Structural Performance of a 10MW Turbine deployed in Offshore Hurricane Wind Conditions

A Case Study for the Gulf of Mexico

Simon Seynaeve

Technische Universiteit Delft

TU Delft

Structural Performance of a 10MW Turbine deployed in Offshore Hurricane Wind Conditions

A Case Study for the Gulf of Mexico

by
door

Simon Seynaeve

to obtain the degree of Master of Science
ter verkrijging van de graad van Master of Science

at the Delft University of Technology,
aan de Technische Universiteit Delft,

to be defended publicly on Wednesday November 20, 2019 at 2:00 PM.
in het openbaar te verdedigen op woensdag 20 november 2019 om 14:00 uur.

Student number:	4756770	
Project duration:	December 1, 2018 – November 20, 2019	
Thesis committee:	Ir. P.G.F. Sliggers,	TU Delft, Chairman
	Dr. ir. A. Jarquin Laguna,	TU Delft, Supervisor
	Ir. P. van der Male,	TU Delft, Supervisor

TU Delft

When the winds of change blow, some build walls,
while others build windmills.
- Chinese Proverb

Abstract

Offshore wind farms are being deployed in ever more challenging conditions. Relatively unexplored are wind farms deployed in hurricane-prone regions. That is exactly the challenge that Mexican government faces as they want to expand their renewable energy resources by developing offshore wind in the Gulf of Mexico. The increased variability in wind resources, due to a combination of a reduced energy-yield design wind speed and increased hurricane structural design wind speed, pushes the overall design challenge of the turbines. Of key importance is the limited knowledge on how hurricane wind affect structures, particularly OWT's.

This study aims to identify how main characteristics of hurricane winds differ from models of regular extreme winds used in engineering simulations, to more accurately quantify hurricane winds loads and response effects on a 10MW turbine and to assess, albeit in a simplified manner, the structural ULS and SLS performance of the turbine under these extreme conditions.

The most important distinction found between hurricane winds and regular extreme winds is the turbulence spectrum: Yu [18] found turbulence energy is shifted towards the lower frequencies for hurricanes while Li [16] found that turbulence energy is shifted towards the higher frequencies. Both agreed that, although disagreeing on the turbulence spectra, that these wind parameters are likely storm-dependent and/or location-dependent. In this study, hurricane parameters are incorporated into a wind generation model adopted from Cheynet [2] and altered to incorporate the hurricane spectra. The wind model is limited to the 1D longitudinal case due to limited available information on other wind components for the hurricane winds. To quantify the loads and response effects due to the different spectra, a numerical approach is considered, using a finite-element blade model developed by Pim van der Male [21] applying the DTU's 10MW reference turbine's structural and simplified aerodynamic properties.

Within the boundaries of the inaccuracies present in the numerical input adn simulations, it was found that both the Yu and Li hurricane spectra show an increased load effect on the turbine blade, the response effect being equally large for both and roughly 20% larger compared to the Kaimal cases. This difference is proven to be predominantly due to the selection of the surface roughness length for hurricane conditions which was found to be larger by both Yu and Li studies [16, 18] for hurricane conditions. The difference due to the spectral change is negligible since the turbulent energy is nearly equal around the natural frequency of the considered 10MW blade thus not giving rise to significant changes in a dynamically amplified response. Selection of accurate hurricane wind parameters such as roughness length are thus equally important as the identified difference in turbulence spectra as they also result in significant changes of about 20% in the final results. Blade orientation has a considerable effect on reducing the response of a single blade if oriented downward. Averaging the thrust forces over all three blades however, effectively negates this advantage.

Structural performance was assessed through failure probabilities of the blade given the results of the aforementioned simulations. It was found that the hurricane wind simulations resulted in the largest failure probabilities, showing a non-linear increase in failure probabilities for larger wind speeds. Bending is the governing failure mode of the blade as these failure probabilities are considerably larger compared to the shear failure probabilities for wind speeds exceeding 50 year return period conditions.

Verifying the blade model response, it was found that the initially assumed three modeshapes were insufficient to accurately described the blade deformations. The model was therefore also

not able to capture the correct internal root shear forces and root bending moments affecting the final results presented.

Acknowledgements

This master thesis is submitted as partial fulfillment to obtain the degree of Master of Science in Offshore and Dredging Engineering Program at the Faculty of Civil Engineering and Geosciences at the Delft University of Technology (TU Delft), The Netherlands. What you are holding in your hand is the culmination of a two year Master study, including 12 months of work, condensed in a paper just over 60 pages long.

To give credit where credit is due, this work could not have been done without my supervisory committee: Ir. Frank Sliggers, Ir Pim van der Male and Dr. Ir. Antonio Jarquin Laguna. First and foremost I would like to thank Pim and Antonio for opening up a relatively unexplored topic of hurricane turbine design to me. And despite me being one of the (self-proclaimed) worst persons to ask for help when needed, were nevertheless always there for advice and useful insight to tackle the problem. Secondly, to Frank, I'd like express my gratitude towards you for showing me that there's more than one way to face problems along the way. That a different perspective can shed a whole new light on the approach and for providing useful feedback during intermediate meetings. It has been an absorbing and challenging experience to say the least, often at times also frustrating, but an interesting topic nonetheless.

Finally, a final word of thanks to my friends I've made along the way at TU Delft, my parents and family for allowing me to vent my frustration on the lack of progress at times without judgement and for all of those things that might have seemed evident in their eyes but to me were never considered as such.

A sincere thank you to all of you!

Simon Seynaeve
Delft, November 2019

List of Figures

List of Tables

Contents

1

Introduction

1.1. The Idea: Mexico's Renewables Objective(s)

Following the global trend of increasing population numbers and energy consumption, Mexico's population has increased by fifty percent in the last three decades (1990 – 2016) while its energy consumption has nearly tripled (100 – 280TWh). These numbers are projected to rise even more in the future. [13]

Even though Mexico's energy mix is, to this day, still dominated by oil and gas, with oil taking up as much as fifty percent of the energy production, a significant percentage of that energy is produced using renewable energy sources (Figure 1.1) [(N)REP: (Non-)Renewable Energy Production]. The overall share, however, of greenly produced electricity has decreased over the years, counting up to about 47TWh (or 17%)(2016) of the total amount of produced power today. Renewable energy contributions are mainly comprised of three land-based components namely hydro-electric, onshore wind and geo-thermal energy (Figure 1.2).[13]

The government's vision to modernise Mexico and its economy, as well as its intention to show leadership on environmental issues have led to a managerial shift in Mexico's energy sector. Setting targets, showing support for clean and responsible energy sources and actually having good wind and solar resources all indicate both willingness and potential for increased power generation from renewable sources. By investing in and applying new technologies across the entire hydrocarbons value chain and attracting new players into the power sector, they plan to ensure cost-efficient investment into both traditional and low-carbon sources of electricity. This reinforces the International Energy Agency (IEA) scenarios indicating that reforms will increase the share of renewable energy sources in the Mexican power sector and slow the growth of carbon dioxide emissions.[13]

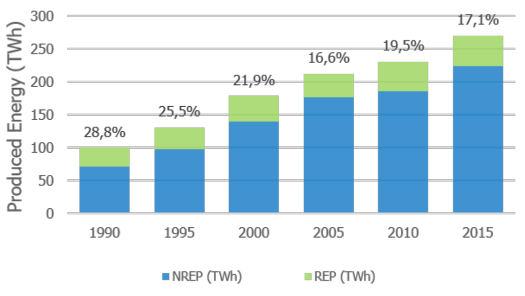

Figure 1.1: Electricity generated from (Non-)Renewable Energy Sources (TWh) [13]

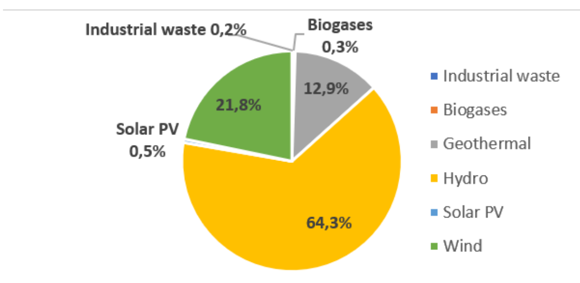

Figure 1.2: Share of Sources in Renewable Electricity Generation (2016) [13]

To meet the increasing energy demands, adhering to the idea of increasing the renewable input, investigating conventional sources of renewable energy yet in more challenging areas can prove to be valuable for further development of the sector locally whilst simultaneously resolving issues other regions are potentially faced with too. Hence, following Europe's movement for offshore wind.

(Offshore) Wind energy in Europe has reached a certain maturity, albeit the overall industry being quite young, compared to other renewable sources of energy and continues to be more widely applied. It is essentially nothing new as it has been used for centuries. Moving offshore has come naturally as a result and consequence from building onshore turbines: develop a simple, working solution and systematically increase its efficiency. Offshore wind development does pose certain challenges due to the harsh oceanic environment (and consequently to its design and price) yet it has considerable advantages compared to an onshore wind development. One only has to think about increasing population numbers to see that available land area is limited. And although the ocean space, both sea floor and water, is occupied by a variety of uses, available area is often not the same issue as it is for onshore applications. Secondly, wind resources offshore are much higher, resulting in larger energy yields. An increased amount of available area and larger energy yield make them more interesting from an economical point of view, despite the larger development price.

1.2. The Challenge: Mexico's Offshore Climate

Moving offshore into the Gulf of Mexico raises a number of red flags. While it is true that moving offshore has advantages, even for the Gulf with its shallower (making for very easy installation) and warmer waters, high accessibility and close proximity to existing oil and gas infrastructure, it is its wind climate that poses major challenges for wind development [20]. A combination of lower than average wind speeds for which conventional turbines are usually designed (and thus lower projected energy yield), in combination with extreme, hurricane conditions (due to its geographical location near the equator) can make turbine and support structure design challenging.

Energy-wise, wind turbines are typically designed to work and optimally within a specific range of wind speeds; DTU's 10MW Turbine is devised to extract energy withing the 4-25[$m.s^{-1}$] wind speed range [9]. Wind speeds for which they are designed structurally are larger e.g. 40-50 [$m.s^{-1}$] for the Central Gulf of Mexico for a return period T of 25-50[years] [3]. Category 3 hurricanes already exceed these design wind speeds generating upwards of 49-58[$m.s^{-1}$] winds. In calmer wind climates, hurricanes cause a larger variability in extreme loads which would translate into higher partial safety factors applied in design standard to achieve a more uniform structural reliability [5]. Underestimation of these extreme design loads could prove to be disastrous for the tower, turbine and the blades. Accompanying wave generation due to these high speeds can have in and of themselves a considerable effect on any offshore structures as evident by the numerous failures of offshore oil and gas platforms in the past. In addition, predicting hurricane occurrences is constrained by the capabilities of current weather models; forecasting is limited to a storm's path and intensity. Therefore it is difficult to estimate how hurricanes will affect wind availability.

Until it is physically possible to actually extract energy from these massive tropical storms[1] rather than fighting or simply withstanding them, the probability of having wind turbines subjected to these extreme loading conditions has to be taken into account into their design. If these issues are left unaddressed during the design of the offshore structure, considering going offshore would not even be an option. Consequently, a huge amount of renewable resources is potentially left unexploited.

[1] This would be an incredible innovation (but an even bigger challenge altogether) given a single tropical storm might releases the equivalent of 600 terawatts of energy, twenty-five percent of that as wind, the vast majority as stored heat. While wind is only a small portion, the amount of power it generates, around 1.5 terawatts, it is enough to meet a quarter of the world's current total electrical generating capacity [1].

1.3. Research Objectives

The objective of this thesis is to assess the structural performance of a conventional three-bladed turbine deployed in Mexico's hurricane-prone climate, more specifically, DTU's 10MW reference turbine [9]. This choice is driven by the fact the wind energy industry keeps expanding both in terms of application rates and turbine sizes and towards harsher conditions. While this is a case study for the Gulf of Mexico, it is not the only region in the world subjected to hurricanes where possibilities for offshore wind development are considered. The evolution towards an increasingly larger sustainable energy output and contribution to the overall energy mix will push offshore wind to even harsher conditions to meet set targets, sparking the need for research into the possibility of deploying wind turbines in these conditions rather than avoiding them.

The structural response of offshore wind turbines subjected to both wind and waves is non-linear and affected by the interaction of aero- and hydrodynamic, structural, operational and geotechnical effects [8]. In this research hydrodynamic, operational and geotechnical effects are ignored since the primary focus will solely be on the turbine blades which will not be directly subjected to wave loading; the foundation will not be modelled and a non-operational, stationary turbine is assumed. This last consideration is perfectly plausible since the hurricane's track size, intensity and path should be sufficiently accurately known and turbine shutdown is to be expected.

Blade tip deflections, root shear forces and root bending moments and will be compared to regular extreme wind conditions to evaluate and compare response effects of hurricane winds on a 10MW turbine blade. It should be noted that the structure should always be designed in its entirety, turbine and support structure included, to come to an optimally performing design; no matter the design conditions it faces. However, the support structure, that is in this definition everything (tower, support structure and foundation) except the turbine itself, are expected to be able to be designed quite straightforward, as load transfer conditions do not change and as such do not pose the major challenge for design in these extreme conditions.

In summary, the research can be condensed in the following set of (sub)questions:

1. Assess hurricanes and identify design conditions;
   (a) Identify hurricane vs. regular extreme wind parameter differences and;
   (b) wherever possible, quantify these differences;
2. Identify critical loading conditions for the blades;
   (a) Assessment of structural blade performance during hurricane conditions through forces, bending moments and stresses (ULS);
   (b) and through blade deflections (SLS);
3. Does structural blade performance change when
   (a) differently oriented?
4. Further estimate blade performance by calculating failure probabilities for
   (a) Root Shear Forces
   (b) Root Bending Moments;

It should be clear that the objective is not to provide the reader with a detailed design approach for extreme hurricane conditions but merely to identify and to quantify, if and wherever possible, probable structural bottlenecks in blade design for the turbine.

1.4. Approach & Methodology

A full diagram of the research approach is presented in Figure 1.3.

The aim of the project is to research the possibility for and Mexico's offshore wind energy potential . To accomplish this, the research of Mexico's wind climate is split into two parts of which this research is only halve (Level I in Figure 1.3). Student colleagues from the Universidad Nacional Autónama (UNA), Mexico will look into the wind energy resource potential of offshore Mexico to determine if developing offshore wind is a reasonable energy source (indicated in grey), while the focus of this research is on the technical or structural performance of OWTs given these extreme hurricane conditions; That is to see if it is structurally feasible to deploy a 10MW turbine in Mexico's hurricane climate.

The Gulf has a rich Oil and Gas history applying API (hurricane) design recommended practices to these installations. Phase I, as depicted in the Figure 1.3, is a literature study. It will consist of relevant research on the definition and mechanics of hurricanes, their effect on offshore structures and the application of hurricane standards. This will be done in function of wind energy design by reducing a hurricane to a simple set of parameters such as, but not limited to, wind velocities and turbulence. These will be compared to regular, extreme winds, The potential threat that hurricanes pose, will be evaluated through the associated risks not limited to the structural challenges.

Hurricane parameters will be incorporated into a numerical wind model generating appropriate wind histories which in turn will be applied to the numerical model of a single turbine blade. If no differences are identified, one would simply be able to apply existing wind turbine design standards, incorporating hurricane wind-characteristic properties. If there are differences, one should consider implementing them first through hurricane design practices (See Figure 1.3), if they exist.

Phase II will address the 10MW turbine blade itself, focusing on the relevant properties for structural evaluation. From an engineering point of view the tower and support structure will not be of primary concern as structural bottlenecks for hurricane design. The focus will therefore be on the blades of the turbine. Due to their slenderness and relatively low stiffness, being subjected to high hurricane wind speeds, they are exposed to large forces and deformations during hurricane events. Choosing a turbine this size is relevant to the current industry practices of installing continuously increasing turbine sizes.

A dynamic approach to the forcing is considered taking into account blade dynamics. At these wind speeds, blade deformations are significant, requiring blade motions to be taken into account. Furthermore, the turbine rotor will be assumed stationary. This is reasonable to assume since wind speeds during hurricanes exceed the operational regime of the turbine. Moreover, should a hurricane develop, even of those intensities below for which they were structurally designed for, warning systems will be triggered shutting down operation of the turbine before the hurricane reaches the turbines.

For evaluation in the Phase III, the Ultimate Limit State (ULS) and Serviceability Limit State (SLS) are considered through rot shear forces and root bending moments (and consequently stresses) and deflections respectively. The Fatigue Limit State (FLS) should also be dealt with for a fully detailed design. After all, severe blade motions give rise to large amounts of fatigue damage where the amount of damage is driven by the number of stress cycles as well as size of stress variations. It is worth investigating which limit state is governing for the design of the blade, the Ultimate Limit State (ULS), Servicability Limit State (SLS) or the Fatigue Limit State (FLS). However, given the complex nature of the fatigue behaviour of composite materials the blades are constructed of, FLS will be excluded from this study, focussing on ULS and SLS.

To perform these calculations, a numerical blade model will be included to assess the structural performance of the more slender turbine blades under the effects of these extreme conditions. Hurricane parameters that cannot be conclusively defined are used in a sensitivity analysis to see how large their influence is on the results.

Lastly, simply changing the blade's orientation effectively aids in reducing loads on the blades.

1.5. Thesis Outline

This research is organised in the following manner. First, Chapter 2 will give a more general insight in the workings of a hurricane. It will describe the mechanics, its lifecycle and anatomy. Risks will be discussed on why hurricanes pose such a significant threat to wind turbines and offshore structures in general, not limited to the structural side of the problem.

In Chapter 3, the similarities and differences between regular extreme winds and hurricane winds are discussed in terms of their implementation in the models in Chapter 4.

Chapter 4 details the workings and approach adopted to simulate the hurricane winds and blade response behaviour.

Chapter 5 presents an overview of the considered calculations, together with their respective results and will be discussed.

Finally, Chapter 6 will summarise the findings in this research, will address the limitations of this work and provide suggestions for future research.

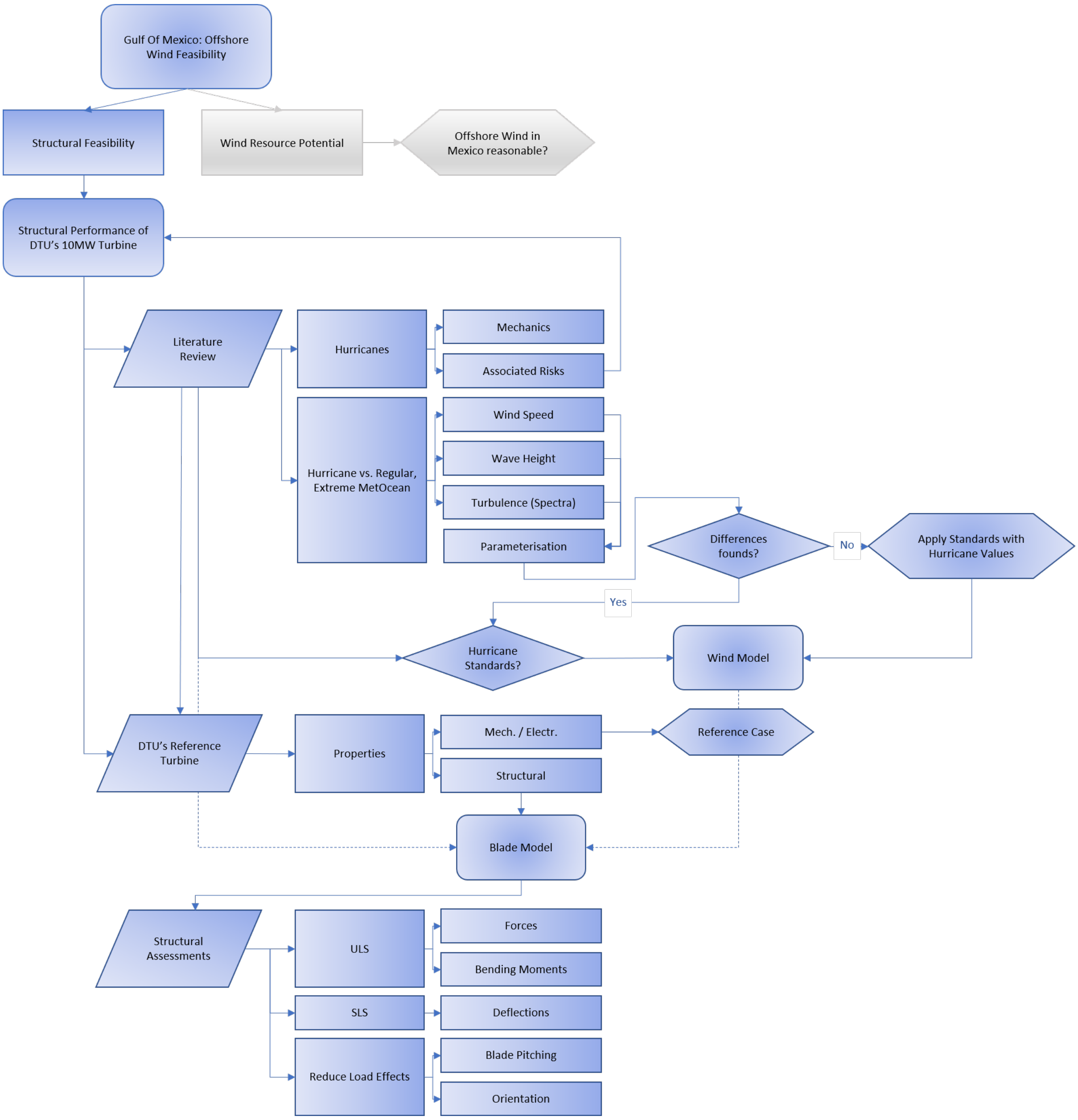

Figure 1.3: Thesis Diagram

2
Hurricanes

Hurricanes have not stolen their name. Derived from a destructive Mayan God *Hurakan*, these tropical storms are one of the most destructive, natural forces on the planet, almost unrivalled in their damage potential in terms loss of life, property and infrastructure. On top of extremely high wind speeds and the associated storm surges, hurricanes bring with them huge amounts of rain leading to flooding of the stricken areas.

Hurricanes, typhoons and cyclones all refer to the same weather event but are named differently based on where they are formed. Hurricanes specifically develop over the North Atlantic Ocean and the Northeast Pacific Ocean (Central American East and West Coast) while cyclones and typhoons are formed over the South Pacific Ocean (Australian East Coast) or the Indian Ocean and The Northwest Pacific Ocean respectively (Japan, China,...).

2.1. Mechanics

Atmospheric pressure is one of the basic principles behind the working mechanism of hurricane. At low altitudes, i.e. near earth's surface, air is warmer due to heating effects by land and ocean (not because of the sun). The density of air here is also higher than air at higher altitudes. Hurricanes only develop in warm, tropical regions where the water temperature is sufficiently high, at least 27[°C], and the air is humid [17, 24]. Figure 2.1 show a radial cross-section of a hurricane.

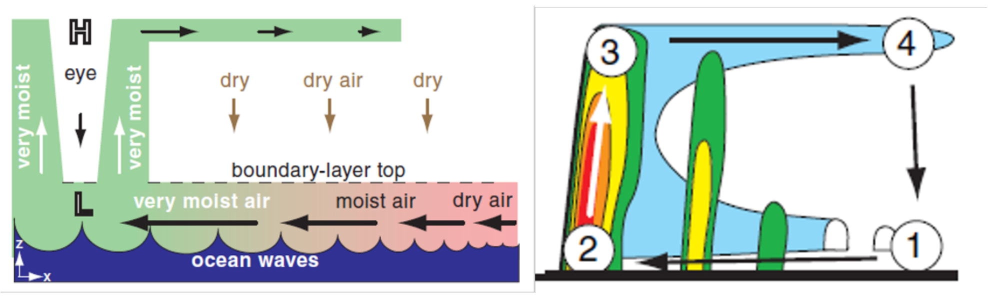

Figure 2.1: The Hurricane Evaporation and Condensation Cycle [24]

Converging, equatorial winds push warm, moist air inwards and upwards (Figure 2.1 [Left] thick black arrows; [Right] (1)-(2)-(3)). As the ocean surface air rises (Figure 2.1 [Right] (2)), it becomes less dense and moves upwards to a new equilibrium state allowing cold air to move downwards. This exchange of hot and cold air is a pressure gradient force. Simultaneously, as the air rises (Figure 2.1 (2)-(3)), it cools down and water vapour condenses to form storm clouds and rain droplets (Figure 2.1 (3)-(4)) developing into rain bands. This convection process combined with Coriolis forces creates circulating winds. The condensation process releases heat or latent heat of condensation in turn heating up surrounding colder air causing it to rise. This deficit is replenished again by warmer ocean surface air through the converging and circulatory winds essentially fuelling and sustaining the hurricane, reinforcing the already ascending air increasing the circulation and the storm's wind speeds.

At altitudes up to 9,000[m] winds further dissipate rising hot air and in even higher atmospheric regions upwards of 9,000[m], high-pressure air also removes heat from the rising air, effectively maintaining a continuous stream from the surface and further driving the air cycle and the hurricane's growth [17, 24].

As long as no disruptive actors are presents i.e. wind shear, and there is a combination of optimal pressure and wind conditions, the storm remains fed by warm ocean air and high-pressure air is sucked into the low-pressure eye of the storms, wind speeds will continue to increase.

2.2. Lifecycle

The largest part of hurricanes that hit the Mexican and United States Eastern Coast develop from thunderstorms, tropical disturbances, off the Western Coast of Africa, as they move out over the ocean waters. Development can take anywhere from hours to days. At this stage they are low-pressure formations with small pressure gradients and little to no rotation. If these disturbance manage to persevere and the thunderstorms keep releasing heat, which warms the area within the region, the cycle of evaporation/condensation cycle that feeds and sustains the hurricane is started as described in the previous section (Ref. Sec2.1).

A hurricane's rotation is induced and its track affected by the Coriolis force. This force affects all fluids and free-moving objects resulting in them not moving along a straight but a curved path: a rightward curvature for the Northern Hemisphere and leftward curvature for the Southern Hemisphere. Winds are deflected similarly. It is this deflection that defines the hurricane's rotation: counterclockwise north of the Equator, clockwise south of the Equator. Its track curvature is similar in the respective directions. This also means that since the Coriolis force is negligible on and near the equator, hurricanes will never form here.

Once a tropical storm has reached hurricane status and has significantly intensified, the only mechanism that can stop it in its track is dissipation. Eventually, it will encounter conditions that cut off the inflow of moist, warm air it feeds on. This happens by either travelling into colder water at higher latitudes where the gradient pressure and wind speeds decrease. Alternatively, the hurricane makes landfall. Condensation and the subsequent release of latent heat decreases and surface friction decreases wind speed causing the wind to move more directly into the eye of storm eliminating the pressure difference that fuels the storm.

2.3. Anatomy

A hurricane is a slow-moving, rapidly rotating 3D wind field often in the range of hundreds of kilometers in diameter (shown in Figure 2.2). It is comprised of three spiral bands as indicated by Figure 2.3, starting from the inside going out, there is its low-pressure, relatively wind still centre, called (a) the eye of the storm. Surrounding the eye is (b) the eye wall, where wind conditions are most severe. Lastly, the thunderstorms moving outward from the eye are referred to as (c) the rain bands.

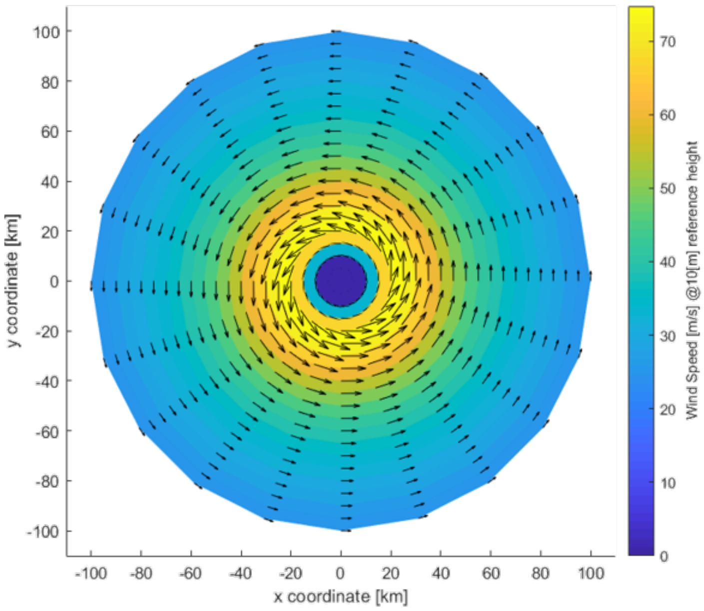

Figure 2.2: 2D Stationary Hurricane Wind Field showing counterclockwise rotation for Northern Hemisphere hurricanes; Conversely, Southern Hemisphere hurricane will rotate clockwise

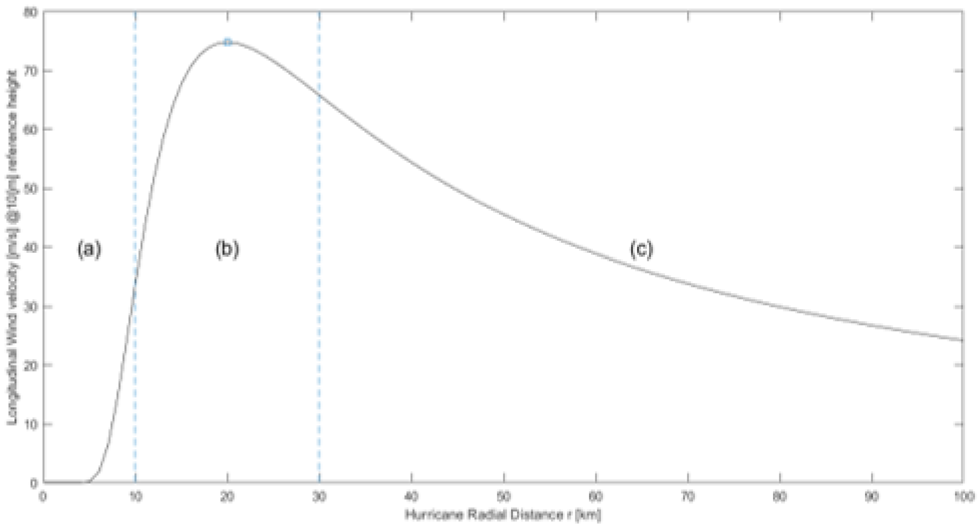

Figure 2.3: Radial longitudinal wind velocity profile @10[m] reference height with (a) the eye, (b) the eye-wall and (c) the rain bands; Additionally indicated is the maximum wind speed v_m at RMW, the radius of maximum wind (20[km]); Note, the dotted lines are merely indicative.

2.4. Hurricane Categories

The Saffir-Simpson Hurricane Wind Scale, elaborated on in Table 2.1, is used to classify North Atlantic hurricanes solely based on their one-minute averaged sustained wind speed [19, 24], as opposed to the more conventional ten-minute averaged wind speed (indicated in brackets) at a reference anemometer height of ten meters; central pressure, storm surge were also used, yet before the 2010 updated scale [24].

Table 2.1: Saffir-Simpson Hurricane Wind Scale for Hurricane Classification for wind speeds @10[m] reference height [19]

Category	**1 min. Wind Speed v** $[m.s^{-1}]$	**Storm Surge** $[m]$	**Central pressure** $[Pa]$	***Damage*** [-]
CAT. 1	≤ 42 (40.1)	≤ 1.5	98.0 - 98.9 · 10^3	*Minimal*
CAT. 2	≤ 49 (46.8)	≤ 2.4	96.5 - 97.9 · 10^3	*Moderate*
CAT. 3	≤ 58 (55.4)	≤ 3.7	94.5 - 96.4 · 10^3	*Extensive*
CAT. 4	≤ 70 (66.9)	≤ 5.5	92.0 - 94.4 · 10^3	*Extreme*
CAT. 5	> 70 (66.9)	> 5.5	< 92.0 · 10^3	*Catastrophic*
Additional				
Tropical depression	≤ 17 (16.2)	≤ 1.0		
Tropical storm	≤ 32 (30.6)	0.0		

This also means that a hurricane's size, i.e. its radial extent as discussed in the previous section, is not indicative for its severity as shown in Table 2.1.

2.5. Risk

Research has been done involving risk assessment of hurricanes for Offshore Wind Turbines (OWT) [8, 23, 28] and O&G structures [25]. [23] only considered tower buckling as a failure mode, neglected loss of blades since they are easily replaceable. Blades however are essential when producing energy from offshore wind thus downtime for repairing or replacing altogether and accompanying additional costs are needed to be limited to a minimum to ensure profitability. Thereby also limiting effects on the grid due to losses.

In engineering design, a statistical approach is typically used to calculate extreme values for larger return periods based on limited duration measurements or data acquisition of environmental conditions. The IEC 61400-3 design standard for Class 1 wind regimes requires that an OWT survive a maximum 10-minute average wind speed with a return period of 50 [years] of $50[m.s^{-1}]$ at hub height [23]. Translating that from a $119[m]$ DTU turbine hub height to a 10[m] reference height at which hurricane wind speeds are defined, shows an exceedance of that value for halve of Category 2 hurricanes (wind speeds between 42-49 $[m.s^{-1}]$).

Moreover, it has been shown that OWT's are particularly vulnerable to loss of yaw control, due to grid connection losses, no longer allowing the turbine to follow the incoming wind's direction [8, 23]. Wind directions can shift rapidly, as much as 30[] in $60[s]$ during Hurricane Bob in 1991 measured $55[km]$ away from the storm's centre, while e.g. the NREL-5 reference turbine is designed to yaw at $0.3[°/s]$ [23]. This yaw speed, although not mentioned in the design report [9], is expected to be in the same order of magnitude if not smaller for the $10[MW]$ due to scaling of the turbine's mass and inertia.

Another contributing factor is the high degree of unpredictability of hurricanes occurrences, both mathematically and statistically. While current weather models have evolved significantly, when and where hurricanes will develop is still virtually impossible to predict [25, 28].

[25] determined that accurate hurricane forecasts would result in fewer 'false' alarms, thereby preventing unnecessary shutdowns, evacuations of and disruptions in production from O&G structures. The same can be said from OWT's albeit they are unmanned structures so disruptions to production are the only factor. At this stage of forecast development it has not been sufficient to create value to the O&G industry nor the offshore wind sector. With improvements in accuracy though, forecast values dramatically increases, yet requires significant investment'[25]. Meteorologists are, to this day, limited to tracking a hurricanes development in terms of size, travel speed and track. Not with absolute certainty but always with a degree of inaccuracy.

Even historically, statistically speaking, extrapolating annual occurrence rates from results from the last 50 years, no discernible trend can be determined to estimate how many hurricanes will occur in the future [28].

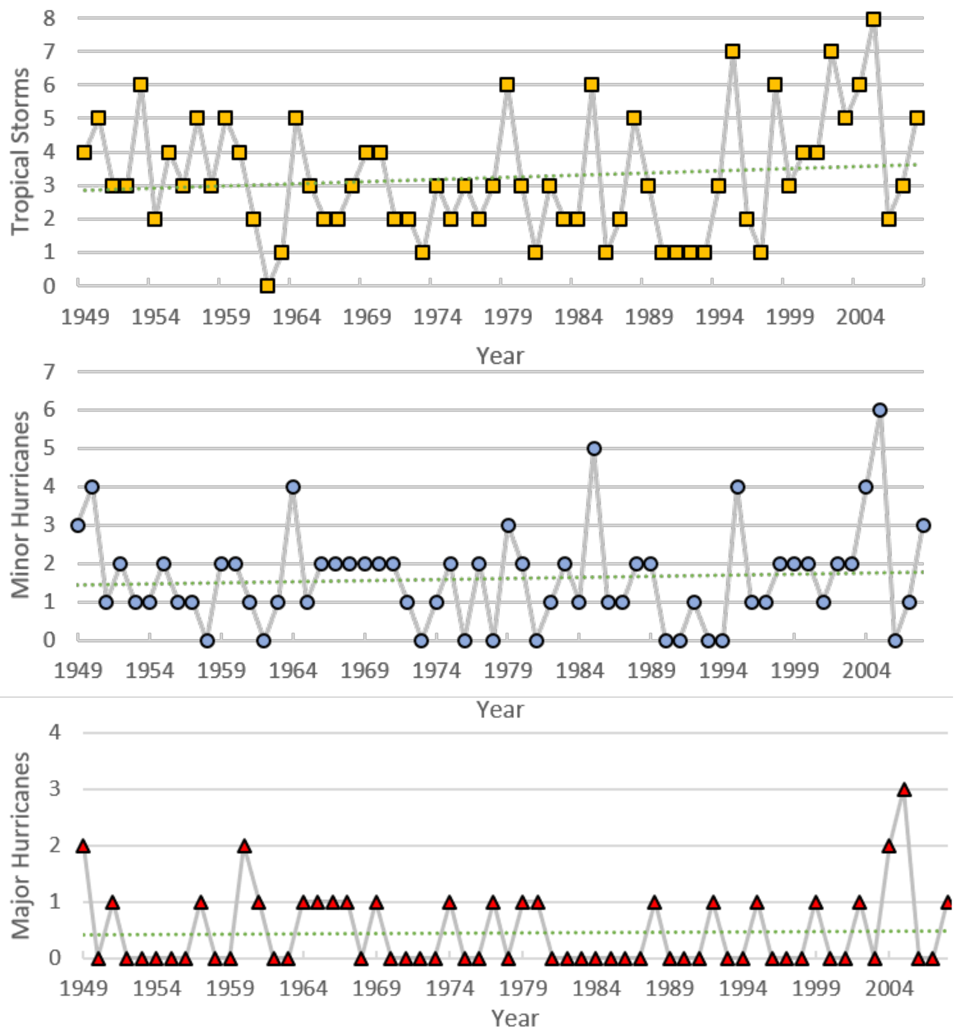

Figure 2.4: Anual Occurences of (1) Tropical Storms (Strength < CAT. 1), (2) Minor Hurricanes (Strength < CAT. 3) and (3) Major Hurricanes (Strength > CAT. 3) as reproduced from [28]

3

Hurricane Winds

Engineering wind is assumed to be comprised of two parts: a mean component and turbulence. This follows from a simplification of the temporal variations of wind speed. On the one hand, there is a clear day-night variation (low-frequent variation) and on the other hand, a somewhat (practically) instantaneous variation (in the range of 1-10 minutes). Firstly, the former suggests, within the considered averaging time of 10 minutes, to assume the low-frequent variation to be zero or i.e. the wind speed to be constant yet non-zero in the considered time frame. Secondly, it has been shown that averaging the high-frequent variations during that same averaging-window results in a zero mean wind speed. This allows for the superposition of time-varying, high-frequency fluctuations in wind speed, also referred to as gust or turbulence, and a constant wind speed. Based on these components, a distinction can be made between regular extreme winds and hurricane winds.

In structural design, a statistical approach is used to calculate extreme values for wind loading. Larger return period wind speeds are based on limited duration measurements of wind speed histories. The API (American Petroleum Institute) standard [3] specifies the wind speed conditions for the Central Gulf of Mexico accordingly, amongst the other Gulf regions, as presented in Table 3.1.

The IEC 61400-1 (v.2005) standard [14] specifies a turbine should be able to withstand a ten minute-average wind speed of 50$[m.s-1]$ for a Class I turbines, which are the higher turbulence characteristics and typically used offshore. That is if the requirements are not otherwise specified by the designer (class S turbines). The API standard defines a characteristic ten-minute averaged wind speed of $50.1[m.s^{-1}]$ for a return period of 50[years]. Based solely on this mean wind component, not taking into account safety factors, any structure designed given these design conditions will not survive the worst Category 3 (46.8-55.4$[m.s^{-1}]$ hurricanes and higher. In order for the structure to survive the least severest of category 5 hurricane conditions, it must be designed for characteristic wind speeds with a return period of 1000[years] as this wind speed exceeds the least severest H5 wind speeds conditions $v_{H5} < v_{c,S,1000}$.

Table 3.1: Independent Extreme Values for Hurricane Wind Speeds @10$[m]$ reference height for the Central Gulf of Mexico [3]

Return Period (years)	10	25	50	100	200	1000	2000	10000
1-hour Mean $[m.s^{-1}]$	33.0	40.1	44.4	48.0	51.0	60.0	62.4	67.2
10-min Mean $[m.s^{-1}]$	36.5	44.9	50.1	54.5	58.2	69.5	72.5	78.7
1-min Mean $[m.s^{-1}]$	41.0	51.1	57.4	62.8	67.4	81.6	85.6	93.5
3-sec Gust $[m.s^{-1}]$	46.9	59.2	66.9	73.7	79.4	97.5	102.5	112.8

Secondly, while hurricane wind-subjected structures and extreme wind speeds-subjected structures are similar behaviour-wise in terms of their constant wind speeds even despite the difference in wind speed amplitude, investigations of hurricanes have indicated different turbulence characteristics [18] from regular extreme winds.

Turbulence intensities are similar for both types of wind [10] according to research on Category 1 hurricanes [16, 18]. The frequency content and distribution of the turbulence is different resulting in different turbulence spectra for hurricane winds and regular extreme winds. The dynamic nature of wind turbines highlights the importance of these distinctions between turbulence frequency content.

3.1. Holland's Hurricane Wind Model

In 1979, Holland developed an analytic, parametric model for wind and sea level pressure profiles for hurricanes [12] which he generalised and revised 30 years later [11]. Its simplicity lies in the equations which only contain two parameters. These may be estimated empirically for hurricane observations or determined climatologically to define a standard hurricane, making it very useful for engineering applications.

Similar to normalised turbulence spectra (Ref. Sec. 3.3.1), normalised hurricane pressure profiles show comparable shapes (Ref. Figure 3.1): low, central pressure within the eye, sharply increasing within the eye-wall and steadily evolving towards an ambient pressure. Hereby normalising the profiles according to Equation 3.1 to remove variations due to differing central and ambient pressure.

$$\frac{(p\,(r) - p_c)}{(p_n - p_c)} \tag{3.1}$$

where $p(r)$ is the pressure at radius r $[km]$, p_c the central pressure and p_n the ambient pressure (which in theory is at $p(\infty)$ but in practice is taken at the first anticyclonically curved isobar). These profiles resemble a series of rectangular hyperbola which he approximated as

$$r^B \ln\left[\frac{(p_n - p_c)}{(p - p_c)}\right] = A \tag{3.2}$$

where A and B are scaling parameters. Rearranging Equation 3.2, he found Equation 3.3 for the pressure profile:

$$p = p_c + (p_n - p_c)\, e^{\frac{-A}{r^B}} \tag{3.3}$$

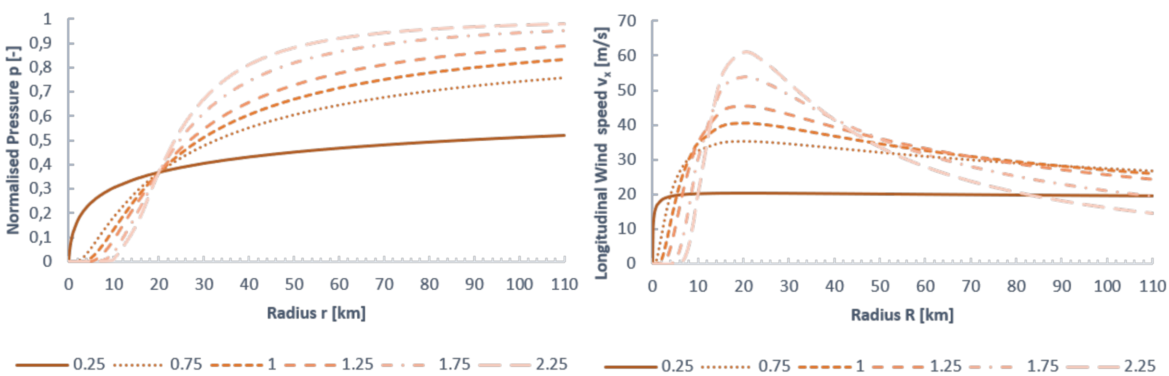

Figure 3.1: Parametric Hurricane profiles (R_{max} = 20[km], p_c = 950 [mbar] and p_n = 1005 [mbar]) with varying B (and consequently A) for [Left] Normalised sea level pressure and [Right] Wind Speed (Recalculated from [12]

Which for the wind profile can be expressed by Equation 3.4, using the gradient wind equations, neglecting the Coriolis force[1] f since it has a negligible contribution in comparison to the pressure gradient in the eye wall and the air being in cyclostrophic balance.

$$v_c(r) = \left[\frac{AB\,(p_n - p_c)\, e^{\frac{-A}{r^B}}}{\rho\, r^B}\right]^{1/2} \tag{3.4}$$

The wind speed profiles according to Equation 3.4 are shown in Figure 3.1 on the right for identically varying B's as for the pressure profiles.

To find the radius at which wind speeds are highest, one can easily state that $dV_c/dr = 0$, thus finding RMW as

$$R_w = A^{1/B} \tag{3.5}$$

Equation 3.5 clearly shows the RMW is independent of the relative values of ambient and central pressure and is defined solely and entirely by scaling parameters A and B. Substituting Equation 3.5 into Equation 3.4, results in an expression for the maximum wind speed V_m

$$v_m = C\,(p_n - p_c)^{1/2} \tag{3.6}$$

where C is often determined empirically through Equation 3.7 to find v_m.

$$C = (B/\rho e)^{1/2} \tag{3.7}$$

and e is the base of natural logarithms. One can also notice that the maximum wind speed is independent from the RMW further supporting a previously-made statement (Ref. Sec. 2.3) that hurricane category (maximum wind speed v_m) is not indicative for a hurricane's size (radial extent). To find v_m however, information is required on the shape of the profile through scale parameter B. A detailed explanation on scaling parameter A and B can be found in [12].

Holland's proposed model ensures radially, symmetrical wind conditions which is rarely the case for real hurricanes. Hurricanes also have a velocity of forward motion or translational velocity v_t which introduces an additional velocity component to the wind profile. Georgiou [28] took into account this additional component to further improve the model as follows

$$v_c(r) = v_H + 0.5\, v_t \sin(\beta) \tag{3.8}$$

where V_H describes the wind profile as proposed by Holland and β is the angle from the direction of forward movement. For Northern Hemisphere with counterclockwise rotating wind fields, this translate in larger winds speeds occurring to the right of the eye and reduces wind speed to the left of it. In the Southern hemisphere this would be opposite. A South-bound, Northern Hemisphere hurricane wind field with translational velocity of $20[m.s^{-1}]$ is shown in Figure 3.2. Note, the increased wind velocity in the right-hand quadrants of the storm.

[1] The Coriolis parameter is calculated as $f = 2\Omega \sin\phi$ where Ω is Earth's rate of rotation ($\frac{2\pi}{T}$ with T = 23 [hr] 56 [m] 4.1 [s]) and ϕ the latitude

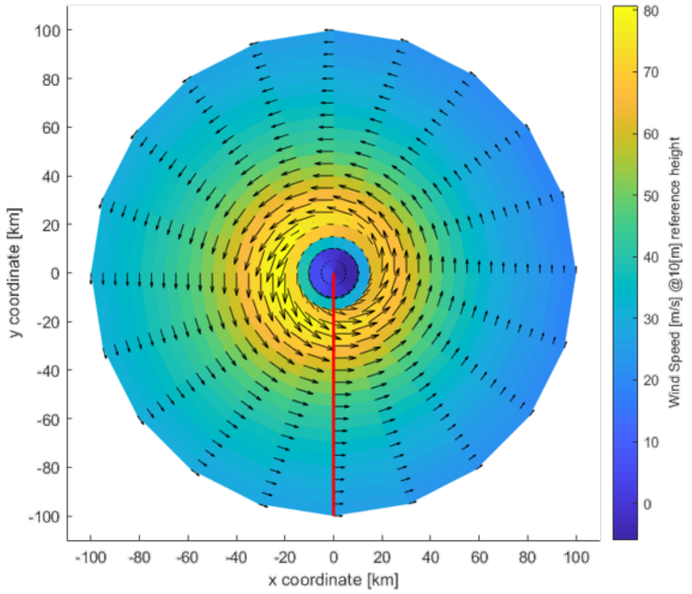

Figure 3.2: South-bound (indicated by the red line), Northern Hemisphere 2D Hurricane Wind Field with a $20[m/s^{-1}]$ translational velocity

3.1.1. Research Relevance of Holland's Wind Model

Since the focus of this research is on ULS and SLS, the physical hurricane and profile itself as proposed by Holland is not of particular interest. ULS focuses on the maximum forces generated by the hurricane winds and maximum stresses experienced by the blade which in this case will coincide with the maximum occurring wind speed found in the eye-wall.

In fact, using Holland's model doesn't require knowing the RMW in order to calculate V_m because of the assumed cyclostrophic balance. As such, it is only V_m that is of interest for the ULS analysis.

However, the duration of a hurricane's passage with respect to its lifetime is short, the turbulent forces exerted on the structure relatively large. Hence, an accurate description of the entire event is recommended including the hurricane as a whole passing the structure when the goal is to estimate fatigue design lifetime of the structure. Assuming maximum hurricane conditions during the entire storm's passage, this might lead to a clear overestimation of fatigue damage experienced, underestimation of fatigue life time and consequently unnecessarily high safety factors.

3.2. Young's Hurricane Wave Model

Before an actual hurricane reaches the offshore turbine, the structure might already experience the effects of said hurricane in the form of swell and waves. Based on a series of simulations, Young [29] developed a parametric hurricane wave prediction model, looking into the relation between hurricane winds and generated waves by running a synthetic series of numerical simulations. He confirmed that both maximum wind speed v_m and translational velocity v_t play an important role in determining not only the magnitude of the generated waves but also their spatial distribution.

A distinction is made depending on the storm's V_t. For slowly moving storms, waves generated in the intense, right-hand wind regions, have group velocities $C_g > V_t$, thus propagating ahead of the storm . They are only subjected to a relatively short equivalent fetch F. If the storm moves fast ($V_t \approx C_g$) the opposite occurs and waves are trapped in the storm with no swell occurring ahead of the storm. For an optimal combination of V_t and v_m, waves spend a maximum amount of time in the high wind region, experience the maximum equivalent fetch and thus produce the highest waves.

$$\frac{g\,H_s(max)}{V_m^2} = 0.0016\left(\frac{g\,F}{V_m^2}\right)^{1/2} \tag{3.9}$$

He developed his model accordingly, using parameters V_t and V_m and RMW, to calculate an equivalent fetch F (Equation 3.9. Further combining this concept with JONSWAP fetch-limited growth relations to provide the means of calculating the size and distribution of these hurricane-generated waves. Important to note here is that his model is only suited for deep water and for hurricanes for which the wind field parameters are relatively constant.

A summary of the model application can be found in Appendix **??**

3.2.1. Research Relevance of Wave Model

One of the reasons that shifted the focus from the entire structure to the turbine blades was the inability to reproduce Young's numerical results based on the proposed model equations. The additional step of selecting the appropriate spatial distribution diagram would make the implementation into the numerical models complex. To avoid this altogether, it was decided to neglect the wave forcing on the structure, while shifting the point of interest towards the turbine itself.

As such, turbine blade will never be directly subjected to wave loading and as such finding an accurate description of the wave loading on the structure is not necessary. An offshore turbine structure is however, a highly dynamic system. A purely static approach to the problem of the blade forcing would mean neglecting additional dynamic effects due to the structure and blade's motion relative to the wind.

From experience, in order to further improve accuracy of the model, a full dynamic description will be needed.

3.3. Hurricane Parameterisation

Describing a complex hurricane wind field by a set of parameters rather than working with the full field description significantly reduces the complexity of the calculations. What follows is a description of important factors, besides the obvious wind speed magnitudes, that differ between regular winds and hurricanes.

3.3.1. Turbulence

Wind is highly variable, both geographically and temporally. These variations persist over a very wide range of scales, both in time and space [26]. The importance of this is amplified due to the squared relationship between wind speed and blade forces. Temporal variations refer to yearly changes in wind or even seasonal and daily variations. Spatial variations refer to differences between climatic regions in the world. Most notable in this, are the variations on more local scales which are largely dictated by physical geography, on smaller scales by topography and on the smallest scale by ground obstacles.

It is at these smaller time scales that the first factor, turbulence, is defined. Turbulence is described as wind speed fluctuations on a relatively fast timescale namely typically less than ten minutes. Its intensity is a measure of the overall level of turbulence and is a defined as

$$I = \frac{\sigma}{\bar{U}} \tag{3.10}$$

where σ is the standard deviation of wind speed variations around a mean $\bar{U}$, usually ten-minute averaged, wind speed and the shear profile often described logarithmically (Equation 3.11).

$$U(z) = U_{ref}\left(\frac{ln(z/z_0)}{ln(z_{ref}/z_0)}\right) \tag{3.11}$$

where z_{ref} [m] is the measurement height of U_{ref} $[m.s^{-1}]$ (typically $10[m]$) and z_0 $[m]$ is the characteristic length for the surface roughness.

The IEC [26] specifies turbulence using Equation 3.12 which was applied in the Wind Generation Model (Ref. Sec.4.1).

$$I_u = I_{ref}(0.75 + \frac{5.6}{\bar{U}}) \tag{3.12}$$

Given the nature of turbulence, it is primarily dependent on the surface roughness characterised by roughness length z_0 and the considered height.

Li [16] found turbulence intensities in the same order of magnitude as regular extreme winds namely 10-14[%]. Be that as it may, the hurricane that was the focus of the research was a Category 1 hurricane. It is possible that for higher category hurricanes this might no longer be true. For the calculations done in this report however, for all wind speeds, a single turbulence intensity of 12[%] is assumed. Further research on other category hurricanes should clarify if this assumption holds.

3.3.2. Turbulence Spectra & Spectral Gap

Turbulence spectra contain information on the distribution of turbulent energy contents for a range of frequencies. The Kaimal [26] spectrum is typically used and described by Equation 3.13 and presented in Figure 3.3 for a 119[m] hub height (as defined by [9] for their 10MW reference turbine, a 10[m] reference wind speed of 50$[m.s^{-1}]$ and turbulence intensity of 10[%]

$$\frac{nS_{uu}(n)}{\sigma_u^2} = \frac{4n\frac{L_k^u}{\bar{U}}}{\left(1+6n\frac{L_k^u}{\bar{U}}\right)^{5/3}} \tag{3.13}$$

where $S_u(n)$ is the autospectral density function for the longitudinal component and L_k^u the turbulence length scale (L_k = 340.2[m]) as defined by Equation 3.14.

$$L_k = 8.1 \cdot \min(0.7 \cdot z; 42) \tag{3.14}$$

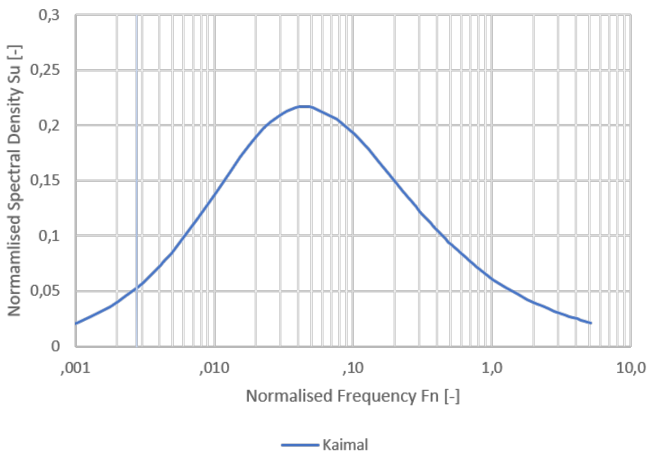

Figure 3.3: Normalised Kaimal Spectrum

Observations and analysis of hurricanes showed that the turbulence spectra of hurricane winds are different from that of regular high winds [10, 18]. Yu et al [18] found that a higher amount of energy is contained within the lower frequencies when compared to the Kaimal Spectrum; Li et al [10, 16], however, found contradicting measurements indicating higher energy within a the higher range of frequencies.

The presented Yu Spectrum [18] (Equation 3.16) was found from measurements at 5[m] and 10[m] reference heights during the passage of four hurricanes at the Florida, US Coast. They concluded that low-frequency turbulence contains more energy for hurricane winds than for regular extreme winds defined by the Kaimal Spectrum. The proposed spectral equation for all 3D components is described by Equation 3.15

$$\frac{nS_u(n)}{u^*} = \frac{p_1 f^2 + p_2 f + p_3}{f^3 + q_1 f^2 + q_2 f + q_3} \tag{3.15}$$

where u^* is the friction velocity and p_i and q_i are constants defined according to Table 3.2 for the respective components. This spectral equation can be normalised to allow for comparison with the Kaimal Spectrum by multiplying it by factor $1/\beta$ where $\sqrt{\beta} = \sigma/u^*$ such that Equation 3.15 becomes

$$\frac{nS_u(n)}{\sigma_u^2} = \frac{1}{\beta}\frac{p_1 f^2 + p_2 f + p_3}{f^3 + q_1 f^2 + q_2 f + q_3} \tag{3.16}$$

Table 3.2: Constants p_i and q_i for respective components of the Yu Spectrum @10[m] reference height

	S_{uu}	S_{vv}	S_{ww}
p_1	-5.980E-03	-0.07044	-0.001399
p_2	1.544E-01	0.2392	0.07417
p_3	1.055E-05	8.606E-05	2.159E-05
q_1	0.4458	1.023	-0.2446
q_2	0.06486	0.2151	0.1565
q_3	9.754E-05	2.2212E-03	8.869E-03

Similarly, Li et al [16] found contradicting evidence, showing higher turbulent energy for higher frequency compared to the Kaimal Spectrum, based on measurements in the South China Sea. The Li longitudinal spectral equation for the back eye wall is expressed by Equation 3.17.

$$\frac{nS_u(n)}{\sigma_u^2} = \frac{16.66f}{1.72 + 237.24 f^{5/3}} \tag{3.17}$$

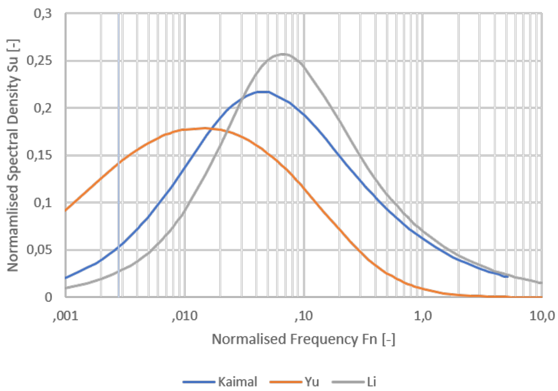

Figure 3.4: Comparison between Kaimal, Yu and Li Spectrum for the longitudinal component u showing a larger energy content in the lower frequency region for Yu and in the higher frequency region for Li

Looking into the turbulence spectra inherently introduces the notion of the 'spectral gap'. Simply stated, it has been shown [7] that for regular winds, relatively speaking, there is almost no turbulent energy in the frequency region between two hours and ten minutes (0.5-10 cycles per hour). This means that often a cut-off frequency of

$$f_0 = \frac{n\, cycles}{hours} = \frac{10}{3600} = 0.00277\,[Hz] \tag{3.18}$$

$0.00277[Hz]$ is used below which the turbulence spectral amplitude can be considered 0.

Since the idea of a spectral gap in hurricane winds does not exist as of yet, and Yu et al has identified a larger energy content in the lower frequency region, assuming this cut-off limit is also valid for hurricane winds might be an oversimplification and will effect the results. Nevertheless, it was chosen to consider this cut-off frequency for all three spectra.

3.3.3. Turbulence Length Scales

Using the Kaimal Spectrum as defined by Equation 3.13 in Sec. **??** requires the definition of the turbulence length scales L_k. These length scales are indicative of the size of the turbulent eddies. They are dependent on the surface roughness z_0 as well as on the height. Proximity to the ground limits the eddie development and thus reduces the length scales. The IEC edition 2 standard defines the longitudinal length scale L_k^u according to Equation 3.14.

Both Yu and Li found different results between hurricanes, agreeing that these length scales are storm dependent.

Specifying these length scales, however, is apparently not needed to use in the proposed hurricane spectra, meaning the hurricane spectra at hub height are assumed equal to the hurricane spectra near sea level. They are calculated in [16, 18] at measurement heights of 5 and 10[m] but relations to extrapolate these values to hub height are not provided.

3.3.4. Roughness Length z_0

References on characteristic roughness lengths for open water during hurricane conditions are limited. A typical value used for a calm, open sea with minimal waves is $z_0 = 0.0002[m]$ [26]. One can expect larger values inside hurricane weather systems due to the generation of extreme waves, varying with wind intensity.

Yu [18] found roughness lengths in the range of [0.0002-0.006][m] for hourly average wind speeds between [12.1-18.5][$m.s^{-1}$] using measured data and applying Equation 3.19a. Li [16] found values in the range of [0.00088-0.0022], using the revised Charnock model (Equation 3.19b) for the back eye-wall. Both are larger than those typically used for non-hurricane winds.

$$z_0 = exp(ln(z) - \frac{\sqrt{\beta}\kappa}{TI_u}) \tag{3.19a}$$

$$z_0 = \alpha_s \frac{u_*^2}{g} + \frac{0.11\nu}{u_*} \tag{3.19b}$$

where $\sqrt{\beta} = \sigma_u/u_*$, u_* is the friction velocity, $\kappa = 0.4$ is the von Karman constant TI_u is the longitudinal turbulence intensity, α_s is the Charnock constant, g the gravitational acceleration and ν the molecular viscosity of air.

With Yu [18] also finding a considerable variation in β values, they both expect this to be a value which will differ, albeit within limits, from storm to storm. This would also likely mean that for increasing storm severities, these values are likely to become even larger. Nevertheless, maximum values found in both researches are applied to remain on the conservative side.

3.3.5. Spatial Coherence

Turbulence spectra as presented above describe variations of turbulence components in time at any given single point. Particularly for moving blades, only describing these temporal variations is not sufficient as these variations are no longer well represented by these single point spectra. Spatial variation is equally important since it is sampled by the moving blades and thus also has an influence on the variations in time [26].

Additional information on the spatial variation is required in order for an accurate description. This means including information on cross-correlations between turbulent fluctuations at different points in space. It is easy to understand that this coherence decreases as the distance between the two points in space increases. But correlations are also smaller for high frequency than for low frequency variations [26]. Coherence is defined as

$$C_i(\Delta r, n) = \frac{S_{ij}(n)}{\sqrt{S_{ii}(n)S_{jj}(n)}} \tag{3.20}$$

where i, j indicate wind components, n is frequency, S_{ij} is the cross-spectrum of variations at two points separated by a distance $\Delta r = \sqrt{\Delta x^2 + \Delta y^2 + \Delta z^2}$ and S_{ii} and S_{jj} are the spectra of variations at each of the points [26].

Yu [18] presented a coherence spectrum between longitudinal and vertical wind components, Li [16] focused on the longitudinal component of the wind alone. Both do not mention spatial coherence for the longitudinal components (S_{xx}) nor the coherence between longitudinal and vertical winds S_{xy}) limiting the study to the 1D longitudinal wind components. It was therefore chosen to also implement spatial coherence for the hurricane spectra according to Equation 3.21 applied by Cheynet [2] which was already implemented for the Kaimal Spectrum.

$$C_i(\Delta r) = exp(-\frac{\sqrt{DecY_u^2 + DecZ_u^2}\, f(n)}{\bar{U}}) \tag{3.21}$$

where f is the frequency of the wind component, $U(z)$ the wind speed at point (Y,Z) Dec_Y^X and Dec_Z^X expressing the spatial decay through coherence decay coefficients C_{ij} using

$$DecY = C_u^y \cdot \delta y \tag{3.22a}$$

$$DecZ = C_u^z \cdot \delta z \tag{3.22b}$$

C_{uy} and C_{uz} can be taken as 10 for the Kaimal case. No indicative values were found for the hurricane spectra and were therefore used in a sensitivity analysis.

4

Wind & Turbine Blade Model

4.1. Wind Model

Chapter 3 has shown hurricane winds are different from regular, extreme wind speeds. To generate hurricane wind histories that can be implemented in the blade model, a wind field simulation script was used, developed by Cheynet [2]. The script allowed for the generation of spatially correlated turbulent wind histories for a predefined geometry, in this case a single turbine blade, for a certain turbulence spectrum. Alterations were made to the script to incorporate the hurricane spectra as described in Section 3.3.2 as well as to introduce the notion of turbulence intensities. Since only the Li Spectrum for the longitudinal wind component is known, a 1D approach is assumed for all spectra.

4.1.1. Wind Signal Definition

Stochastic processes such as wind histories can be simulated using a spectral representation method [6]. Wind histories can be produced computationally efficient by using a cosine series equation. As long as the number N of cosine components is sufficiently large, these wind histories accurately reflect the prescribed statistic properties. If the Power Spectral Density function $S_{f_0 f_0}$ of the wind series is known, one can accurately recreate a signal akin to the stochastic properties of the wind. A signal can be (re)produced as an infinite sum of cosines described by

$$f(t) = \sqrt{2} \sum_{n=0}^{N-1} A_n \cos(\omega_n t + \Phi_n) \tag{4.1}$$

Where the amplitude A_n of each cosine component depends on the spectral density value at a certain frequency ω_n and Φ_n is a phase shift uniformly and randomly distributed between $[0 - 2\pi]$. A_n can be calculated as

$$A_n = \left(2S_{f_0 f_0}(\omega_n)\,\Delta\omega\right)^{1/2}, \qquad n = 0, 1, 2, \dots, N-1 \tag{4.2}$$

where ω_n and $\Delta\omega$ are defined as

$$\omega_n = n\Delta\omega, \qquad n = 0, 1, 2, \dots, N-1 \tag{4.3}$$

$$\Delta\omega = \omega_u / N \tag{4.4}$$

and the following property should be enforced.

$$A_0 = 0 \quad or \quad S_{f_0 f_0}(\omega_0 = 0) = 0 \tag{4.5}$$

In Equation 4.4, ω_u represents an upper cut-off frequency for which the power spectral density function value $S_{f_0 f_0}(\omega)$ may be assumed zero. It is a fixed value, hence $\Delta\omega \longrightarrow 0$ as $N \longrightarrow \infty$ increasing the accuracy since $S_{f_0 f_0}$ is more densely sampled.

The wind histories will be periodic with period T_0

$$T_0 = 2\pi/\Delta\omega \tag{4.6}$$

As dicussed before, spatial coherence was introduced by Cheynet using Davenport's model in the form of an exponential function.

$$Coh = exp(\frac{-\sqrt{DecY_u^2 + DecZ_u^2}\, f(n)}{\bar{U}}) \tag{4.7}$$

where

$$DecY = C_u^y \cdot \delta y \quad DecZ = C_u^z \cdot \delta z \tag{4.8}$$

and C_u^y and C_u^z are decay coefficients assumed to be 10 for regular extreme winds and dy and dz are spatial distances between nodes in respective y (lateral) and z (vertical) direction.

Since no information was found on spatial coherence in hurricane winds, a matrix was constructed applying as-needed coherence between nodes following Equation **??** specified before.

Three wind histories are presented in Figures 4.1 through 4.3, for the Kaimal, Yu and Li spectra respectively, more specifically the turbulence component. A reference wind speed of $10[m,s{-}1]$ at $10[m]$ reference height was used with a 12[%] turbulence intensity, at a $119[m]$ hub height. Kaimal always includes coherence, while for the hurricane spectra, although, coherence in this particular case is assumed equal. The assumed roughness lengths z_0 were assumed 0.0002 and 0.006 for Kaimal and the hurricane spectra respectively. Note that only the wind histories for a single node are presented, while in reality a wind history for each single node is generated.

From these histories, the effect of the different spectra can already be seen. In the Yu wind history in Figure 4.2, there's a considerably smaller contribution of the higher frequencies, noticeable through the less erratic changes in wind gust, reflecting the smaller energy and thus smaller amplitude of high frequency wind components.

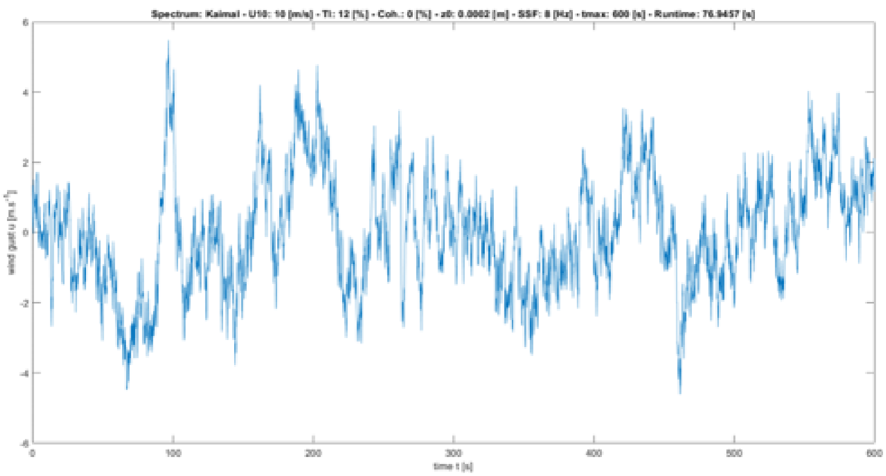

Figure 4.1: Example of a $10[min]$ Kaimal Spectrum Wind History (TI: 12 [%], SSF: 8 $[Hz]$, z_0: $0.0002[m]$)

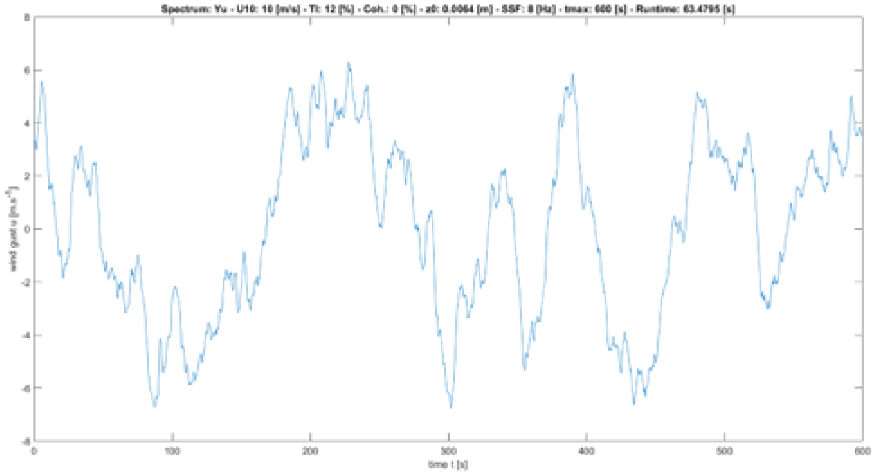

Figure 4.2: Example of a 10[min] Yu Spectrum Wind History (TI: 12 [%], SSF: 8 [Hz], z_0: 0.006[m])

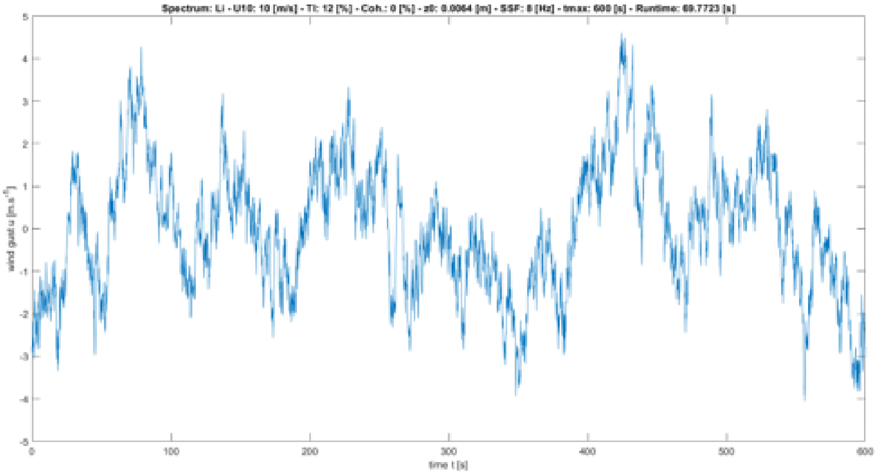

Figure 4.3: Example of a 10[min] Li Spectrum Wind History (TI: 12 [%], SSF: 8 [Hz], z_0: 0.006[m])

4.1.2. Wind Model Validation

To validate the workings of the wind generation model, a number of scenarios was run to determine if the model behaved as was to be expected. An overview is presented in Table 4.1.

Table 4.1: Validation scenarios of the wind generation model

Seed [-]	1	3	5		
SSF [Hz]	1.0	3.0	5.0	7.0	10.0
T.I. [%]	10.0	12.0	15.0		
C_i^i [-]	1	5	10	20	

Implementing pseudo-randomness rather than complete randomness into the generation of the wind histories, more specifically in the selection of an arbitrary phase value ϕ_n (Equation 4.1), allows to recreate previously generated wind signals in order to re-evaluate its effects. It ensures reproducibility of the results. When looking into the results of the seed selection, shown in Appendix B Figure B.1, three distinct signals can be seen, confirming pseudo-randomness was implemented correctly.

Choosing a proper Spectrum Sampling Frequency (SSF) has an important effect on further calculations. The higher the sampling frequency chosen, the more accurate the spectrum is captured in the generated signal (Appendix B Figure B.2). Indefinitely increasing this sampling frequency however, causes the computational time to increase drastically (as shown in Table 4.2) without significantly increasing the accuracy of the wind signal (which is not all that clear from the same table); a phenomenon in numerical modelling referred to as convergence. This has an effect both in the generation of the time signal first and secondly, later on when evaluated by the ODE solver in the Blade Model (ref. Sec. 4.2). A good balance between numerical accuracy and computational time needs to be maintained. Therefore it was chosen to use a SSF of $10[Hz]$.

Table 4.2: Convergence of Wind Histories for increasing Spectrum Sampling Frequency

SSF $[Hz]$	**Runtime** $[s]$	**Gust** u_x $[m.s^{-1}]$	**Accuracy** [%]
1	1.68	-3.42	-
3	9.51	-3.51	-2.6
5	25.19	-3.76	-7.2
7	43.57	-3.12	17.0
10	83.98	-3.13	-0.3

Turbulence was validated for all three spectra in Figures B.3, B.4 and B.5. All show the same expected trend, increasing the turbulence intensity changes the amplitude of the signal but not its shape.

Lastly, the implementation of the coherence was checked. Since no values are known regarding hurricane coherence, any positive value can be chosen, a zero coherence decay coefficient indicating full coherence at all nodes meaning that there is a perfect spatial relation between the different wind signals at different nodes i.e. each wind signal is completely dependent and equal for each node. This is shown in Figures B.6, B.7 and B.8 where for full coherence complete overlap of the signals at the first three nodes are shown, indicating the implementation of the coherence is correct.

4.2. Blade Model

A finite-element model of a single blade developed in [21] was adopted to evaluate loads and load effects. Structural vibrations are assumed small allowing the model to be geometrically linear with structural properties based on the conceptual 10MW DTU turbine [9] and (Ref. Appendix C).

Steady aerodynamics were assumed, i.e. no flow separation is occurring, implying forces are developed instantaneously along the blade. More simply stated, this means changes in wind speed translate to an immediate change in aerodynamic forces. Furthermore, a no flow separation assumption, means the and changes in the angle of attack α are assumed to remain relatively small.

4.2.1. Blade Element Theory

The Blade Element Theory is a method to analytically determine aerodynamic forces based on blade section geometry i.e. airfoil properties. These forces acting on consecutive differential elements of the blade are calculated based on the relative velocity experienced by the blade. The most important assumption made by the theory states that the behaviour of an individual element is not affected by other elements along the blade. The forces acting on the blades are thus fully governed by the lift and drag properties of the airfoil [22]. The airfoil properties along the blade length are not stated by DTU's report [9] but assuming that the airfoil is symmetrical, furthermore adopting the thin plate analogy, the lift coefficient C_l can then be expressed by Equation 4.9a while the assumption of attached flow conditions means pressure drag is negligible and the only contributing factor to drag is due to friction and the drag coefficient can be defined according to Equation 4.9b.

$$C_l(r) = 2\pi \sin(\alpha(r)) \tag{4.9a}$$
$$C_d \approx 0.02 \tag{4.9b}$$

The blade is divided into N sections, each elements containing discretised distributed mass and stiffness properties, sectional properties in the form of blade twist and aeroelastic properties according to Equations 4.9a and 4.9b. Figure 4.4 shows a cross-section of a blade element. The resultant flow velocity $W(r,t)$ experienced by a blade section distance r removed from the hub, consists of two components: an incoming, out-of-plane wind field component $U_\infty(r,t)$ and the in-plane velocity $V(r,t)$ due to the blade's rotation

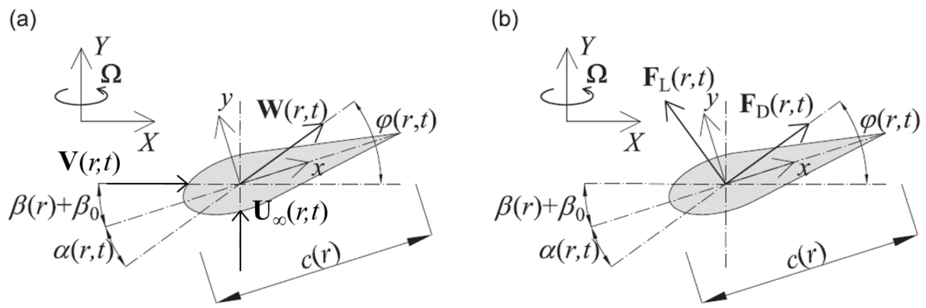

Figure 4.4: (a) Velocity and (b) force diagram at the rotor plane for a rotating wind turbine blade [21]

resulting in a normal, tangential and resultant velocity at a each blade element. In addition to the incoming wind, the blade also experiences a velocity component $\dot{u}$ due to its own motion such that the velocity components become

$$U = U_\infty - \dot{u}_{OP}, \quad V = \Omega r - \dot{u}_{IP}, \quad W = \sqrt{U^2 + V^2} \tag{4.10}$$

with u_{OP} and u_{IP} denoting the out-of-plane and in-plane deflections caused by lift and drag forces and the 'dot' ($\dot{u}$) signifying the time-derivative of the respective deflections. The two components of the relative wind speed W introduce two static aerodynamic forces as indicated in (b) in Figure 4.4: A lift force dF_L, defined perpendicular to the relative flow and a drag force dF_D, defined parallel to the relative flow, and expressed according to

$$\delta F_L(r) = \frac{1}{2}\rho c(r) C_l(\alpha) W(r)^2 = \rho c(r)\sin(\alpha(r)) W(r)^2 \tag{4.11a}$$
$$\delta F_D(r) = \frac{1}{2}\rho c(r) C_d(\alpha) W(r)^2 \tag{4.11b}$$

where $c(r)$ is the chord length of the blade section, $C_l(\alpha)$ and $C_d(\alpha)$ are lift and drag coefficients as a function angle of attack $\alpha(r,t)$. From the same diagram, the relation between inflow angle $\phi(r,t)$, (local) blade twist $\beta(r)$, (global) blade pitch β_0 and angle of attack $\alpha(r,t)$ can be found as

$$\alpha = \phi - (\beta_i + \beta_0), \quad \tan\phi = \frac{U}{V} \tag{4.12}$$

Assuming the blades are stationary ($\Omega = 0$), this simplifies to

$$W = \sqrt{(U_\infty - \dot{u}_{OP})^2 + (\dot{u}_{IP})^2} \tag{4.13}$$

Furthermore, adopting a $\beta_0 = 90°$ pitch angle due to the turbine being in non-operational conditions [9].

4.2.2. Analysis Procedure

The entire analysis procedure and accompanying derivations are described in detail in [21] and thus, for the sake of brevity, will not be reproduced in full.

All n $(N+1)$ nodes comprising the model, shown in Figure 4.5, have 4 degrees of freedom: 2 deflections (u, v) and 2 rotations (θ, ϕ).

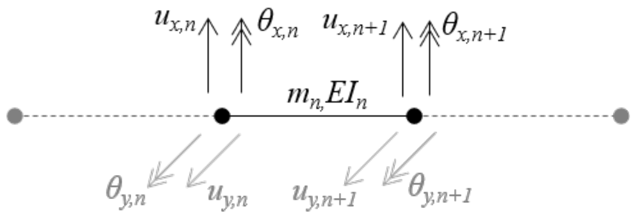

Figure 4.5: 8 Nodal degrees of freedom for blade element n

The system is described by two coupled nonlinear fourth-order partial differential equations 4.19a where $(\mathbf{M}, \mathbf{K}) \in \mathbb{R}^{4N\times 4N}$, $\mathbf{u_i} \in \mathbb{R}^{4N}$ and $\mathbf{F_{i,n}} \in \mathbb{R}^{4N\times 1}$.

$$\mathbf{M}(r)\ddot{\mathbf{u}}_{\mathbf{i,n}}(r,t) + \mathbf{K}(r,t)\mathbf{u}_{\mathbf{i,n}}(r,t) = \mathbf{F}_{\mathbf{i,n}}(r,t), \quad \mathbf{u}_{\mathbf{i,n}} = [u_{i,n}, \theta_{i,n}]^T, \quad i = x, y;\, n = 1 \ldots N \tag{4.14}$$

The differential equations are coupled via the off-diagonal terms in the stiffness matrix $\mathbf{K}$ and are nonlinear through the effect of the blade's motion on the blade forces. With the full force vector $\mathbf{F_{i,n}}(r,t)$ written as:

$$\begin{bmatrix} F_1(t)_{IP} \\ M_1(t)_{IP} = 0 \\ F_1(t)_{OP} \\ M_1(t)_{OP} = 0 \\ \vdots \\ F_n(t)_{IP} \\ M_n(t)_{IP} = 0 \\ F_n(t)_{OP} \\ M_n(t)_{OP} = 0 \end{bmatrix} \tag{4.15}$$

and Equations 4.16a and 4.16b referring to the, albeit simplified, instantaneous out-of-plane and in-plane nodal forces respectively at nodes 1 to n. No external bending moments are applied thus can be set to zero.

$$\mathbf{F}(r,t)_{OP} = \mathbf{F}_D(r,t) + \mathbf{F}_L(r,t) = \frac{1}{2}\rho c(r)(U_\infty - \dot{u}_{OP})^2)\Big(C_d(\alpha,r) + C_l(\alpha,r)\Big) \tag{4.16a}$$

$$\mathbf{F}(r,t)_{IP} = \mathbf{F}_D(r,t) + \mathbf{F}_L(r,t) = \frac{1}{2}\rho c(r)(-\dot{u}_{IP})^2)\Big(C_d(\alpha,r) + C_l(\alpha,r)\Big) \tag{4.16b}$$

The analysis is based on the modal reduction of the system; the forced vibrations of the system are described by a superposition of n eigenmodes $\mathbf{E} \in \mathbb{R}^{N\times N}$ multiplied by an unknown time-vector $q_n(t)$ [15, 21]

$$\mathbf{u}(t) = \sum_{i=1}^{n} \hat{\mathbf{u}}_i A_i sin(\omega_i t + \phi_i) = \sum_{i=1}^{n} \hat{\mathbf{u}}_i q_i(t) = \mathbf{E}_i \mathbf{q}_i(t) \tag{4.17}$$

where the eigenmodes $\mathbf{E}_i$ are found as a solution to the eigenvalue problem using a finite-element model of the blade:

$$\{\mathbf{K}(r) - \omega_i^2 \mathbf{M}(r)\}\mathbf{E}_i(r) = \mathbf{0} \tag{4.18}$$

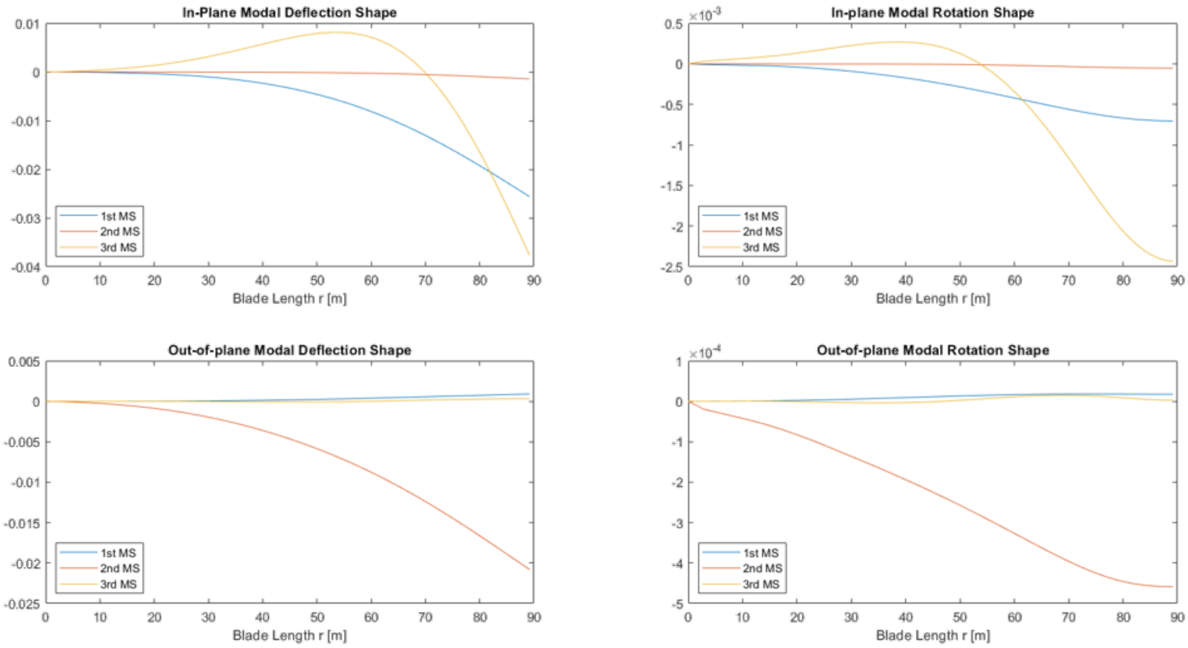

Figure 4.6: First three blade modeshapes for deflection and rotation In-plane and Out-of-Plane

ω_n and $\mathbf{E}_n(r)$ represent the nth natural frequency and the mode respectively. Solving the eigenvalue problem using Matlab's *eig*-algorithm results in finding the natural frequencies (Table 4.3) and the accompanying modeshapes (Figure 4.6).

Table 4.3: Comparison between Model Natural Frequencies and DTU 10MW identified Natural Frequencies

Mode	Model $\omega_n [Hz]$	DTU 10MW ω_n $[Hz]$	Error [%]	*Description*
6	0.609	0.6339	-3.9281	*1st Blade Collective Flap*
7	0.9028	0.9220	-2.0824	*1st Blade Assymetric Edgewise*
11	1.7096	1.7633	-3.0454	*2nd Blade Collective Flap*

Table 4.3 provides a first way to validate the numerical model (Ref. 4.2.3). If the natural frequencies of the model match those found for the DTU reference turbine, one can say that the structural properties are modelled accurately and thus the dynamic behaviour captured accurately within the boundaries of the made assumptions. For a system with N degrees of freedom, N natural frequencies can be distinguished. Table 4.3 shows that the natural frequencies are systematically underestimated with an average error of 3% indicating either an underestimation of stiffness or overestimation of mass. This error could not be further reduced and was deemed acceptable in further calculations.

Use of the orthogonality property, allows to increase numerical efficiency, by premultiplying with the transposed eigenvector $\mathbf{E}^T$, turning Equation 4.19a into a set of ordinary differential equation which remain coupled through the force vector:

$$\mathbf{E}^T\mathbf{M}(r)\mathbf{E}\ddot{\mathbf{q}}(t) + \mathbf{E}^T\mathbf{C}(r)\mathbf{E}\dot{\mathbf{q}}(t) + \mathbf{E}^T\mathbf{K}(r)\mathbf{E}\mathbf{q}(t) = \mathbf{E}^T\mathbf{F}(r,t) \tag{4.19a}$$

$$\mathbf{M}^*(r)\ddot{\mathbf{q}}(t)\mathbf{C}^*\dot{\mathbf{q}}(t) + \mathbf{K}^*\mathbf{q}(t) = \mathbf{E}^T\mathbf{F}(r,t) \tag{4.19b}$$

which can be solved numerically using Matlab's *ODE* solver to find $q(t)$.

4.2.3. Blade Model Validation

A second way to validate the blade model, beside the natural frequency validation discussed before, is to evaluate its static deflection (Ref. Table 4.4). To that end, a uniform, constant wind speed was considered, acting on a horizontal blade with non-uniform blade properties. Given the linearity of the model, twice the force should result in a deflection twice as large. Knowing the quadratic relation between force and wind speed, the deflection should increasing with a factor of 4 as wind speed doubles.

Table 4.4: Static Numerical Deflections and Forces for TI = 0[%], $z_0 = 0.0002$[m]

	Out-of-Plane		In-Plane	
U_{ref} $[m.s^{-1}]$	$x_{s,n}$ $[m]$	$F_{x,n}$[kN]	$y_{s,n}$ $[m]$	$F_{y,n}$ $[kN]$
5	0.0227	160.04	-0.0083	-2.22
10	0.0909	640.14	-0.0332	-8.88
20	0.3635	2560.58	-0.1328	-35.53
40	1.4541	10242.30	-0.5310	-142.13

A few things can be determined from the results presented above. Doubles the wind speed does in fact result in the increase of deflections and forces with a factor 4, confirming the linearity of the model. Out-of-plane deflections and forces are considerable larger than the in-plane deflections. When pitching the blades to 90° the larger forces acting on the blades are due to aerodynamic drag resulting in out-of-plane motions. Due to the blade twist, however, there will always a lift component generated albeit only a fraction of the size the drag force. The negative value for the In-Plane force indicate that the blade is pushed downwards.

These results can be compared to a simple cantilever beam with constant, mean properties as defined according to Table 4.5. The results of which are shown in Table 4.6 where lift and drag can be calculated simply by filling in Equations 4.11a and 4.11b. The lift coefficient is taken $C_L = 0$ with $C_L = \pi \sin(\beta_r + \beta_0)$ where $(\beta_r + \beta_0)$ is assumed 90[°] along the entire blade length and C_D can be assumed 0.02 for a pitched blade [21].

Table 4.5: Mean Cantilever Beam Properties for Static Deflection and Forces

air density ρ $[kg.m3]$	1.25
blade length l $[m]$	89.2
chord length c $[m]$	3.93
C_D [-]	0.02
C_L [-]	0
Ei_{xx} $[N.m^2]$	$5.73\ 10^8$
Ei_{yy} $[N.m^2]$	$1.57\ 10^{10}$

Table 4.6: Static Analytical Deflections and Forces for a cantilever beam

	Out-of-Plane		In-Plane	
$x_{s,a}$ $[m]$	$F_{x,a}$ $[N]$	$y_{s,a}$ $[m]$	$F_{y,a}$ $[N]$	
5	0.0256	165.57	0	0.00
10	0.1024	662.29	0	0.00
20	0.4096	2649.15	0	0.00
40	1.6385	10596.60	0	0.00

Even with the assumed mean properties, these results are similar to the ones found numerically, indicating a good validity of the applied model for the static case.

Lastly, to check the assumption of attached flow conditions, the magnitude of the angle of attack α is checked for the highest wind speed conditions (T10000). The angle of attack along the blade is presented in Figure 4.7. Typically values of 10-12[°] are used for small angles of attack, the maximum value here is 14.58° which is pushing that limit of the small angle of attack approximation. Nevertheless, it was considered acceptable within the other inaccuracies of the model.

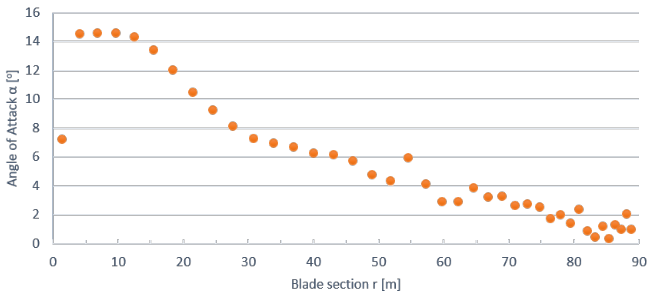

Figure 4.7: Variation of the Angle of Attack α along the blade for the highest wind speed (T10000)

5 Simulations & Results

5.1. Simulations

To evaluate the performance of a single blade of DTU's reference turbine, 3x14 simulations were run, detailed in Table 5.1, representing all 14 ten-minute averaged wind speeds including nine design return periods and the lower limit of each one of the five hurricane categories for each of the three spectra. Simulations were run for a duration of $660[s]$, neglecting the first $60[s]$ thus removing the transient response of the blade from the results. An equal amount of coherence was assumed for Kaimal, Yu and Li spectra by adopting a decay coefficient $C_i i$ equal to 10. In addition, a turbulence intensity TI of 12[%]] was selected. Furthermore, a surface roughness length $z_0 = 0.0002$ and $z_0 = 0.006$ was chosen since they represent the typical value used for regular, extreme wind speed and the maximum value found for hurricanes, respectively. The latter hereby allowing calculations to be the most conservative given the relation between z_0 and the wind velocity profile. As discussed before, a stationary blade was assumed, with a pitch angle $\beta_0 = 90°$ and an azimuth angle of $0[°]$ i.e vertical, pointing upward).

The Kaimal case was chosen as the overall reference case, given its common application in the current industry standard, while *Rated* wind speed was selected since at this wind speed, for an operating turbine, blade forces (i.e thrust forces on the rotor) are highest.

Table 5.1: Simulations to compare regular extreme-wind and hurricane-wind blade responses

	U_{10} $[m.s^{-1}]$	T [years]
1	11.4	Rated
2	30.6	[H1
3	36.5	10
4	40.1	[H2
5	44.9	25
6	46.8	[H3
7	50.1	50
8	54.5	100
9	55.4	[H4
10	58.2	200
11	66.9	[H5
12	69.5	1000
13	72.5	2000
14	78.7	10000

In the following sections, the use of the term 'forces' refers to both the root shear forces and root bending moment if not explicitly defined; response(s) refers to forces, bending moments and deflections; ratio's refer to either the relative magnitude of the hurricane spectra response to the Kaimal response or to any response relative to its reference case.

5.2. Blade Tip Deflections, Shear Forces & Bending Moments

The full results of the simulations specified in Table 5.1 are given in tabulated form in Table D.1 through D.6 in Appendix D for the respective spectra and out-of-plane (OP) and in-plane (IP). They are also presented in Figures 5.1, 5.3 and 5.5 for the deflection, shear forces and bending moments respectively. Since we are not particularly interested in the absolute values, yet the relative magnitude of the internal forces and bending moments and displacements, the ratio's of the blade responses are presented in Figures 5.2, 5.4 and 5.6.

The resultant deflections δ, forces F and bending moments M (in- and out-of-plane) (discrete time traces) were assumed to be normally distributed in time, hence, after statistical processing, resulting in 4 values: a 95%, a mean or 50% and a 5% characteristic exceedance value of the responses, and a standard deviation $\sigma_{(\delta,F,M)}$. The mean value reflects the 'mean' behaviour of the blade i.e. the response to the mean component of the wind while the 5% and 95% value reflect the turbulent behaviour i.e. the variation around the mean response. These values refer to a single statistical value of which can be said that this value is not exceeded by that percentage of forces and deflections i.e. the 95% value will only be exceeded 5% of the time (in this case in the simulated ten-minute time window). This 95% value is often used as the characteristic value for design calculations, either multiplied with or divided by a safety factor (for loads and material strength respectively) to arrive at the actual design values.

Firstly and most importantly, looking at the response ratio's, they clearly show a trend indicating the hurricane spectra responses are a factor $\gamma = 1.2$ larger than the Kaimal response. This means that for equal wind speed conditions, the blade response is higher for the hurricane spectra as compared to the Kaimal extreme winds. Given the definition of these load cases however, these results still contain the added effect of the roughness length z_0 as this value was not kept equal across spectra in this comparison.

Furthermore, the tabulated data in Appendix D shows, Tables D.7 through D.10, that on average, the Yu responses are marginally larger (2-3%) than the Li responses. Moreover, the respective OP and IP response ratios within the same spectrum are slightly smaller, about 10%, smaller for the IP response compared to the OP response. That is the case for all three considered spectra.

Secondly, the results also reflect the non-linearity system. Linearity would imply Equation 5.1 to be held for all simulations i.e. forces (F, M) are proportional to wind velocity (U^2) and deflections are linearly proportional on the forces (Ref. Equations 4.11a and 4.11b).

$$\frac{U_{i+1}}{U_i} = \sqrt{\frac{F_{i+1}}{F_i}} = \sqrt{\frac{\delta_{i+1}}{\delta_i}} \tag{5.1}$$

Verifying this statement using Figures 5.7, 5.8 5.9 seem to be showing a linear relation. The tabulated values (Ref. Tables D.11 through D.16) in Appendix D) help clarify that the relation is in fact non-linear.

As wind speed increases, so does the blade response (blade deflection, velocity and acceleration) which amplifies the loading on the blade by increasing its relative wind speed, resulting in this non-linear relation. This non-linear effect increases with an increasing wind speed as the difference between the linear ratios and actual ratios becomes relatively larger.

In addition to the established trend of the response ratios being smaller for the IP response relative to the OP response, the linearity check shows the same behaviour where the non-linearity ratios are relatively smaller compared to the OP ratios (Ref. Tables D.11 through D.16).

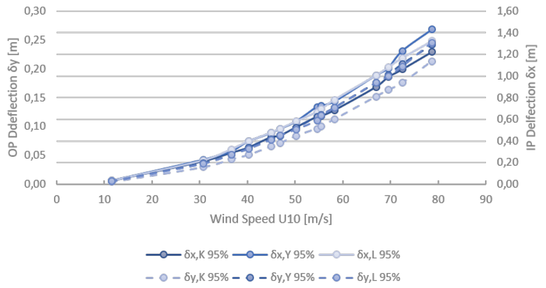

Figure 5.1: Blade Deflections (δ) for the in Table 5.1 presented Simulations

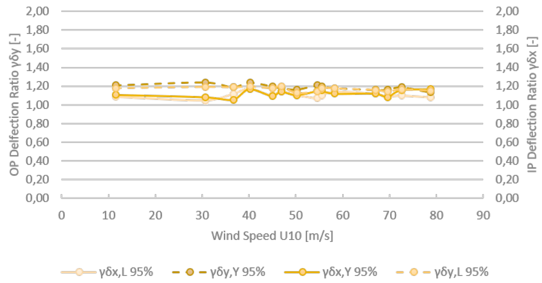

Figure 5.2: OP and IP Deflection Ratios for Yu($U_{10}(n)$) and Li($U_{10}(n)$) vs. Kaimal($U_{10}(n)$)

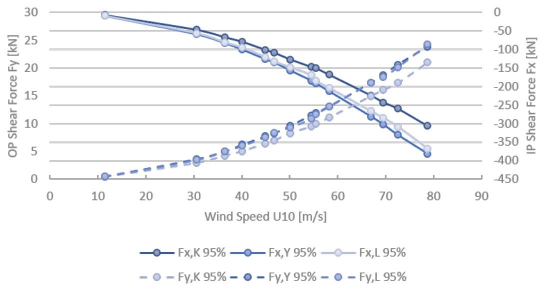

Figure 5.3: Shear Forces (F) for the in Table 5.1 presented Simulations

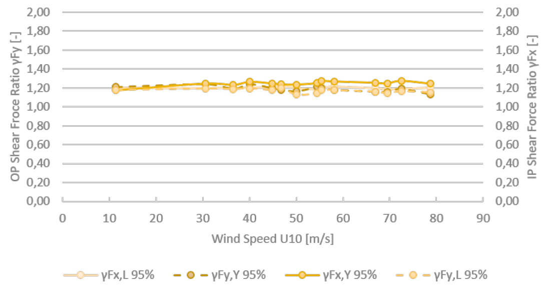

Figure 5.4: OP and IP Shear Force Ratios for Yu($U_{10}(n)$) and Li($U_{10}(n)$) vs. Kaimal($U_{10}(n)$)

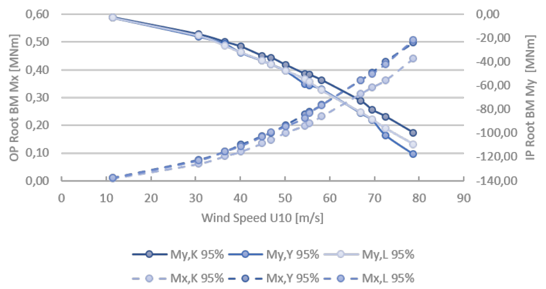

Figure 5.5: Bending Moments (M) for the in Table 5.5 presented Simulations

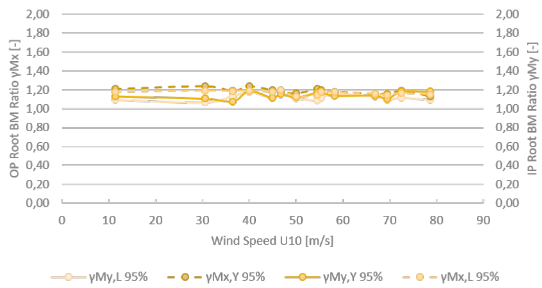

Figure 5.6: OP and IP Bending Moment Ratios for Yu($U_{10}(n)$) and Li($U_{10}(n)$) vs. Kaimal($U_{10}(n)$)

It should be noted again that both hurricane spectra could not be scaled to hub height. In the case of Kaimal, extrapolating the turbulence spectrum to hub height, shifts the turbulent energy towards lower normalised frequencies, increasing the total turbulent energy. Certainly an increase in turbulent energy will also be the case for the hurricane spectra thereby affecting the simulation findings. This can both positively and negatively affect the found load ratios depending on which direction the turbulent energy shifts towards. Especially when energy gets 'redistributed' towards the natural frequencies of the blade leading to an increased dynamic response of the system thereby also increasing the non-linear response effects.

Nevertheless, a turbine blade subjected to hurricane winds, assuming an increased roughness length results in an larger response of the system which needs to be taken into account in further design of the blade.

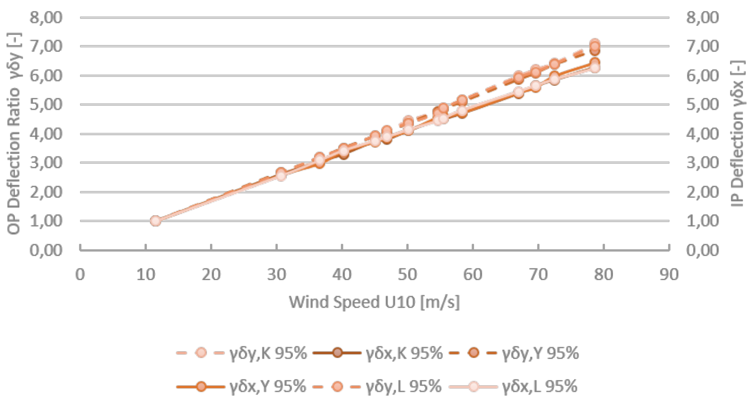

Figure 5.7: Model Deflection (δ) Linearity Properties

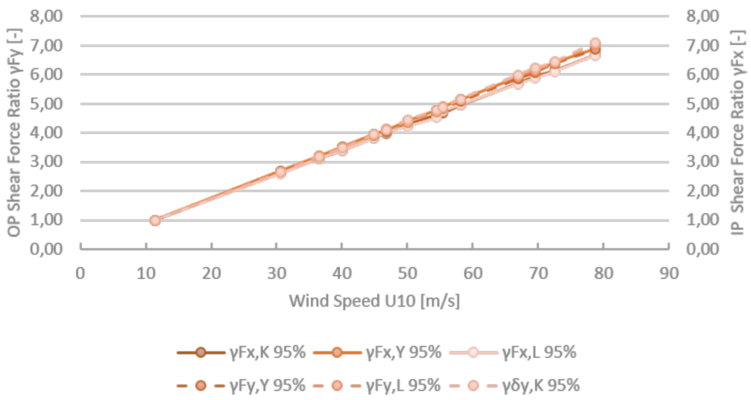

Figure 5.8: Model Shear Force (F) Linearity Properties

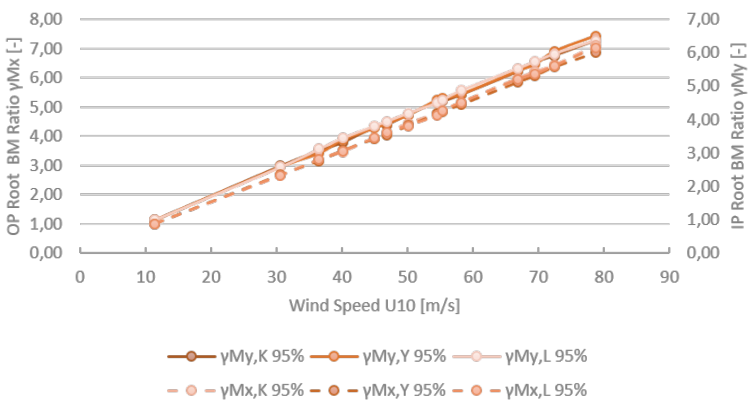

Figure 5.9: Model Bending Moment (M) Linearity Properties

Evaluating the response of the blade in the frequency domain by means of the Fourier transformation of the IP and OP deflection shows that the response is in fact comprised of three frequencies. This is indicated by the three peaks in the spectrum in Figure 5.10. Actually four frequency peaks can be distinguished if one considers the zero frequency component which reflects the mean components of the response. These three frequencies coincide with each one of the eigenfrequencies indicating that the response is a summation of all three modeshapes. The

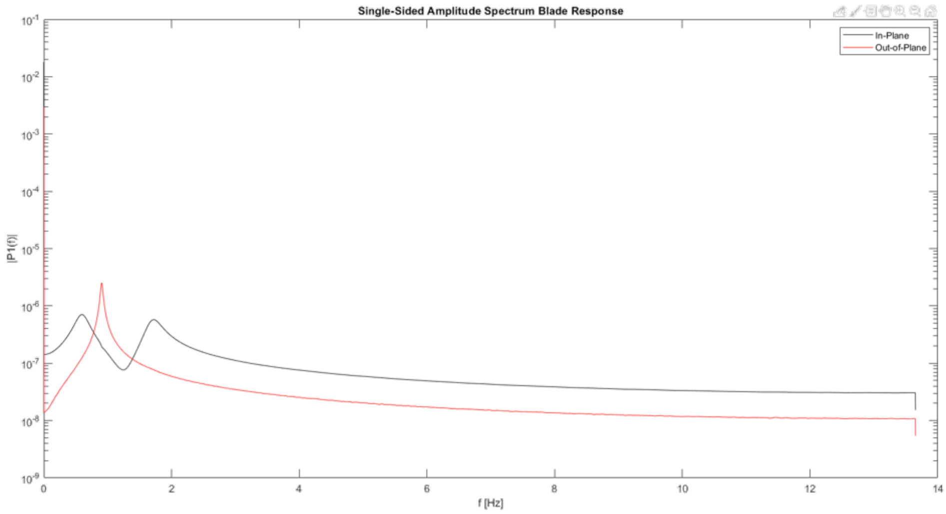

Figure 5.10: Fourier Analysis of the Dynamic IP and OP Blade Deflection Response for the Kaimal Rated Wind Speed

The unknown functions with which the eigenmodes are multiplied can be found in Figure 5.11.

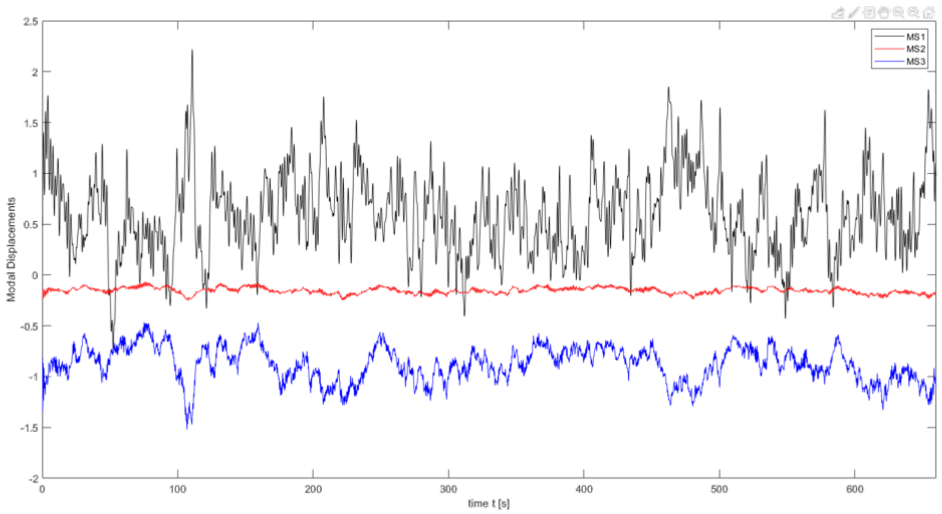

Figure 5.11: Unknown Time Functions for Modal Analysis Approximation of the Kaimal Rated Wind Speed Load case

5.3. Sensitivity Analysis

Since information on hurricane wind parameters is limited, an assumption was made as to which value was used in the calculations above. A sensitivity analysis was done to see how and to which degree these parameter choices affected the simulation results.

To save computational time, all sensitivity analysis simulations were run for 330[s] neglecting again the first 30[s] and removing the transient response. A wind speed of 54.5[$m.s^{-1}$] was chosen as this represented the 100[year] return period wind speed. All simulation were run for a blade AA of 0[°].

Detailed simulation results can be found in Appendices E, F and G for the roughness length, coherence and orientation simulations respectively.

5.3.1. Roughness Length

Two different comparison were made in order to say something useful about how the choice of roughness length (RL)z_0 affects the loading of the blade. The full absolute simulation results can be found in Appendix E, Tables E.1- E.6 and are graphed in Figures 5.12, 5.14 and 5.16.

The six RL specified in Table 5.2 were selected for the RL sensitivity analysis. Roughness lengths vary from the 0.0002 to 0.0128, spanning the range of extreme, regular wind values to a value slightly larger than the value assumed for the hurricane spectra simulations.

R.L. z_0 [m]	0.0002	0.0004	0.0008	0.0016	0.0032	0.0064	0.0128

Table 5.2: Rouhgness Lengths z_0 selected for the Sensitivity Analysis

The sensitivity analysis consists of two steps. First, the simulation results for the hurricane spectra are compared to the corresponding Kaimal simulation results i.e. the ratios of Yu, Li($z_0(n)$) to Kaimal($z_0(n)$) are calculated. These results are given in Tables E.7 through E.10 and presented in Figures 5.12, 5.14 and 5.16. Their respective ratios are shown in Figures 5.13, 5.15 and 5.17.

Where there was a difference identified in blade response given the base load cases presented in Sec. 5.2, the response ratios now reduce to $\gamma_{\delta,F,M)} = 1$. This means that for the established base calculations the difference in response can be attributed to the difference in roughness length.

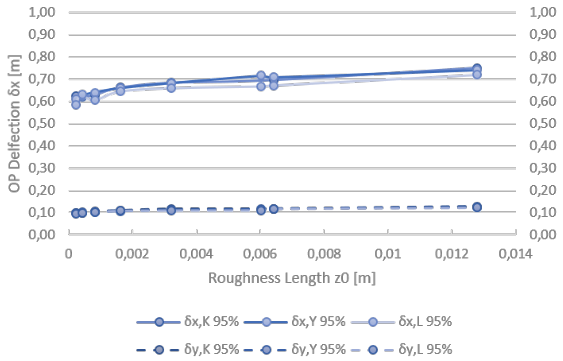

Figure 5.12: Blade Deflections (δ) for the in Table 5.2 presented Roughness Lengths z_0

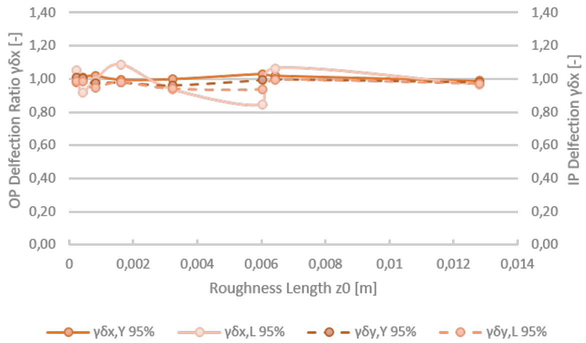

Figure 5.13: Blade Deflection Ratios (γ_δ) for the in Table 5.2 presented Roughness Lengths z_0 - Yu, Li($z_0(n)$) vs. Kaimal($z_0(n)$)

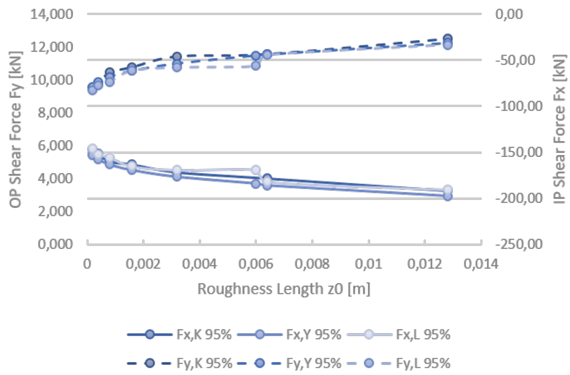

Figure 5.14: Root Shear Forces (F) for the in Table 5.2 presented Roughness Lengths z_0

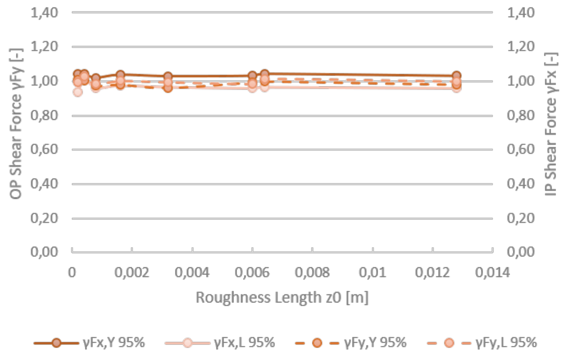

Figure 5.15: Root Shear Force Ratios (γ_F) for the in Table 5.2 presented Roughness Lengths z_0 - Yu, Li($z_0(n)$) vs. Kaimal($z_0(n)$)

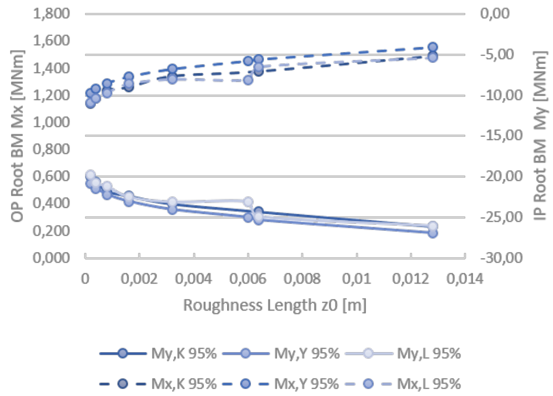

Figure 5.16: Root Bending Moments (M) for the in Table 5.2 presented Roughness Lengths z_0

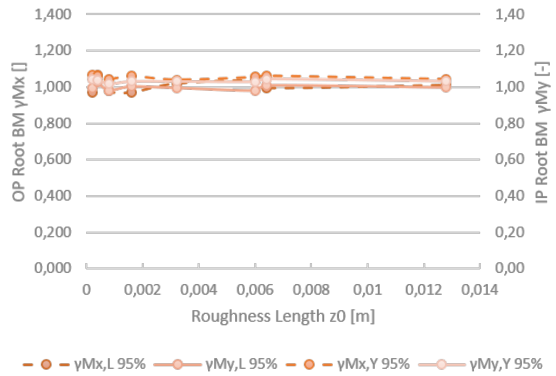

Figure 5.17: Root Bending Moments Ratios (γ_M) for the in Table 5.2 presented Roughness Lengths z_0- Yu, Li($z_0(n)$) vs. Kaimal($z_0(n)$)

Secondly, the simulation results for both hurricane spectra were compared to the initially assumed the reference spectrum case with a roughness length $z_0 = 0.0002$ and $z_0 = 0.006$ respectively yet for the T100 wind speed i.e. Yu, Li($z_0(n)$) vs. Yu, Li($z_0 = 0.006$ and Kaimal($z_0(n)$) vs. Kaimal($z_0 = 0.0002$). These results are given in Tables E.11 through E.16 and shown in Figures 5.18 to 5.20. They represent a true sensitivity in that they show how much the response varies (%) when the RL varies.

In the case of the Kaimal results, varying the RL from 0.0002 to 0.006 shows an increase in response of 20%. For the hurricane spectra, the increased response is smaller: 14-16%. This means that the response ratio of $\gamma = 1.2$ found before is due to a combination of spectral effects and choice of RL.

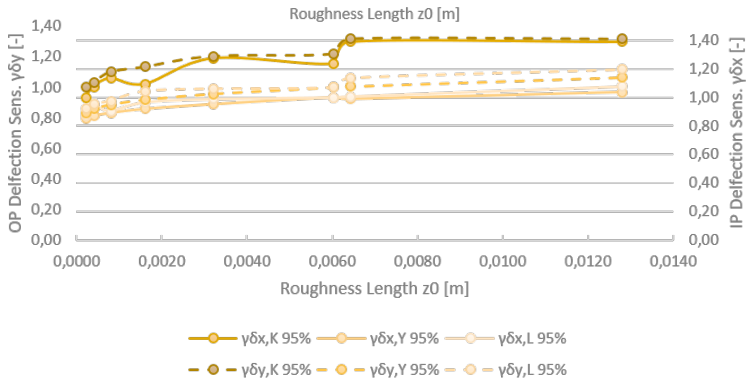

Figure 5.18: Blade Deflection Sensitivity (γ_δ) for the in Table 5.2 presented Roughness Lengths z_0 - Yu, Li($z_0(n)$) vs. Kaimal($z_0 = 0.0002$)

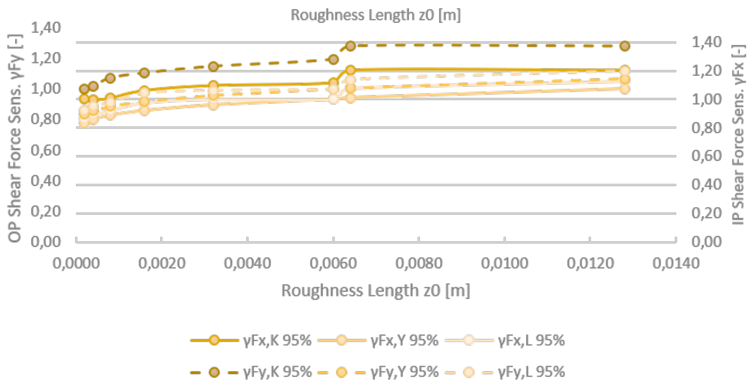

Figure 5.19: Shear Force Sensitivity (γ_F) for the in Table 5.2 presented Roughness Lengths z_0 - Yu, Li($z_0(n)$) vs. Kaimal($z_0 = 0.0002$)

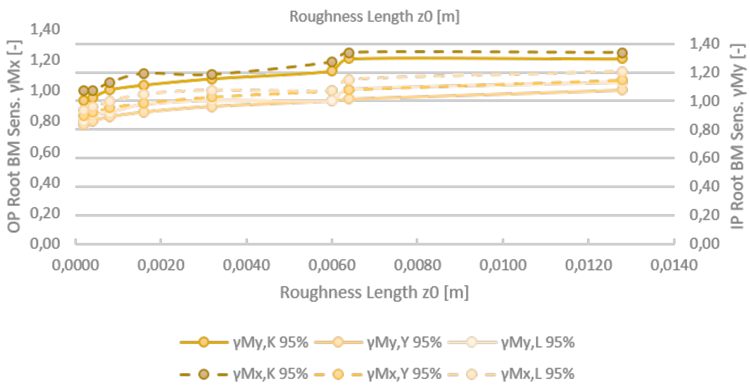

Figure 5.20: Bending Moment Sensitivity (γ_M) for the in Table 5.2 presented Roughness Lengths z_0 - Yu, Li($z_0(n)$) vs. Kaimal($z_0 = 0.0002$)

Larger values for the roughness lengths also have to be considered. The research done on actual hurricane wind measurements [16, 18] were limited to smaller hurricanes. Given that the roughness length is function of the wind speed, larger wind speed could therefor lead to even larger lengths. Which evidently would lead to even larger load effects.

5.3.2. Coherence

To investigate in the sensitivity towards coherence, the same methodology applied for the RL sensitivity was applied as well. A number of coherence decay coefficients were selected for this purpose and are presented in Table 5.3. The full tabulated numerical results can be found in Appendix F in Tables F.1 to F.6 and are presented in Figures 5.21, 5.23 and 5.25 respectively for deflections, shear forces and bending moments.

C_{ii} [-]	5	10	15	25	50

Table 5.3: Coherence Decay Coefficients C_{ii} selected for the Sensitivity Analysis

Due to lack on detailed information on the definition of coherence in hurricane winds, as stated before, Equation 4.7 was used to define coherence in all spectral winds. According to this Equation as the decay coefficients C_{ii} become smaller the spatial coherence decays slower in space essentially increasing the effect the wind at a certain point has on the wind speed in different point in space. This causes the wind speeds along the blade to be more 'averaged' out. In other words, for $C_{ii} = 0$ the wind speed at each point of the blade in space would be the same albeit different in time given wind turbulence. This more 'synchronous' loading of the blade is expected to result in a larger overall response.

The OP Kaimal (Table F.1) and OP Li results (Table F.5) verify this idea and show that for larger decay coefficients C_{ii} the response does indeed decrease, albeit only a small amount. This is contradicted by the other results showing either a nearly constant response in the case of OP Yu response (Ref. Table F.3) or an increased response with an increasing decay coefficient (IP Kaimal, Ref. Table F.1) - IP Yu, Ref. Table F.4 - IP Li, Ref. Table F.6).

Equation 4.7 also states that coherence is dependent on the frequency content of the turbulent wind and the wind speed with coherence. Coherence decreases for lower wind speeds (and thus consequently when decreasing) RL and for higher frequencies. Yu has higher energy in the lower frequency regions while Li has a higher energy content in the higher frequencies compared to the Kaimal Spectrum. Since both hurricane spectra results are generated using the same RL and thus the same result mean wind speed, the only difference is found in the frequency content of the wind and thus in the turbulent response. Yet both show similar response ratio ranging from $\gamma = 1.10$ to $\gamma = 1.2$ depending on the direction and spectrum.

The degree to which a change in coherence decay coefficient affects the response is thus smaller than the effect of a change in roughness length. This is confirmed by the second part of the coherence, presented in Figures 5.27, 5.28 and 5.29 sensitivity analysis showing an almost constant relation between an change of the decay coefficient and the change of the response in the range of decay coefficients studied in this thesis.

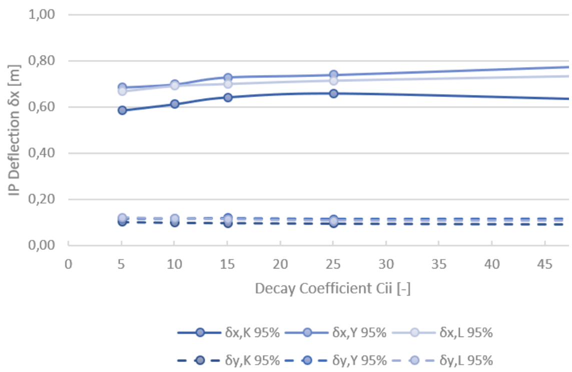

Figure 5.21: Blade Deflections (δ) for the in Table 5.3 presented Decay Coefficients C_{ii}

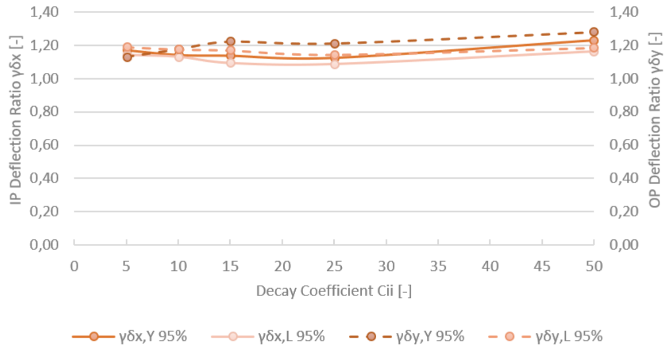

Figure 5.22: Blade Deflection Ratios (γ_δ) for the in Table 5.3 presented Decay Coefficients C_{ii}- Yu, Li($C_{ii}(n)$) vs. Kaimal($C_{ii}(n)$)

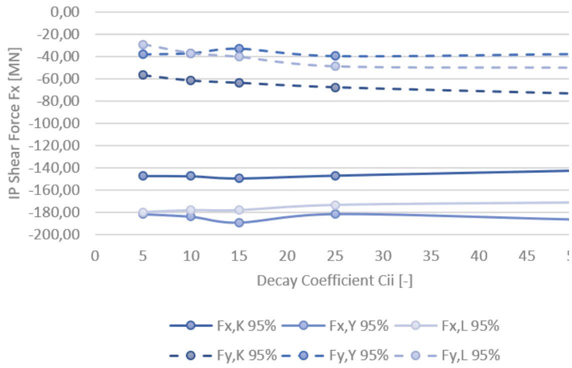

Figure 5.23: Root Shear Forces (F) for the in Table 5.3 presented Decay Coefficients C_{ii}

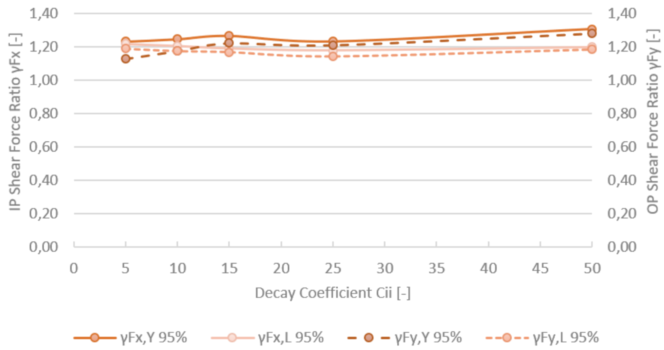

Figure 5.24: Root Shear Force Ratios (γ_F) for the in Table 5.3 presented Decay Coefficients C_{ii} - Yu, Li($C_{ii}(n)$) vs. Kaimal($C_{ii}(n)$)

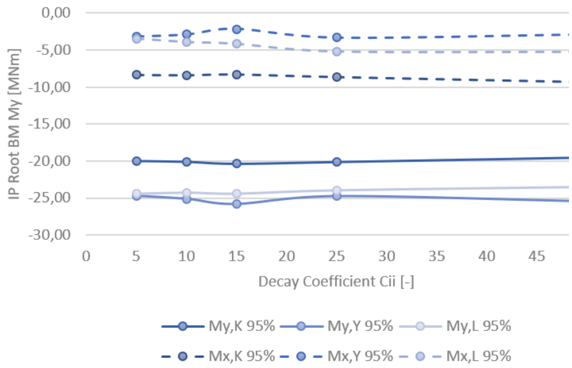

Figure 5.25: Root Bending Moments (M) for the in Table 5.3 presented Decay Coefficients C_{ii}

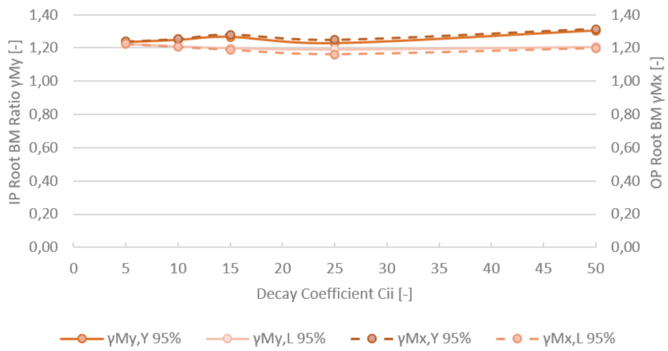

Figure 5.26: Root Bending Moments Ratios (γ_M) for the in Table 5.3 presented Decay Coefficients C_{ii}- Yu, Li($C_{ii}(n)$) vs. Kaimal($C_{ii}(n)$)

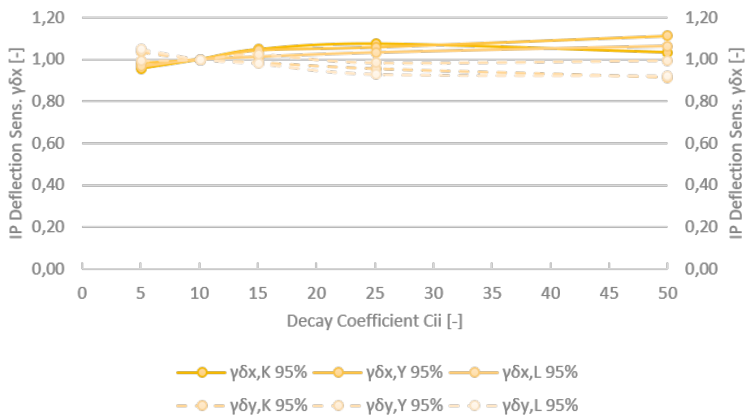

Figure 5.27: Blade Deflection Sensitivity (γ_δ) for the in Table 5.3 presented Decay Coefficients C_{ii}- Yu, Li($C_{ii}(n)$) vs. Kaimal($C_{ii} = 10$)

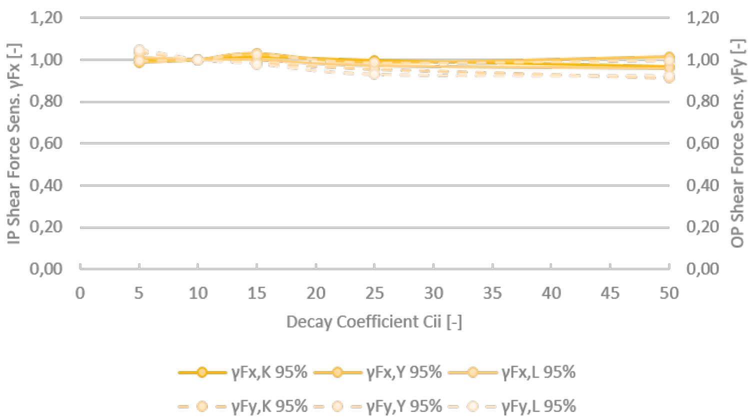

Figure 5.28: Shear Force Sensitivity (γ_F) for the in Table 5.3 presented Decay Coefficients C_{ii}- Yu, Li($C_{ii}(n)$) vs. Kaimal($C_{ii} = 10$)

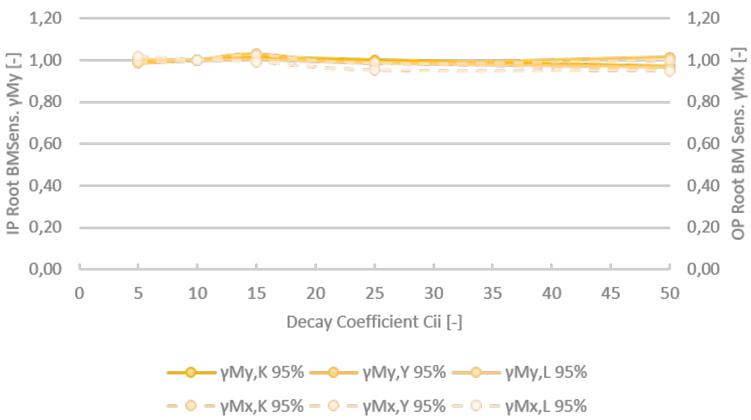

Figure 5.29: Bending Moment Sensitivity (γ_M) for the in Table 5.3 presented Decay Coefficients C_{ii}- Yu, Li($C_{ii}(n)$) vs. Kaimal($C_{ii} = 10$)

5.3.3. Blade Orientation

It's worth investigating what the effect is of changing the blade orientation on the response of the blade. Given the size of the blades, wind shear profile and magnitude of the wind speed itself, changing the orientation could have a significant effect on the response. Just like before, the fully detailed numerical results are given in Appendix G, Tables G.1 to G.6. They are also visualised in Figures 5.30, 5.32 and 5.34.

For all three spectra, a single blade was considered in at different positions in 15° intervals from the 0° angle (vertically pointing upward) up to a 180° (pointing downward) (Ref. Table 5.4). The resulting ratios of the responses are shown in Tables G.7 to G.10 and visualised in the Figures 5.31, 5.33 and 5.35 alongside the responses for the deflections, shear forces and bending moments respectively.

AA ϵ [°]	[0:15:180]

Table 5.4: Azimuth Angles (AA) ϵ [°] selected for the Sensitivity Analysis

Additionally, evaluating the response of the blade at different orientations, allows symmetry to be applied and the thrust force to be estimated on a three-bladed turbine. It can potentially indicate a configuration of the turbine to ensure a minimum amount of force is developed on the turbine should it interact with a passing hurricane.

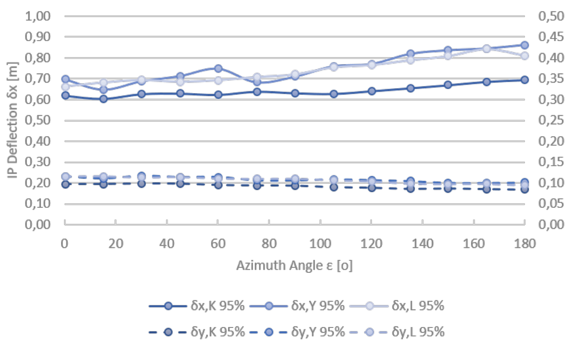

Figure 5.30: Blade Deflections (δ) for the in Table 5.4 presented AA $\epsilon(n)$

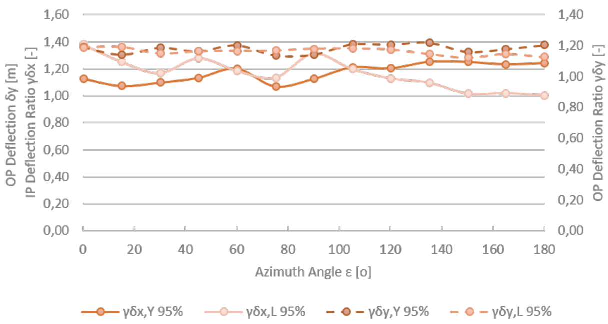

Figure 5.31: Blade Deflection Ratios (γ_δ) for the in Table 5.4 presented AA $\epsilon(n)$ - Yu, Li(AA $\epsilon(n)$) vs. Kaimal(AA $\epsilon(n)$)

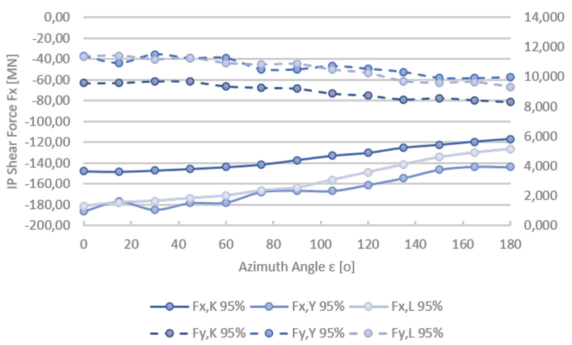

Figure 5.32: Root Shear Forces (F) for the in Table 5.4 presented AA $\epsilon(n)$

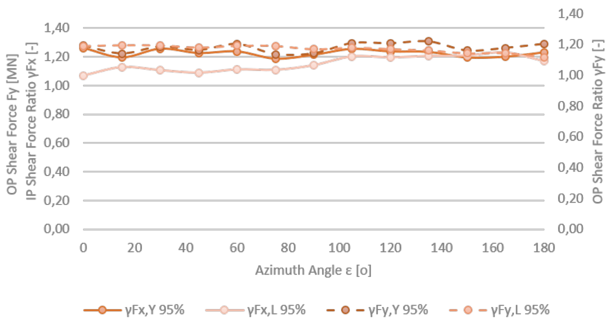

Figure 5.33: Root Shear Force Ratios (γ_F) for the in Table 5.4 presented AA $\epsilon(n)$ - Yu, Li(AA $\epsilon(n)$) vs. Kaimal(AA $\epsilon(n)$)

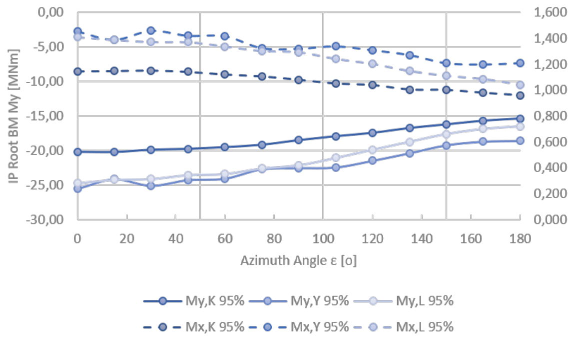

Figure 5.34: Root Bending Moments (M) for the in Table 5.4 presented presented AA $\epsilon(n)$

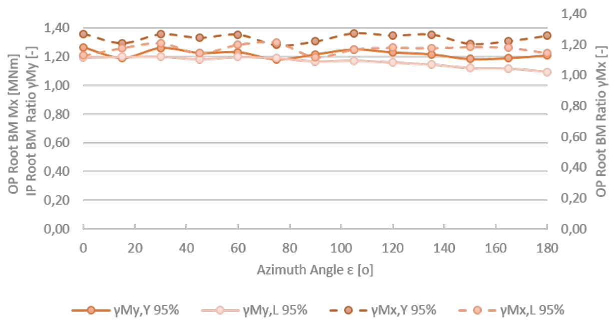

Figure 5.35: Root Bending Moments Ratios (γ_M) for the in Table 5.4 presented AA $\epsilon(n)$ - Yu, Li(AA $\epsilon(n)$) vs. Kaimal(AA $\epsilon(n)$)

Unsurprisingly, changing the orientation of a single blade has a considerable effect on the overall loads the blade reducing as much as -21% for the Kaimal spectrum, -23% for the Yu spectrum and -30% for the Li Spectrum. And while the OP deflections also present the expected result, the IP deflections do not. This is improbable given what is known from previous results; no additional effects explain why the deflections would suddenly increase in such a manner rather than decrease. The only possible explanation remaining is that there is an error or inaccuracy in the used blade model.

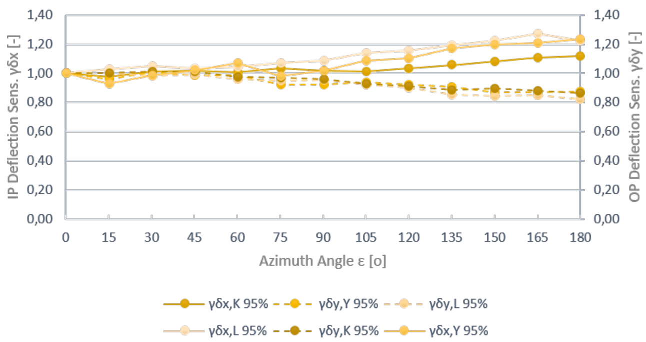

Figure 5.36: Deflection Sensitivity (γ_δ) for the in Table 5.4 presented Azimuth Angles ϵ - $\epsilon(n)$ vs. ϵ = 0°

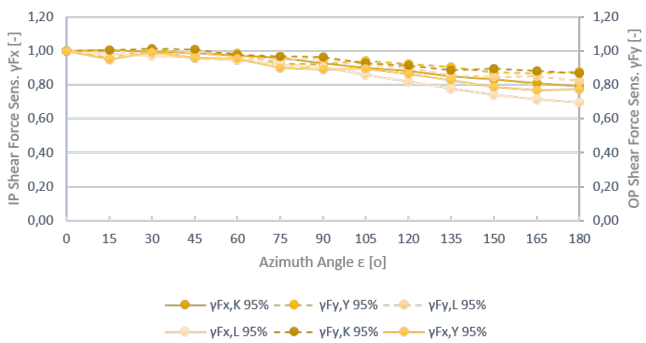

Figure 5.37: Shear Force Sensitivity (γ_F) for the in Table 5.4 presented Azimuth Angles ϵ - $\epsilon(n)$ vs. ϵ = 0°

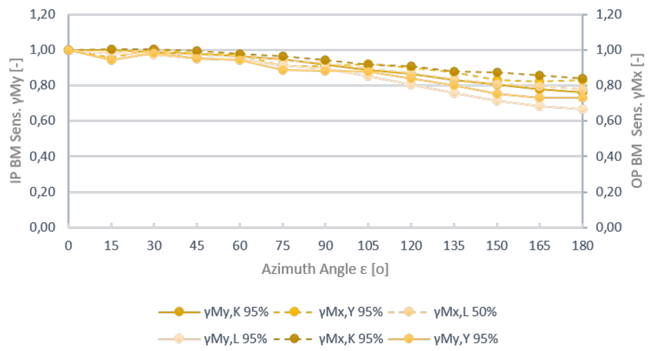

Figure 5.38: Bending Moment Sensitivity (γ_M) for the in Table 5.4 presented Azimuth Angles ϵ - - $\epsilon(n)$ vs. $\epsilon = 0°$

Lastly, as mentioned before, the thrust force on the turbine was calculated assuming symmetry of the system. The results are tabulated in Table G.17 where they were calculated according to Table 5.5. The results are presented in Figure 5.39 and sensitivities in Figure 5.40 and are given in Tables G.11 to G.16.

Table 5.5: Overview of Blade Orientation and combinations for Thrust Force F_t Calculation

Orientation ϵ [°]	AA ϵ
0	0 [°] + 2×120 [°]
15	15 [°] + 135 [°] + 105 [°]
30	30 [°]+ 90 [°] + 150 [°]
45	45 [°] + 75 [°]+ 165 [°]
60	2×60 [°] + 120 [°]

In terms of relative magnitude of the thrust forces this yields no new information. As expected, extrapolating the results to a three-bladed turbine still yields a response ratio $\gamma_{F,M} = 1.2$. The previously found benefit of reducing the loads on the blade by changing its orientation, is negated by the addition of the two other blades effectively resulting in very similar results for turbine thrust forces no matter the orientation. This is shown in Figure 5.40 indicated by a nearly constant relation between thrust force and orientation angle of the blades.

On average the difference is only 1-3% which occurs at the 60° angle indicating that one of the blades should be pointing downward in order the reduce the loading. The difference however is quite negligible at the investigated wind speed of 54.5 m/s, higher wind speed will likely yield different results due to the non-linearity of the response.

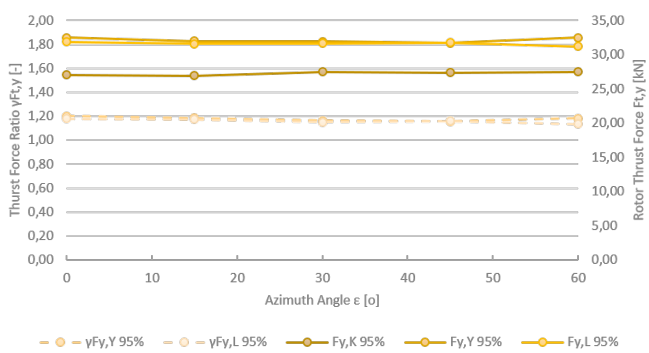

Figure 5.39: Three-bladed turbine Thrust Force F_t and Thurst Force Ratio γ_{Ft}

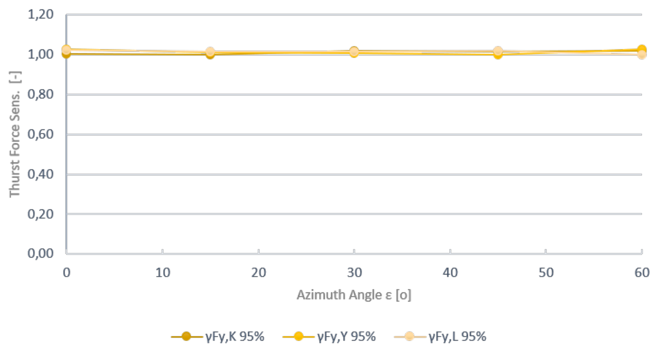

Figure 5.40: Three-bladed turbine Thrust Force Sensitivity - Max(F_t)/$F_t(n)$

5.4. Constant Wind Speed Response

It is well worth investigating what the response of the blade is for a constant wind speed. If a constant wind speed is applied to the blade, constant both in time and space, the dynamics of the system no longer affect the response. This response is defined as the quasi-static response of the beam. In other words, the term $M.\ddot{u}$ in the equations of motion becomes zero as the blade no longer experiences any accelerations in its steady-state response.

$$\underline{\underline{K}}.\underline{u} = \underline{F} \tag{5.2}$$

The response $\underline{u}$ is only governed by the stiffness of the blade $\underline{\underline{K}}$ and the external forces $\underline{F}$ acting on it and becomes constant in time as shown in Figure 5.41.

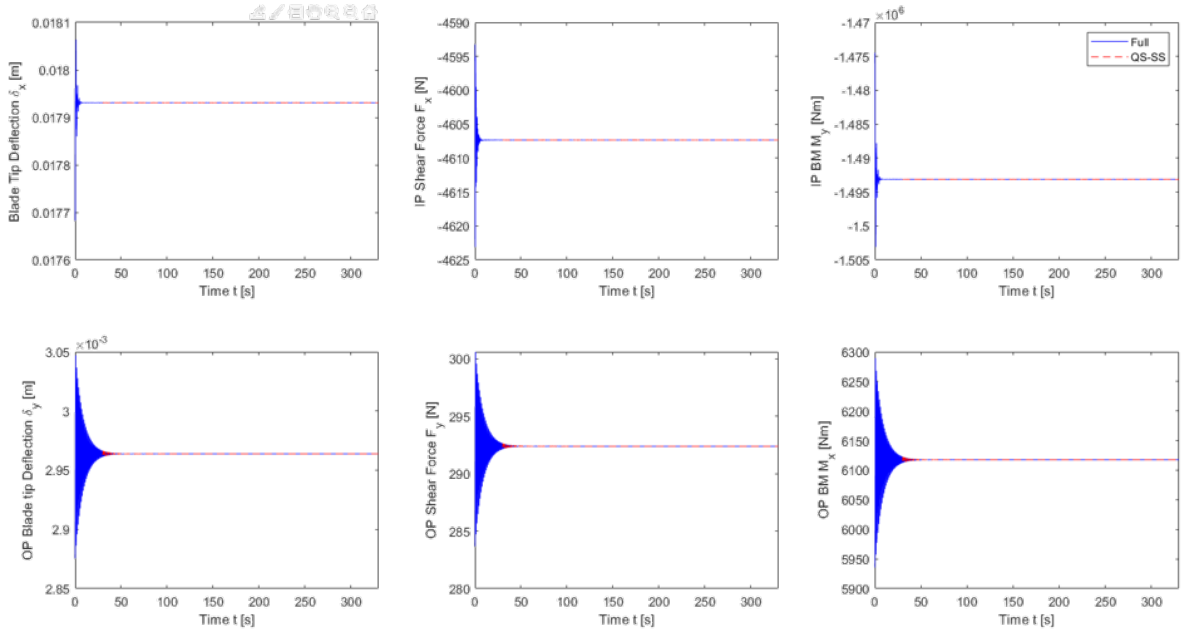

Figure 5.41: Quasi-Static IP and OP response of the blade

For the quasi-static response we know that the internal and external stresses should be equal. Trying to very this, yields the following results shown in Figures 5.42 and 5.43 for the Rated wind speed and summarised for all wind speeds in Tables for the external forces and bending moments (Table 5.6) and internal forces and bending moments (Table 5.7). The summarised results are graphed in Figures 5.44, 5.45 and 5.46. Since the response is static, evaluation of the response only gives mean values.

All figures and tables below show that the internal and forces do not match, proving a poor quasi-static behaviour approximation of the applied model. This means that the number of modes initially chosen to approximate the deformation of the blade was too small. Since the deformation of system resulting from the acting external forces on the blade is poorly approximate, the resulting internal forces are inaccurate.

Furthermore, since the approximation of the deformation by modal shapes is independent from the dynamics of the system, the dynamic internal forces approximation is equally poor. In fact, for an increasing wind speed, the difference between internal and external forces increase non-linearly for the constant wind speed. Since the response of dynamic system also increase non-linearly the error might prove to be even worse.

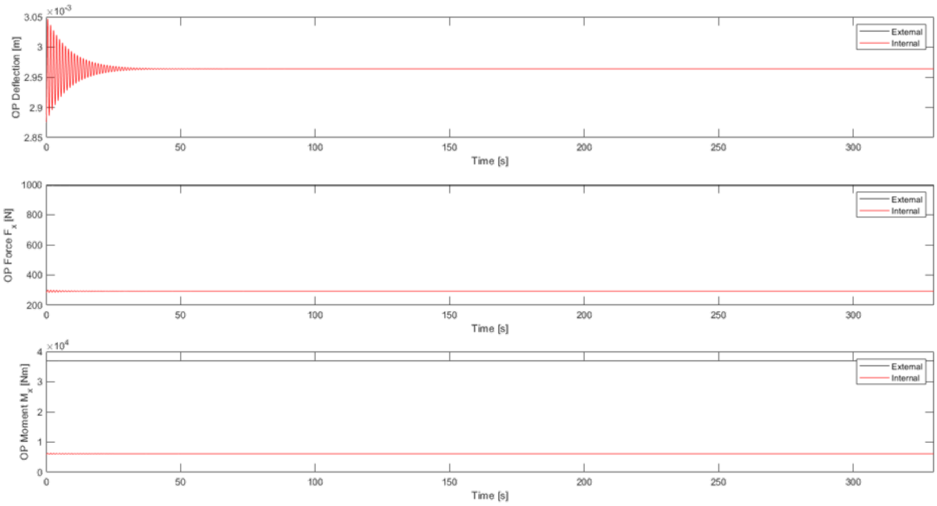

Figure 5.42: Comparison of External [black] and Internal [red] OP Forces and Bending Moments

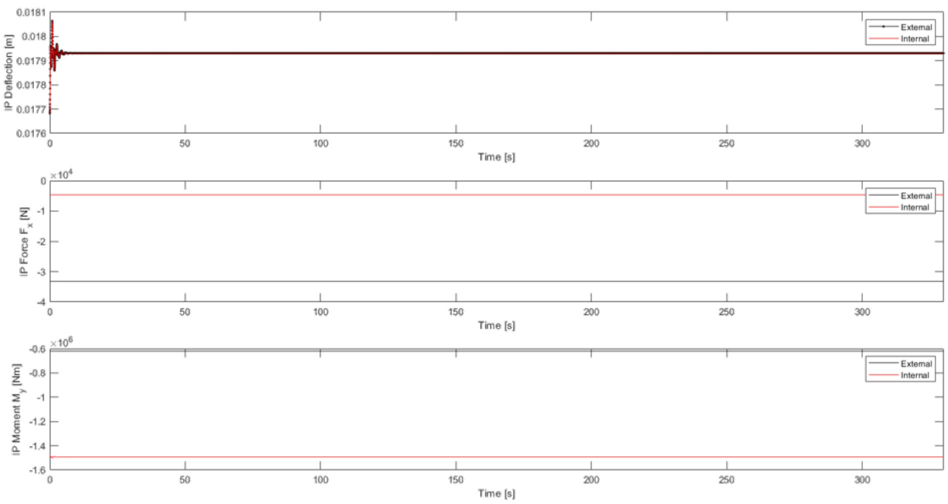

Figure 5.43: Comparison of External [black] and Internal [red] IP Forces and Bending Moments

Table 5.6: Blade Deflections (δ) and External Root Shear Forces (F_{ext}) and Root Bending Moments (M_{ext}) for a Constant Wind Speed U_{10} ($T.I. = 0\%$) ([black] in Figures 5.42,5.43)

		Out-of-Plane			In-Plane		
		δ [m]	F [kN]	M [MNm]	δ [m]	F [kN]	M [MNm]
U10 [m/s]	T [years]	δ_y 50%	$F_{y,ext}$ 50%	$M_{x,ext}$ 50%	δ_x 50%	$F_{x,ext}$ 50%	$M_{y,ext}$ 50%
11.4	Rated	0.00	0.99	0.04	0.02	-33.19	-0.62
30.6	[H1	0.02	7.15	0.27	0.13	-239.15	-4.46
36.5	10	0.03	10.17	0.38	0.18	-340.27	-6.35
40.1	[H2	0.04	12.27	0.46	0.22	-410.70	-7.67
44.9	25	0.05	15.38	0.57	0.28	-514.90	-9.61
46.8	[H3	0.05	16.71	0.62	0.30	-559.40	-10.44
50.1	50	0.06	19.15	0.71	0.35	-641.07	-11.97
54.5	100	0.07	22.67	0.84	0.41	-758.62	-14.16
55.4	[H4	0.07	23.42	0.87	0.42	-783.88	-14.63
58.2	200	0.08	25.85	0.96	0.47	-865.12	-16.15
66.9	[H5	0.10	34.15	1.27	0.62	-1143.10	-21.34
69.5	1000	0.11	36.86	1.37	0.67	-1233.68	-23.03
72.5	2000	0.12	40.11	1.49	0.73	-1342.48	-25.06
78.7	10000	0.14	47.26	1.76	0.85	-1581.91	-29.53

Table 5.7: Blade Deflections (δ) and Internal Root Shear Forces (F_{int}) and Root Bending Moments (M_{int}) for a Constant Wind Speed U_{10} ($T.I. = 0\%$) ([red] in Figures 5.42,5.43)

		Out-of-Plane			In-Plane		
		δ [m]	F [kN]	M [MNm]	δ [m]	F [kN]	M [MNm]
U10 [m/s]	T [years]	δ_y 50%	$F_{y,int}$ 50%	$M_{x,int}$ 50%	δ_x 50%	$F_{x,int}$ 50%	$M_{y,int}$ 50%
11.4	Rated	0.00	0.29	0.01	0.02	-4.61	-1.49
30.6	[H1	0.02	2.11	0.04	0.13	-33.20	-10.76
36.5	10	0.03	3.00	0.06	0.18	-47.23	-15.31
40.1	[H2	0.04	3.62	0.08	0.22	-57.01	-18.47
44.9	25	0.05	4.54	0.09	0.28	-71.47	-23.16
46.8	[H3	0.05	4.93	0.10	0.30	-77.65	-25.16
50.1	50	0.06	5.65	0.12	0.35	-88.98	-28.84
54.5	100	0.07	6.68	0.14	0.41	-105.30	-34.13
55.4	[H4	0.07	6.90	0.14	0.42	-108.81	-35.26
58.2	200	0.08	7.62	0.16	0.47	-120.08	-38.92
66.9	[H5	0.10	10.07	0.21	0.62	-158.67	-51.42
69.5	1000	0.10	10.07	0.21	0.62	-158.67	-51.42
72.5	2000	0.12	11.83	0.25	0.73	-186.34	-60.39
78.7	10000	0.14	13.93	0.29	0.85	-219.58	-71.16

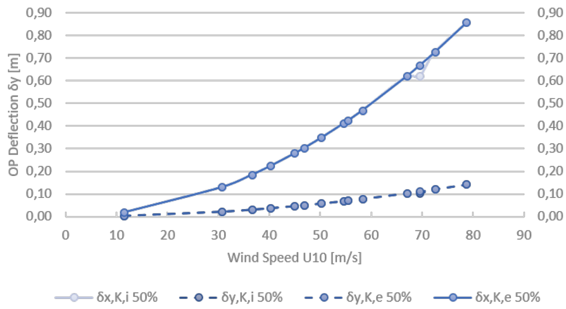

Figure 5.44: Deflection (δ) Comparison for a constant Wind Speed U_{10}

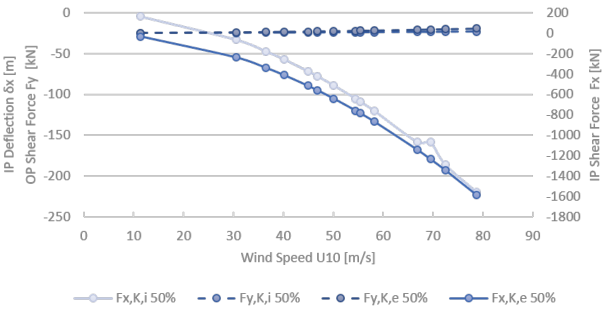

Figure 5.45: Internal (F_{int}) vs. External (F_{ext}) Shear Force Comparison for a constant Wind Speed U_{10}

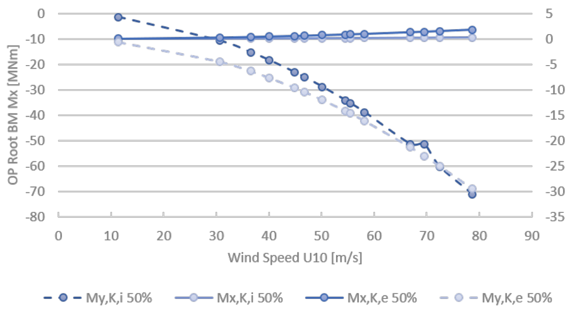

Figure 5.46: Internal (M_{int}) vs. External (M_{ext}) Bending Moments Comparison for a constant Wind Speed U_{10}

The comparison between external and internal forces and bending moments for the Rated wind speed dynamic solution is presented in Figures 5.47 to 5.49 below.

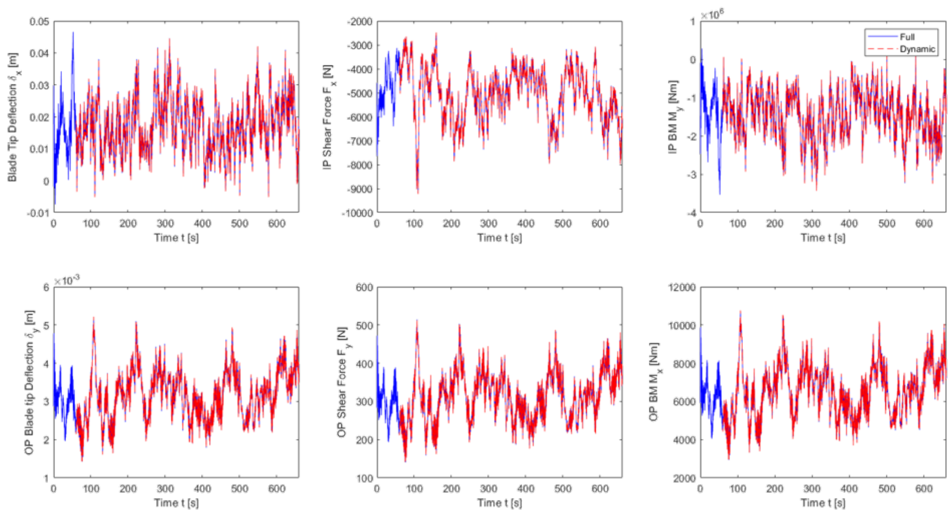

Figure 5.47: Comparison of Dynamic External [black] and Internal [red] OP Forces and Bending Moments for the Kaimal Rated Case

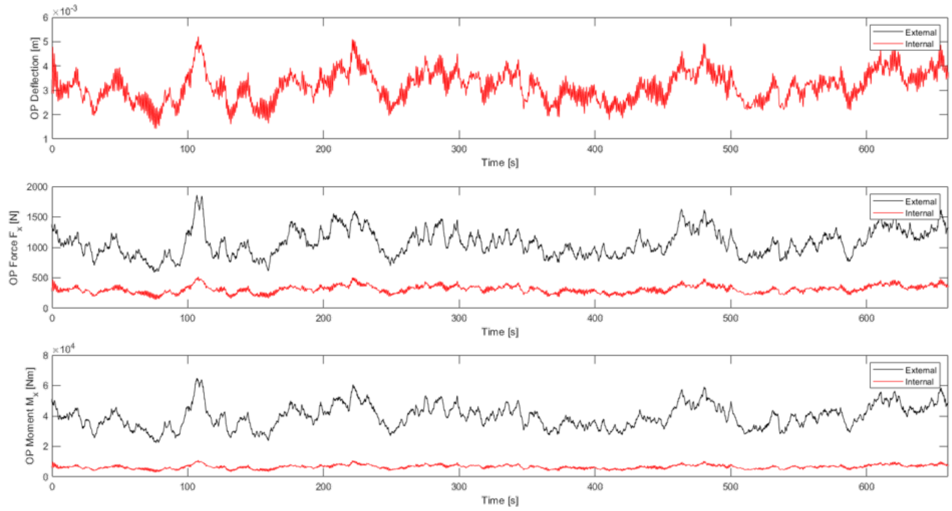

Figure 5.48: Comparison of Dynamic External [black] and Internal [red] OP Forces and Bending Moments for the Kaimal Rated Case

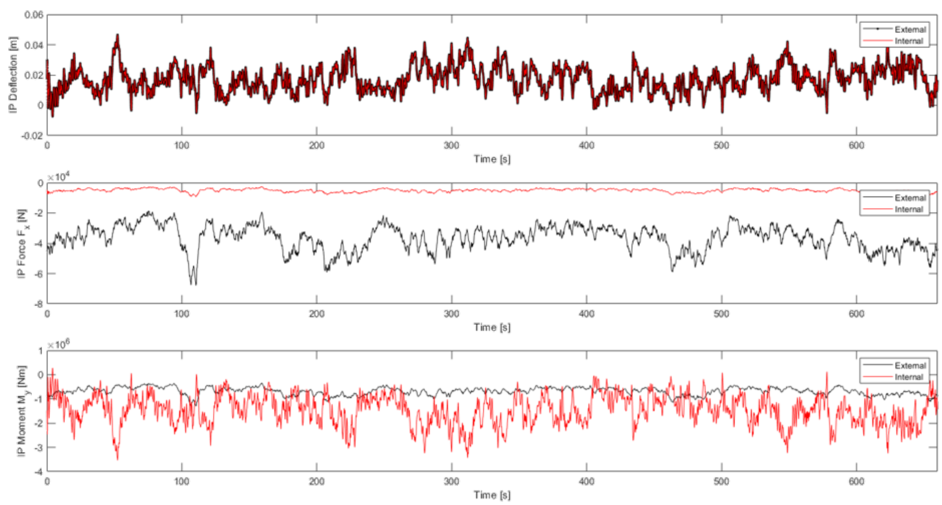

Figure 5.49: Comparison of Dynamic External [black] and Internal [red] IP Forces and Bending Moment for the Kaimal Rate case

As expected, even for the constant response of the blade, the OP and IP deflection responses remain a superposition of 3 modeshapes as indicated in Figure **??**.

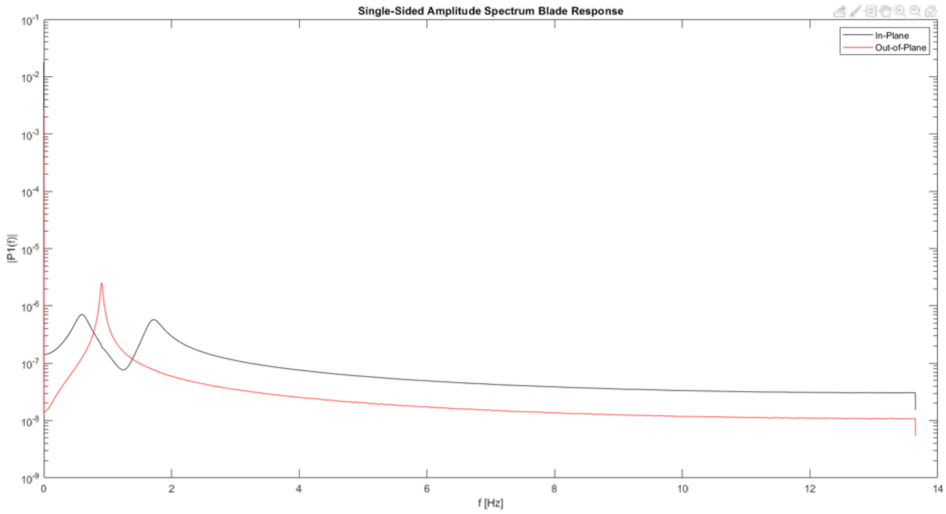

Figure 5.50: Fourier Analysis of the Constant IP and OP Blade Deflection Response for the Kaimal Rated Wind Speed

The unknown functions with which the eigenmodes are multiplied can be found in Figure 5.51 and are unsurprisingly constant in time..

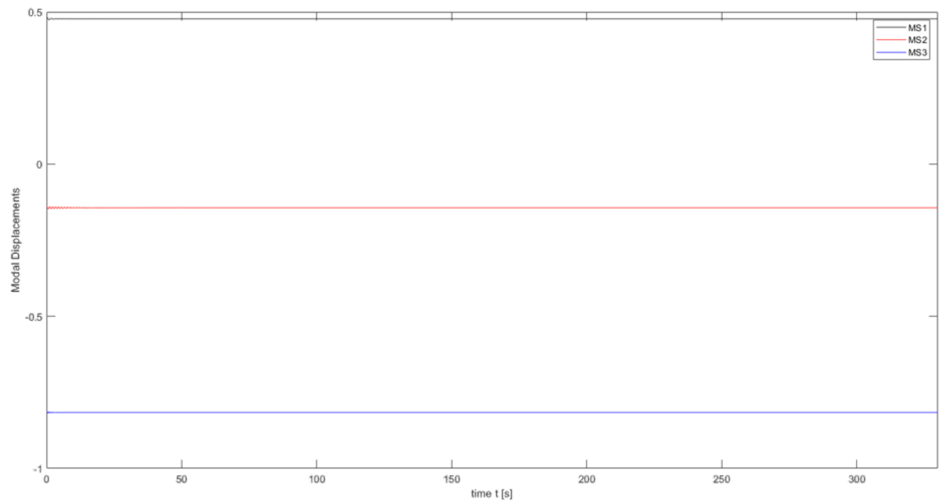

Figure 5.51: Unknown Time Functions for Modal Analysis Approximation of the Kaimal Rated Constant Wind Speed case

5.5. Failure Probability

To assess the structural performance of the blade, the probabilities of failure in shear and bending were calculated given the resultant forces and bending moments calculated in Section 5.2. A reliability design model defines both load and material strength as probabilistic random variables [4]. Figure 5.52 shows the reliability formulation in which the risk depends on the overlap between the two curves. An important conclusion from this figure is that there's no such thing as a risk-free system.

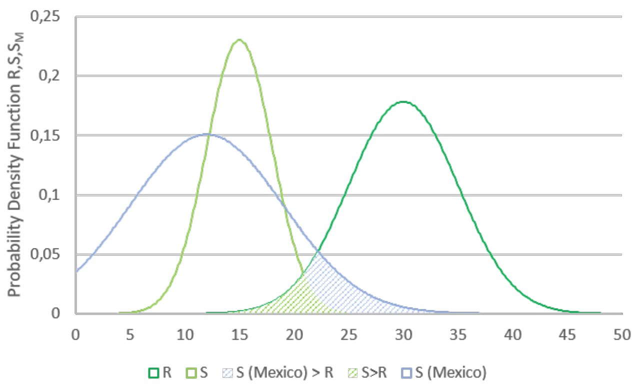

Figure 5.52: Indicative Reliability formulation in which risk depends on the overlap between the 2 curves, Resistance R and and Loading S

It was established in Chapter **??** that Mexico's offshore climate poses a significant threat to offshore wind development. It has a lower mean wind speed, shifting the blue curve to the left of the light green one. Hurricanes cause the variability of wind speed to increase and thus loading to increase, widening the curve. The net result shows a larger overlap between resistance R and loads S indicating a larger probability that the loads actually exceed the material capacity.

To calculate the probability of failure of a single blade, a level II method is used as described in [27], where the mean of the base variables and their standard deviations are used to determine the failure probability of a certain limit state function Z (LSF). The failure probability is no longer dependent on the overlap between two curves but on the area of the curve where $Z < 0$, visualised in Figure 5.53. Again, having a lower average wind speed, the increased variability increases the area of the curve below $Z = 0$, indicating increased probabilities of failure in Mexico's offshore climate for a system with identical material properties.

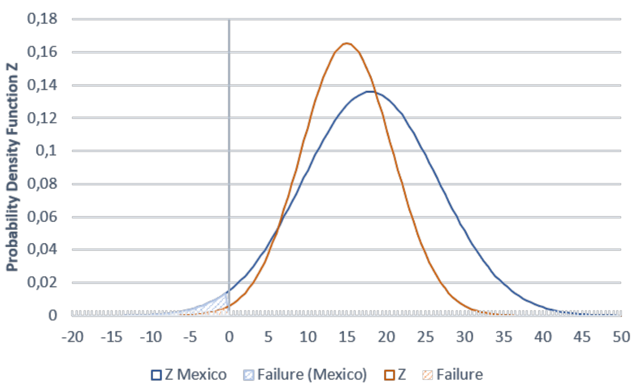

Figure 5.53: Indicative Reliability formulation in which risk depends on the area of the curve where $Z < R - S < 0$

In this case, the LSFs can be written as the difference between the material stress capacity and the acting, internal stress using Equation 5.3a for shear failure and Equation 5.3b and bending failure respectively:

$$Z = R - S = \frac{\pi}{4}(D_o^2 - (D_o^2 \cdot t)^2) \cdot f_{y,s} - \sqrt{F_x^2 + F_y^2} \tag{5.3a}$$

$$Z = R - S = \frac{\pi}{32 \cdot D_o}(D_o^4 - (D_o - 2 \cdot t)^4) \cdot f_{y,b} - \sqrt{M_y^2 + M_x^2} \tag{5.3b}$$

with D_o the outside diameter of the circular blade section connecting it to the hub, t the thickness of the material, $f_{y,s}$ the shear yield stress of the blade multiply material, $f_{y,b}$ the bending yield stress of the multiply material, F_x and F_y the respective IP and OP forces and M_y and M_x the respective IP and OP bending moments. Since the shear stress properties for the material weren't specified in DTU's reference report [9], it was assumed that 60% of a quarter of the steel tension yield stress ($235N/mm^2$) would be used as the mean (μ) shear yield stress, which is often taken around 50% of the tensile stress thus $f_{y,s}$ = $35.25N/mm^2$. The standard deviation (σ) was set at $4N/mm^2$. For the allowable bending stress a quarter of the steel tensile strength was used: $f_{y,b} = 58.75N/mm^2$ with a standard deviation of $10N/mm^2$. Material properties were kept identical for all spectra.

Table 5.8: Adopted Material Strength Properties for the Calculation of Failure Probabilities

Failure Mode	Yield Stress $[N/mm^2]$	σ $[N/mm^2]$
Shear	35.25	4
Bending	58.75	10

The presented LSFs are non-linear with respect to their design variables. Simplifying the approach and assuming the material dimensions are deterministic (which in fact, they are not), the remaining design values are the material strength properties $f_{y,s}$ and $f_{y,b}$ the acting forces F_i and bending moments M_i found from the simulations run in Section 5.2. Iteratively, the failure probability can then be found from the reliability index β by linearising the limit state function in the so-called design point X_i^*. The reliability index β is defined according to Equation 5.4. The design point hereby refers to the combination of design variables which yields the highest probability of failure

$$\beta = \frac{\mu_Z}{\sigma_Z} \tag{5.4}$$

with μ_Z the mean value of the linearised LSF and σ_Z its standard deviation can be determined according to

$$\mu_Z = Z(X_1^*, X_2^*, X_3^*) + \sum_{i=1}^{n}(\mu_{X_i} - X_i)\frac{\partial Z}{\partial X_i}(X_i^*) \tag{5.5a}$$

$$\sigma_Z^2 = \sum_{i=1}^{n}\left(\frac{\partial Z}{X_i}(X_i^*)\right)^2 \cdot \sigma_{X_i^*}^2 \tag{5.5b}$$

A fully detailed desription can be found in the TU Delft CIE4130 Probabilistic Design Lecture Notes [27] and will therefor not be repeated in detail here. Full including intermediate results for all failure probability calculations are given in Appendix I.

The failure probabilities of a single blade subjected to a combined out-of-plane and in-plane shear force are presented in Table 5.9 and visually shown in Figure 5.54.

Probabilities of failure tend to increase non-linearly as wind speed increases. This is perfectly reasonable given the non-linear relation between wind speed and internal forces. Given the actual magnitude of failure probabilities, the blade is highly unlikely to fail in shear. As wind speeds increase, blades subjected to hurricane winds have an increasingly larger chance of failing compared to non-hurricane Kaimal Spectrum. Note that these failure probabilities do include the specified difference in RL between spectra as these were the most conservative conditions for the hurricane spectra.

Table 5.9: Single Blade Shear Failure Probability P_f for all Wind Speed Conditions and Spectra

	Spectrum	Kaimal	Yu	Li
T [years]	U_{10} [m/s]	Failure Probability		
Rated	11.4	1.83E-07	1.83E-07	1.83E-07
H1	30.6	1.95E-07	1.98E-07	1.98E-07
T10	36.5	2.02E-07	2.06E-07	2.06E-07
H2	40.1	2.06E-07	2.13E-07	2.11E-07
T25	44.9	2.13E-07	2.21E-07	2.20E-07
H3	46.8	2.16E-07	2.25E-07	2.24E-07
T50	50.1	2.22E-07	2.30E-07	2.29E-07
T100	54.5	2.29E-07	2.44E-07	2.35E-07
H4	55.4	2.30E-07	2.47E-07	2.44E-07
T200	58.2	2.37E-07	2.54E-07	2.51E-07
H5	66.9	2.59E-07	2.80E-07	2.77E-07
T1000	69.5	2.67E-07	2.91E-07	2.84E-07
T2000	72.5	2.71E-07	3.08E-07	2.95E-07
T10000	78.7	2.94E-07	3.36E-07	3.24E-07

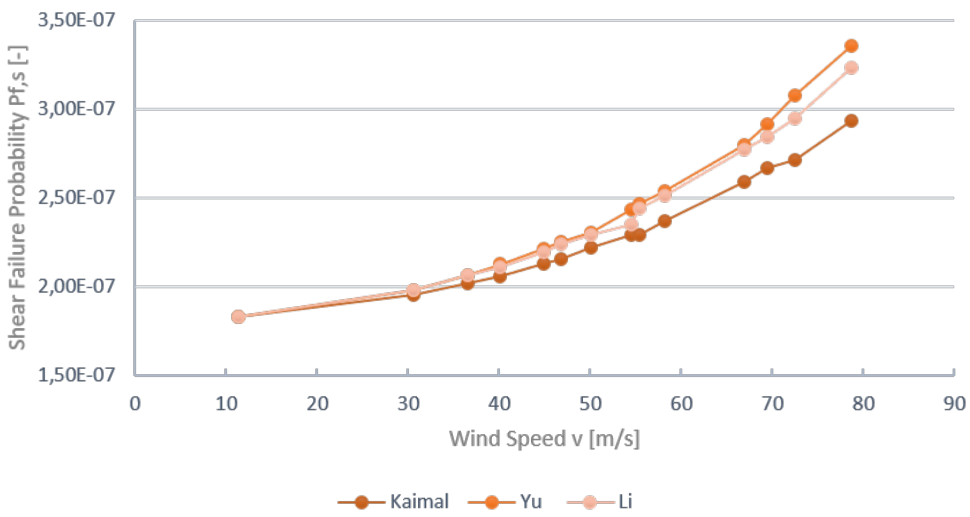

Figure 5.54: Shear Failure Probability $P_{f,x}$ evolution for increasing Wind Speed U_{10}

The failure probabilities of a single blade subjected to a combined out-of-plane and in-plane bending moment are presented in Table 5.10 and visually shown in Figure 5.55.

Chances of the blades breaking in bending are considerably larger than for shear for the higher wind speeds. Once wind speeds exceed the T100 design period wind conditions, probabilities of failure increase drastically to an almost certain failure at T10000 conditions irrespective of the spectra.

Due to the fact that the model inaccurately describes the deformation of the blade using only three modeshapes consequently inaccurately describing the internal forces, as well as due to the fact that the actual material properties are unknown, the accuracy of the failure probabilities should be taken cautiously. The overall trend however, seems to be as expected.

Table 5.10: Single Blade Failure Probability P_f for all Wind Speed Conditions and Spectra

	Spectrum	Kaimal	Yu	Li
T [years]	U_{10} [m/s]	Failure Probability		
Rated	11.4	0.00E+00	0.00E+00	0.00E+00
H1	30.6	5.33E-15	0.00E+00	0.00E+00
T10	36.5	2.38E-13	0.00E+00	5.24E-14
H2	40.1	1.97E-13	2.02E-12	1.24E-11
T25	44.9	6.49E-11	2.01E-12	3.63E-13
H3	46.8	3.78E-13	1.25E-09	7.67E-10
T50	50.1	8.32E-09	2.21E-06	1.17E-06
T100	54.5	3.28E-05	4.22E-03	4.33E-04
H4	55.4	5.27E-05	6.39E-03	1.51E-03
T200	58.2	8.73E-04	2.10E-02	2.49E-02
H5	66.9	1.59E-01	4.75E-01	4.58E-01
T1000	69.5	3.40E-01	6.60E-01	6.29E-01
T2000	72.5	4.93E-01	8.17E-01	7.98E-01
T10000	78.7	8.28E-01	9.47E-01	9.74E-01

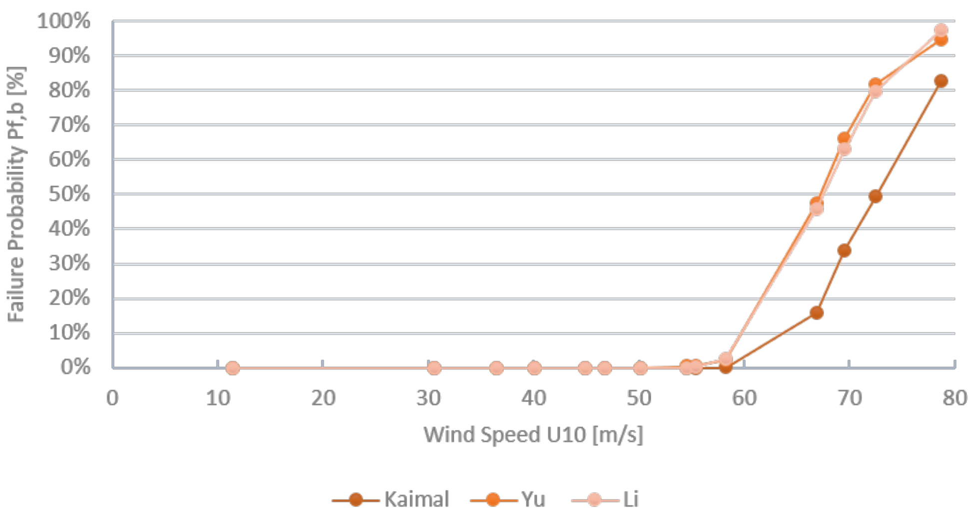

Figure 5.55: Failure Probability $P_{f,b}$ evolution for increasing Wind Speed U_{10}

5.6. Design Return Period Exceedances

Standards state design return periods for which systems should be designed in order to ensure a safe and adequate, fit-for-purpose design. Taking into account the additional load effects, in this case mainly driven by the choice of roughness length during hurricane conditions, the design period exceedance probabilities of hurricane responses are tabulated in Tables 5.11 to 5.16 for all five category hurricanes, for all three spectra (top to bottom). A distinction is made between shear response (Tables 5.11, 5.13 and 5.15 on the left) and bending response (Tables 5.12, 5.14 and 5.16 on the right).

Similarly to how the failure probabilities where determined in Sec.5.5 using an LSF, these value where calculated using a much simpler LSF.

$$Z_s = S_{T,s} - S_{H,s} \tag{5.6a}$$

$$Z_b = S_{T,b} - S_{H,b} \tag{5.6b}$$

where $\mu_{S_{T,s}}$, $\mu_{S_{H,s}}$, $\sigma_{S_{T,s}}$ and $\sigma_{S_{T,b}}$ are calculated as

$$\mu_{S_{T,s}} = \sqrt{\mu^2_{F_{x,T}} + \mu^2_{F_{y,T}}} \tag{5.7a}$$

$$\sigma_{S_{T,s}} = \sqrt{\sigma^2_{F_{x,T}} + \sigma^2_{F_{y,T}}} \tag{5.7b}$$

$$\mu_{S_{H,b}} = \sqrt{\mu^2_{M_{x,H}} + \mu^2_{M_{y,H}}} \tag{5.7c}$$

$$\sigma_{S_{H,b}} = \sqrt{\sigma^2_{M_{x,H}} + \sigma^2_{M_{y,H}}} \tag{5.7d}$$

respectively such that

$$\mu_{Z_i} = \mu_{S_{T,i}} - \mu_{S_{H,i}} \tag{5.8a}$$

$$\sigma_{Z_i} = \sqrt{\sigma^2_{S_{T,i}} + \sigma^2_{S_{H,i}}} \tag{5.8b}$$

$$\beta_{Z_i} = \frac{\mu_{Z_i}}{\sigma_{Z_i}} \tag{5.8c}$$

This is to show that while the design period wind speeds may exceed the maximum expected wind speed, the response of the system can be larger due to additional response effects thus exceeding the design response. Say, one wants to design a structure to withstand H3 wind speed conditions. The obvious choice would be to select a T200 return period as this wind speed exceeds the maximum H3 wind speeds (or the minimum H4 wind speeds). The tables show however, that if one would select T200 design conditions, these H4 conditions would exceed the selected period roughly 35-40% of the time. Which entails that the design is not that safe at all.

Table 5.11: Kaimal Hurricane Shear Exceedance Probability $P_{f,s}$ (%) of Design Return Periods (T)

		H1	H2	H3	H4	H5
T [years]	U_{10} [m/s]	30.6	40.1	46.8	55.4	66.9
Rated	11.4	100.00	100.00	100.00	100.00	100.00
T10	36.5	8.56	75.20	96.70	99.89	99.99
T25	44.9	0.42	18.49	62.88	95.31	99.76
T50	50.1	0.08	4.52	29.31	78.45	98.34
T100	54.5	0.01	1.06	11.80	55.64	94.58
T200	58.2	0.00	0.35	4.80	34.46	86.83
T1000	69.5	0.00	0.01	0.20	3.25	36.61
T2000	72.5	0.00	0.00	0.07	1.51	25.65
T10000	78.7	0.00	0.00	0.02	0.35	9.67

Table 5.12: Kaimal Hurricane Bending Exceedance Probability $P_{f,b}$ (%) of Design Return Periods (T)

		H1	H2	H3	H4	H5
T [years]	U_{10} [m/s]	30.6	40.1	46.8	55.4	66.9
Rated	11.4	99.13	99.82	99.92	99.94	99.98
T10	36.5	24.32	65.21	86.01	95.56	99.28
T25	44.9	7.72	30.95	57.22	82.17	96.35
T50	50.1	3.00	15.62	36.64	67.10	91.53
T100	54.5	1.68	8.84	23.29	51.86	84.10
T200	58.2	0.90	5.21	15.45	40.70	76.91
T1000	69.5	0.26	1.20	3.66	12.97	41.22
T2000	72.5	0.22	0.95	2.82	10.13	34.69
T10000	78.7	0.07	0.30	0.97	4.21	19.46

Table 5.13: Yu Hurricane Shear Exceedance Probability $P_{f,s}$ (%) of Design Return Periods (T)

		H1	H2	H3	H4	H5
T [years]	U_{10} [m/s]	30.6	40.1	46.8	55.4	66.9
Rated	11.4	100.00	100.00	100.00	100.00	100.00
T10	36.5	11.89	76.44	96.51	99.69	99.93
T25	44.9	0.82	22.16	63.20	93.53	99.12
T50	50.1	0.32	8.35	34.76	78.76	96.64
T100	54.5	0.03	1.74	13.17	55.46	90.71
T200	58.2	0.03	0.94	6.81	37.07	81.36
T1000	69.5	0.01	0.11	0.77	7.00	39.34
T2000	72.5	0.00	0.04	0.30	3.39	26.89
T10000	78.7	0.00	0.01	0.07	0.96	12.30

Table 5.14: Yu Hurricane Bending Exceedance Probability $P_{f,s}$ (%) of Design Return Periods (T)

		H1	H2	H3	H4	H5
T [years]	U_{10} [m/s]	30.6	40.1	46.8	55.4	66.9
Rated	11.4	99.59	99.83	99.97	99.97	99.99
T10	36.5	19.70	68.79	0.90	97.22	99.57
T25	44.9	4.18	29.47	0.58	85.19	97.14
T50	50.1	1.95	15.87	0.38	71.68	93.04
T100	54.5	1.49	9.34	0.23	54.13	84.29
T200	58.2	0.37	4.03	0.13	41.67	77.34
T1000	69.5	0.08	0.69	0.03	12.62	41.45
T2000	72.5	0.16	0.83	0.02	9.68	31.66
T10000	78.7	0.09	0.43	0.01	5.04	19.17

Table 5.15: Li Hurricane Shear Exceedance Probability $P_{f,s}$ (%) of Design Return Periods (T)

		H1	H2	H3	H4	H5
T [years]	U_{10} [m/s]	30.6	40.1	46.8	55.4	66.9
Rated	11.4	100.00	100.00	100.00	100.00	100.00
T10	36.5	8.27	75.17	97.43	99.73	99.99
T25	44.9	0.24	16.47	65.06	94.00	99.80
T50	50.1	0.03	3.46	31.19	78.44	98.72
T100	54.5	0.00	0.56	11.94	57.93	95.94
T200	58.2	0.00	0.32	5.02	33.98	86.19
T1000	69.5	0.00	0.01	0.19	3.75	37.92
T2000	72.5	0.00	0.00	0.08	1.82	25.80
T10000	78.7	0.00	0.00	0.02	0.39	9.00

Table 5.16: Li Hurricane Bending Exceedance Probability $P_{f,b}$ (%) of Design Return Periods (T)

		H1	H2	H3	H4	H5
T [years]	U_{10} [m/s]	30.6	40.1	46.8	55.4	66.9
Rated	11.4	99.79	99.74	99.97	99.99	99.99
T10	36.5	20.59	65.27	88.76	97.62	99.52
T25	44.9	4.56	29.38	59.44	86.07	97.19
T50	50.1	1.54	14.32	37.71	70.94	93.03
T100	54.5	0.65	7.36	23.27	55.28	86.86
T200	58.2	0.44	4.13	13.78	38.98	76.55
T1000	69.5	0.10	0.78	2.92	11.72	42.16
T2000	72.5	0.06	0.48	1.81	7.80	32.94
T10000	78.7	0.01	0.07	0.34	2.21	16.29

6 Conclusions

The goal of this research was to study the structural performance of a 10MW reference turbine in hurricane conditions in The Gulf of Mexico. The work was divided into three main sub-objectives: 1. Identify the main characteristic differences between hurricane winds and regular extreme wind; 2. study the effects of different wind conditions i.e. regular extreme winds vs. hurricane winds on blade response through forces, bending moments and deflections; 3. Investigate the influence of selected hurricane wind parameters i.e. roughness length and coherence on these responses and 4. to assess the structural reliability or probability of failure of a blade given hurricane conditions. The fulfilment of these objectives is discussed in Section6.1. Section 6.2 offers recommendations to further improve the results and expand on this research.

6.1. Conclusions

The first objective of this thesis was to investigate the load effects of hurricane winds compared to regular extreme winds on a 10MW turbine blade. To this end, Chapter 3 discussed wind parameters including turbulence, turbulence intensity, turbulence length scales, roughness length and coherence, in order to be able to make a distinction between regular extreme wind and hurricane winds.

It was established that the most notable difference were the turbulence spectra, i.e. the turbulent energy distribution over the frequency components. The Yu Spectrum [18] contained more turbulent energy within the lower frequency regions compared to the regularly applied Kaimal Spectrum. Li [16] found contradicting evidence stating that there was more energy found within the higher frequency regions compared to the Kaimal Spectrum. Moreover, Yu and Li found roughness lengths to be overall larger compared to the values typically used for offshore turbine design. However, they both investigated smaller category hurricanes. Given the relation between roughness length and wind speed, it can be expected that roughness lengths will increase even more for larger category hurricanes.

Turbulence intensities in hurricane winds were found to be of a comparable percentage as regular extreme winds. Turbulence length scales were introduced for both hurricane spectra studies, yet how to include them into the turbulence spectra was not addressed in the respective sources. The 10[m] hurricane spectra were therefore assumed to be valid at hub height as well i.e. not height correction was incorporated.

Neither addressed in the Li Spectrum Research [16] was spatial coherence between longitudinal wind velocity components and between upward a longitudinal wind components, limiting the simulations to a 1D longitudinal approach where spatial coherence was implemented as an exponential decay function dependent on coherence decay coefficients. Both authors of respective works were in agreement that these discussed hurricane wind parameters, with the exception of the turbulence spectra, are most likely storm-dependent and/or location-dependent.

Secondly, in Chapter 4, findings from Chapter 3 where implemented in a wind history model developed by Cheynet [2], to which mainly turbulence intensity and the two different hurricane spectra were added to incorporate the hurricane wind findings. To generate the numerical results, use was made of a blade model developed by Pim van der Male [21] applying modal reduction techniques on a Finite-Element Model of the turbine blade with DTU's 10MW turbine structural properties and simplified aerodynamic characteristics. Blade deformations and consequently its response were analysed based on the superposition of three modeshapes of the blade. Verification of this approach showed that three modeshapes were insufficiently accurate to describe the deformation, indicated by a considerable difference between internal and external forces for the quasi-static state which should be equal.

The modal analysis resulted in out-of-plane and in-plane deflections and forces through the non-uniform turbine blade stiffness indicating that for an even more accurate description of the problem a 2D or even 3D approach should be considered requiring more information on all hurricane wind components including temporal and spatial coherence.

Chapter 5.2 detailed the findings of the simulations including their sensitivity to definition of roughness length z_0 and coherence. Results showed clearly the importance of a correct definition of surface roughness length as it considerably affects the response ratios for the hurricane spectra increasing the Kaimal response with a factor $\gamma = 1.2$. As expected, increasing the roughness length, increases the response of the blade due to its relation through the wind shear profile. The coherence was defined for the hurricane spectra winds using the same exponential decay function. No references were found detailing the coherence in hurricane winds. This is apparent for all wind parameters specifically concerning hurricane winds: there is only a limited amount of information available on these particular values resulting in a large uncertainty on the input and thus also on the results presented in this work. Nevertheless, given the dynamic nature of OWT's and the difference in turbulence spectra, it is expected that the response will be different compared to regular extreme winds. To what degree will be dependent on the blade choice as the natural frequency plays an important role.

From the results found in Section 5.2, it can be concluded that there is a difference in response when comparing hurricane spectra to the regular extreme wind Kaimal spectrum response. The difference is predominantly explained by the choice of roughness length z_0 as indicated by the sensitivity analysis. The small difference between the turbulent energy in the three spectra the around the natural frequency of the blade gives is not enough to cause a change in response of the blade. It doesn't lead to any significant increased dynamic response.

Lastly in section 5.5 the failure probability of a single blade was calculated using the forces and bending moments found in Section 5.2. A level II reliability method approach was used to determine the probability of failure given a simple, non-linear limit state function. Material properties were not provided in DTU's report [9] thus assumptions were made regarding blade laminate properties. Sixty percent of halve the tensile yield stress of S235 steel was taken as the shear yield stress. For bending, halve of the yield stress of steel was chosen.

Failure probabilities were highest for the hurricane spectra including the different choice of the roughness length and increased non-linearly with increasing wind speeds. Failure probabilities were also larger for failure in bending compared to failure in shear.

A more accurate wind containing less uncertainty on hurricane parameters, a more accurate blade model by including more modeshapes, and less uncertain material properties would yield much more representative findings leading to an overall better assessment of the blade performance of a 10MW turbine in hurricane conditions.

6.2. Future Work

The approach adopted in this thesis, based on limited available references and sources on hurricane winds and hurricane wind design, leaves room for further improvement and expansion on the current work. Most importantly with respect to the uncertainty of input parameters namely hurricane turbulence (intensity, spectra and turbulence length scales) and the accuracy of the blade model. More measurements need to be done for real hurricanes in different regions of the world for all categories to effectively establish if the values are storm-dependent, location-dependent or both. It would at least lead to a range of more plausible values for which the degree of accuracy is relatively high. It would furthermore allow the design of structures to be tuned to the region for best-performance, fit-for-purpose, structures.

The Wind model used in this research is limited to a 1D longitudinal wind field applied to a single blade of which only the maximum wind speed is used to say something about the ULS and SLS performance of the turbine blade. Hurricanes are extreme events on a large scale. A full 3D wind field could not only increase the accuracy on single blade results but could also be employed to investigate the performance of an entire wind farm subjected to a single hurricane. Moreover, design of a structure requires also FLS to be investigated. This was not done in the current work due to the limited knowledge on fatigue behaviour of multiply materials.

The accuracy of the blade model to calculate the response was deemed inaccurate by including only three modeshapes to approximate the blade deformation. Incorporating more modeshapes should lead to more accurate static and dynamic responses. Furthermore, the blade model adopted considered only symmetrical airfoils, and applied the thin plate analogy to simply define aerodynamic properties C_l and C_d instead of using the actual airfoil data. Inclusion of these properties would increase the accuracy of the responses even more.

Lastly, something not mentioned in the research is the use of model scale testing. Researchers at WindEEE have developed a hexagonal wind tunnel specifically for this purpose to generate full 3D wind field including hurricanes. However, to accurately capture these events in a wind tunnel, enough data must be collected.

Being able to safely design turbines to survive even more extreme wind conditions could lead to a significant increase in wind resource exploitation.

Bibliography

[1] Michelle Z. Donahue (2016). Can we capture energy from a hurricane? https://www.smithsonianmag.com/innovation/can-we-capture-energy-hurricane-180960750/.

[2] E. Cheynet (2019). Wind field simulation (the user-friendly version). https://www.mathworks.com/matlabcentral/fileexchange/50041-wind-field-simulation-the-user-friendly-version), MATLAB Central File Exchange.

[3] American Petroleum Institute. Api 2int-met: Interim guidance on hurricane conditions in the gulf of mexico. 2007.

[4] American Pertroleum Institute (API). Recommended practice for planning, designing and constructing fixed offshore platforms - load and resistance factor design. *API RP 2A-LRFD*, 1993.

[5] S.R. Arwade A.T. Myers and J.F. Manwell. Consideration of hurricanes and tropical cyclones in the design of offshore wind turbines. page 11, 2015.

[6] M. Shinozuka; G. Deodatis. Simulation of stochastic processes by spectral representation. *Applied Mechanics Reviews*, 44(4), 1991.

[7] I. Van der Hoven. Power spectrum of horizontal wind speed in the frequency range from 0.0007 to 900 cycles per hour. *Journal of Meteorology*, 14:160–164, 1957.

[8] Spencer T. Hallowell et al. Hurricane risk assessment of offshore wind turbines. *Elsevier - Renewable Energy*, 125:234–249, 2018.

[9] Christian Bak et al. (DTU Wind Energy). Light rotor: The 10-mw reference wind turbine. 2014.

[10] Bejoy P. Alduse Gholamreza Amirinia, Sungmoon Jung. Effect of different hurricane spectra on wind turbine loads and responses. *AWEA Wind Power Conference Paper*, 141: 1–11, 2017.

[11] James I Belanger Greg J. Holland and Angela Fritz. A revised model for radial profiles of hurricane winds. *Monthly Weather Review*, 12:9, 2019.

[12] Greg J. Holland. An analytic model of the wind and pressure profiles in hurricanes. *Monthly Weather Review*, 9:7, 1980.

[13] International Energy Agency (IEA). Mexico. https://www.iea.org/countries/Mexico/.

[14] International Electrotechnical Commission, IEC. Iec 61400-1 : Wind turbines part 3 - design requirements for offshore wind turbines (draft) (2014). 2005.

[15] J.M.J. Spijkers; A.W.C.M. Vrouwenvelder; E.C. Klaver. *Structural Dynamics CT4140 Part 1 - Structural Vibrations*. Delft University of Technology, Faculty of Civil Engineering and Geosciences, 2005.

[16] A. Kareem L. Song P. Qin L. Li, Y. Xiao. Modeling typhoon wind power spectra near sea surface based on measurements in the south china sea. *Journal of Wind Engineering and Industrial Aerodynamics*, pages 565–576, 2012.

[17] M. Brain; C. Freudenrich (PH.D); R. Lamb;. How hurricanes work. https://science.howstuffworks.com/nature/natural-disasters/hurricane.htm.

[18] B. Yu; A.G.Chowdhury; F.J. Masters. Hurricane wind power spectra, cospectra and integral length scales. *Boundary-Layer Meteorology*, 129(3):pp 422–430, December 2008.

[19] National Hurricane Center and Central Pacific Center (National Oceanic and Atmospheric Administration [NOAA]). The saffir-simpson hurricane wind scale.

[20] OffshoreWind.biz. Nrel to study feasibility of gulf of mex-

ico offshore wind. https://www.offshorewind.biz/2017/07/18/nrel-to-study-feasibility-of-gulf-of-mexico-offshore-wind/.

[21] A.V. Metrikine P van der Male, K.N. van Dalen. The effect of the nonlinear velocity and history dependencies of the aerodynamic force on the dynamic response of a rotating wind turbine blade. *Journal of Sound and Vibration*, 383:191–209, 2016.

[22] S.N. Walker R.E. Wilson, P.B.S. Lissaman. Aerodynamic performance of wind turbines. *ERDA/NSF/04014-7611*, 1976.

[23] 1 Mitchell J. Small Iris Grossmann Stephen Rose, Paulina Jaramillo and Jay Apt. Quantifying the hurricane risk to offshore wind turbines. *Proceedings of the National Academy of Sciences (PNAS)*, 2012.

[24] Roland Stull. *Practical Meteorology: An Algebra-based Survey of Atmospheric Science - Chapter 16 Tropical Cyclones*. Dept. of Earth, Ocean Atmospheric Sciences, University of British Columbia, 2017.

[25] Barry Posner Craig H. Bishop Timothy J. Considine, Christopher Jablonowski. The value of hurricane forecasts to oil and gas producers in the gulf of mexico. *Journal of Applied Meteorology*, 43:12, 2004.

[26] David Sharpe Tony Burton, Nick Jenkins and Ervin Bossanyi. *Wind Energy Handbook, Second Edition*. John Wiley & Sons, 2011.

[27] S.N. Jonkman; R.D.J.M. Steenbergen; O. Morales-Nápoles; A.C.W.M. Vrouwenvelder & J.K. Vrijling. Probabilistic design: Risk and reliability analysis in civil engineering. *TU Delft Lecture Notes*, v.4, 2017.

[28] Lian Xie, Kristen Foley Shaowu Bao, Leonard J. Pietrafesa, and Montserrat Fuentes. A real-time hurricane surface wind forecasting model: Formulation and verification. *Monthly Weather Review*, 5:16, 2006.

[29] Ian R. Young. Parametric hurricane wave predicition model. *Journal of Waterway Port Coastal and Ocean Engineering*, (9):16, 1988.

A

Appendix A : Young's Hurricane Wave Model - Wave Height Estimation

Knowing the hurricane's V_m, V_t and its RMW, an estimation of the significant wave height can be calculated by first finding the effective radius of the storm as expressed by

$$R' = 22.5 \cdot 10^3 \log(R) - 10.3 \cdot 10^3 \tag{A.1}$$

where R' and R have units of $[m]$. The equivalent fetch can then be calculated using

$$\frac{F}{R'} = a \cdot V_m^2 + b \cdot V_m V_t + c \cdot V_t^2 + d \cdot V_m + e \cdot V_t + f \tag{A.2}$$

where constant a through f are defined according to Table A.1.

Table A.1: Equivalent Fetch Parameters

	Value [-]
a	$-2.175 \cdot 10^{-3}$
b	$1.506 \cdot 10^{-2}$
c	$-1.223 \cdot 10^{-1}$
d	$2.190 \cdot 10^{-1}$
e	$6.737 \cdot 10^{-1}$
f	$7.980 \cdot 10^{-1}$

Substitution of the equivalent fetch F and V_m in the adopted JONSWAP fetch-limited growth relationship, as formulated by Solving Equation A.3 will yield the maximum significant wave height.

$$\frac{g\, H_s(max)}{V_m^2} = 0.0016 \left(\frac{g\, F}{V_m^2} \right)^{1/2} \tag{A.3}$$

where U_{10} was replaced by V_m, an appropriate wind scaling parameter for hurricanes, F is the fetch length and g gravity.

The spectral peak frequency of the maximum waves f_m in the storm can also be found similarly using Equation A.4.

$$\frac{g}{2\pi f_m(max) V_m} = 0.045 \left(\frac{g\, F}{V_m^2} \right)^{1/3} \tag{A.4}$$

By selecting the appropriate spatial distribution diagram according to V_m and V_t, values for the ratio's $H_s/H_s(max)$ and $f_m/f_m(max)$ can be calculated.

B

Appendix B : Wind Model Validation

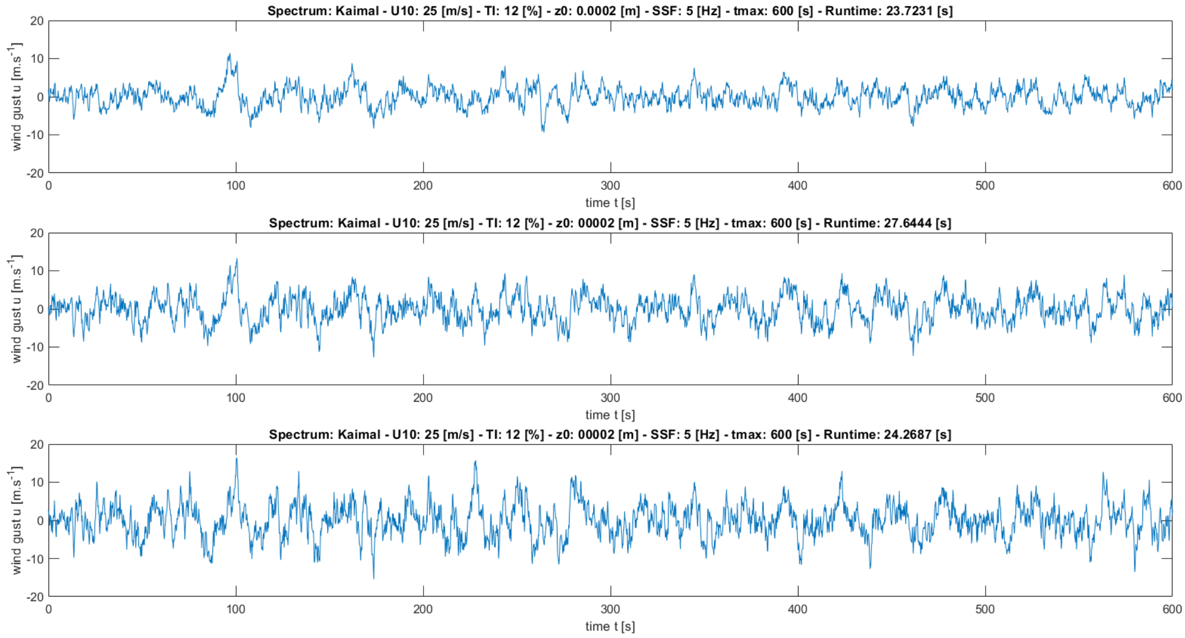

Figure B.1: Pseudo-random generated wind histories based on seed selection (1-3-5[-])

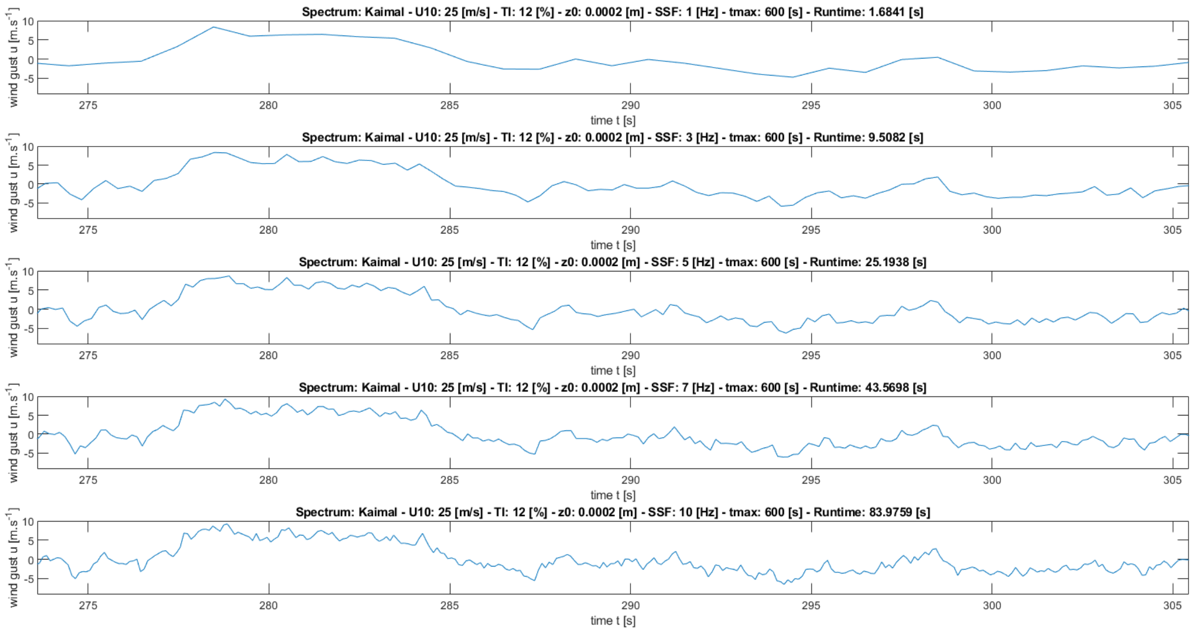

Figure B.2: Generated wind histories as a function of the Spectrum Sampling Frequency (SSF) (1-3-5-7-10[Hz]

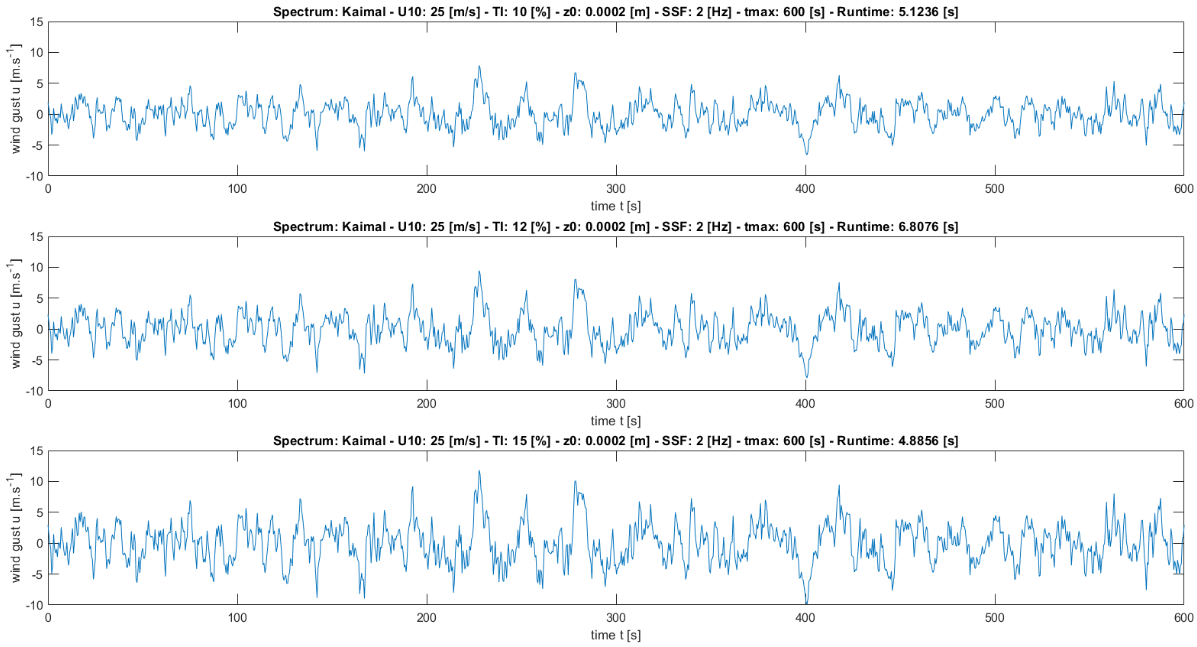

Figure B.3: Generated wind histories using the Kaimal Spectrum for a series of Turbulence intensities (10-12-15(%)

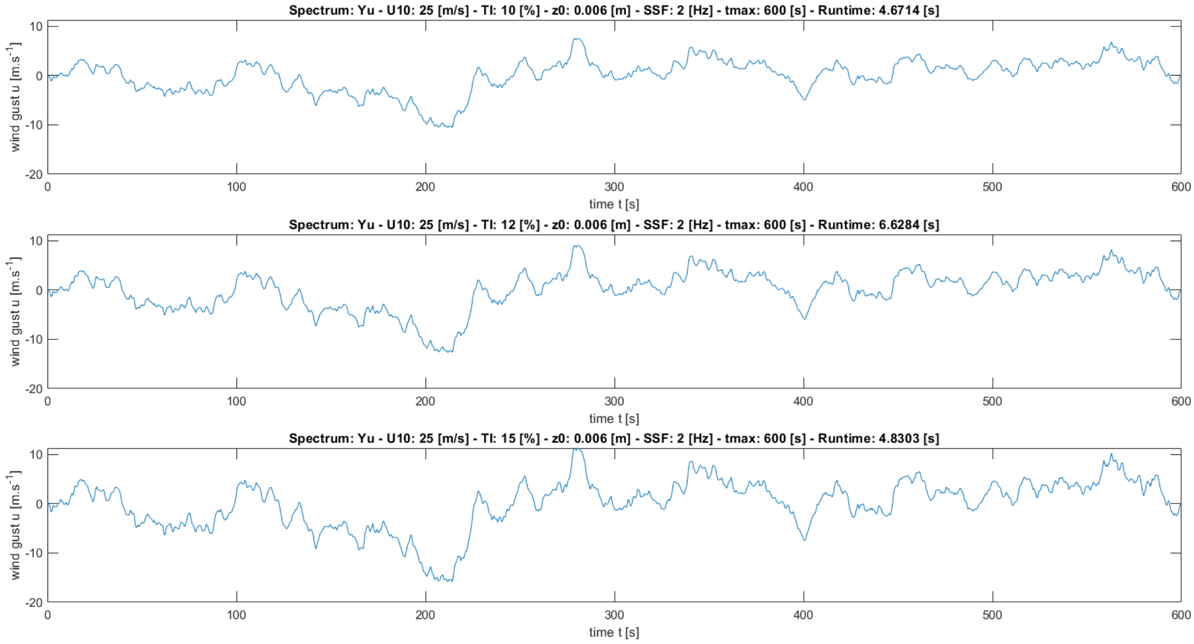

Figure B.4: Generated wind histories using the Yu Spectrum for a series of Turbulence intensities (10-12-15(%)

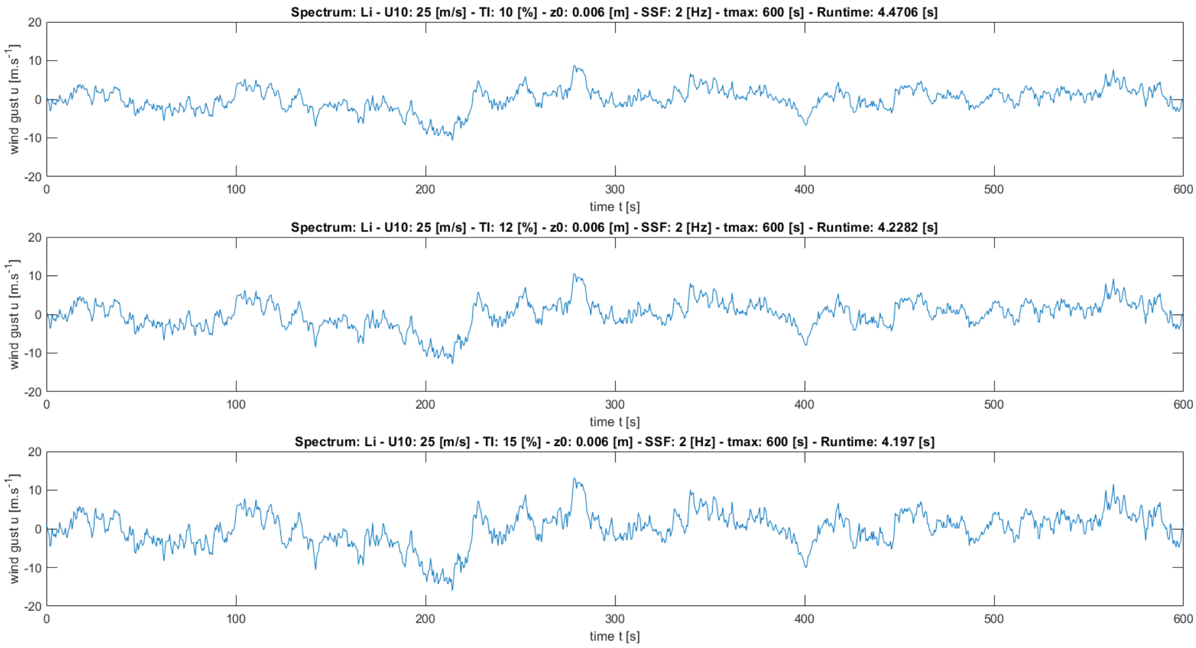

Figure B.5: Generated wind histories using the Li Spectrum for a series of Turbulence intensities (10-12-15(%)

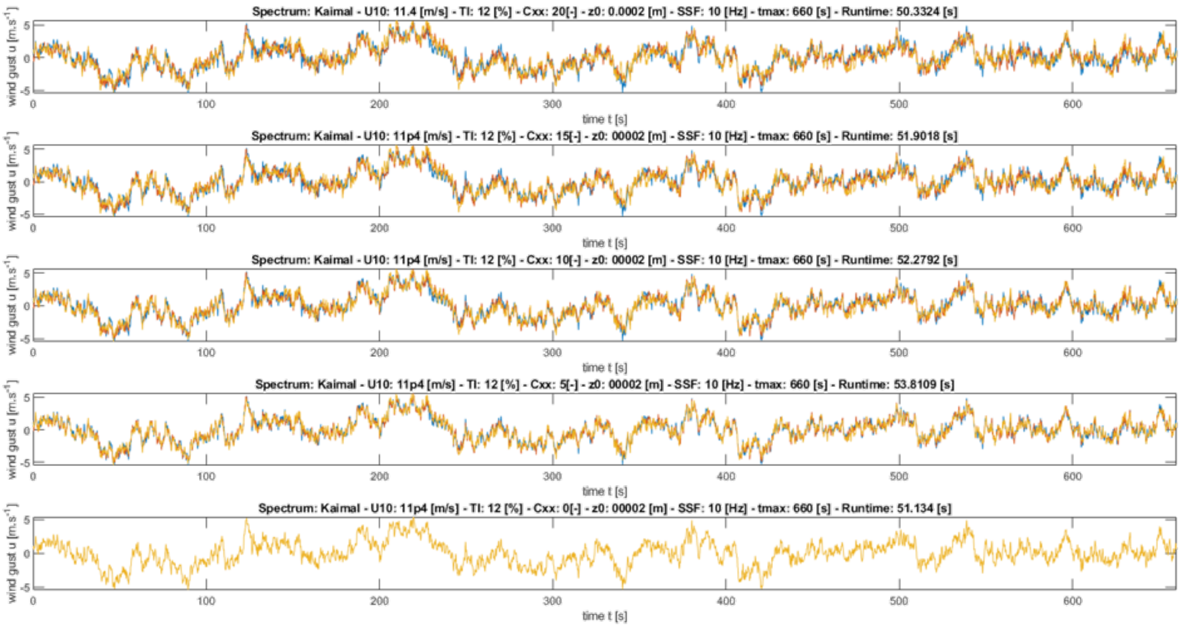

Figure B.6: Generated Hurricane wind histories (Kaimal Spectrum) as a function of the Coherence Decay Coefficients (20,15,10,5,0[-]) for the first 3 nodes

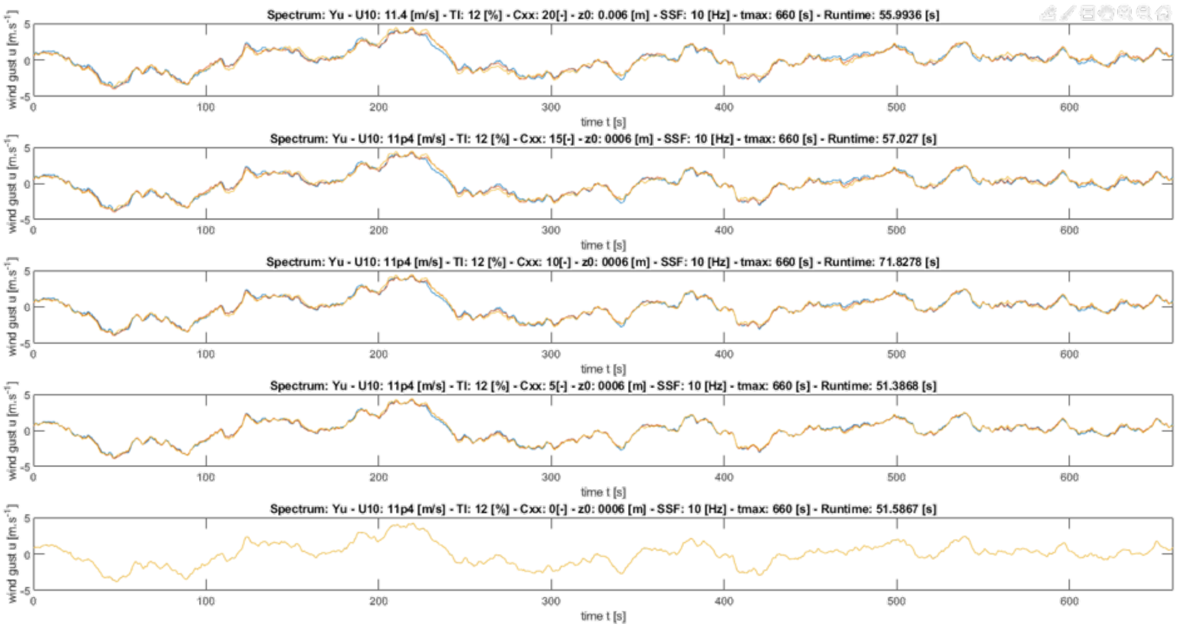

Figure B.7: Generated Hurricane wind histories (Yu Spectrum) as a function of the Coherence Decay Coefficients (20,15,10,5,0[-]) for the first 3 nodes

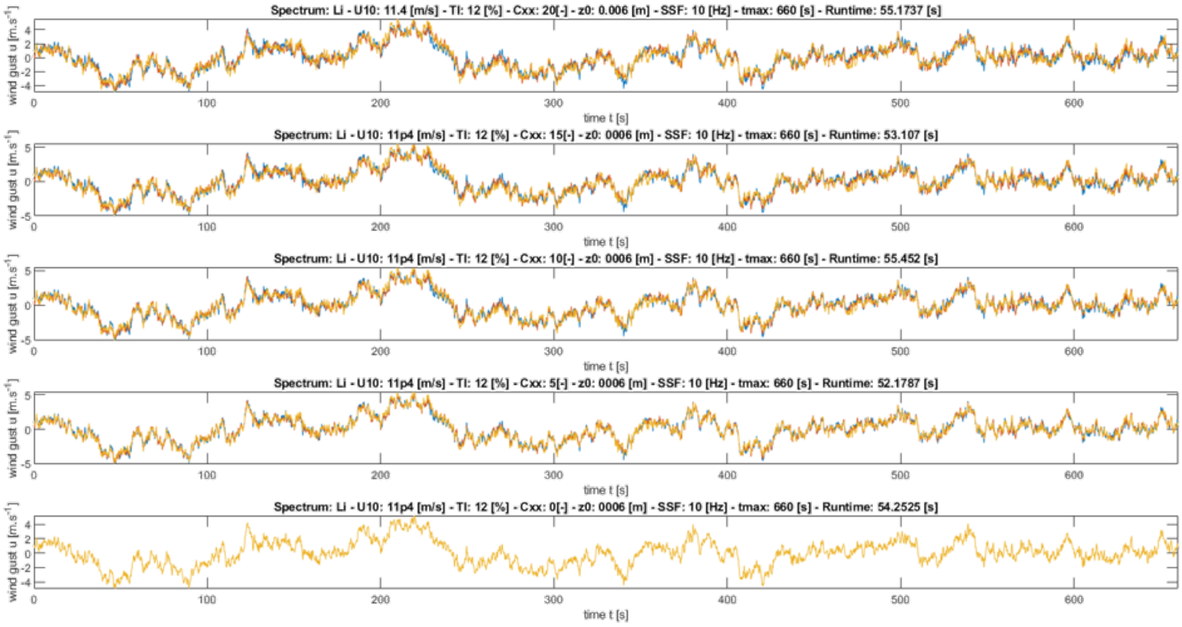

Figure B.8: Generated Hurricane wind histories (Li Spectrum) as a function of the Coherence Decay Coefficients (20,15,10,5,0[-]) for the first 3 nodes

C

Appendix C : Structural and Aero-elastic Properties of DTU's 10MW Turbine

Table C.1: General properties of the DTU 10MW turbine [9]

Cut-in wind speed $[m.s^{-1}]$	4
Cut-out wind speed $[m.s^{-1}]$	25
Rated wind speed $[m.s^{-1}]$	11.4
Number of blades $[-]$	3
Rotor Diameter $[m]$	178.3
Hub Height $[m]$	119.0

Table C.2: Full System Natural Frequencies @0 [rpm] excl. grav. loads. aerod. loads & structural damping [9]

Mode	**HAWC2** $[Hz]$	**Description**
1	0.249	1st Tower SS
2	0.251	1st Tower FA
3	0.502	1st Drive Train
4	0.547	1st Blade Asym. Flapwise Yaw
5	0.590	1st Blade Asym. Flapwise tilt
6	0.634	1st Blade Collective Flap
7	0.922	1st Blade Asym. Edgewise 1
8	0.936	1st Blade Asym. Edgewise 2
9	1.376	2nd Blade Asym. Flapwise Yaw
10	1.550	2nd Blade Asym. Flapwise tilt
11	1.763	2nd Blade Collective Flap
12	1.969	2nd Tower SS
13	2.247	2nd Tower FA

Table C.3: Blade Planform Properties (N=40) [9]

Section	x $[m]$	y $[m]$	z $[m]$	Twist $[°]$	Chord c $[m]$
1	0.00	0.00	0.00	0.00	5.38
2	0.00	0.00	2.80	-14.50	5.38
3	0.00	-0.01	5.44	-14.50	5.38
4	0.00	-0.02	8.18	-14.50	5.38
5	0.00	-0.04	11.00	-14.43	5.45
6	0.00	-0.06	13.90	-13.89	5.64
7	0.00	-0.08	16.87	-12.55	5.87
8	0.00	-0.11	19.90	-10.61	6.07
9	0.00	-0.14	22.96	-8.89	6.18
10	0.00	-0.18	26.06	-7.80	6.20
11	0.00	-0.22	29.18	-7.02	6.14
12	0.00	-0.28	32.31	-6.38	6.02
13	0.00	-0.34	35.42	-5.78	5.85
14	0.00	-0.41	38.52	-5.23	5.65
15	0.00	-0.48	41.57	-4.67	5.42
16	0.00	-0.57	44.58	-4.09	5.19
17	0.00	-0.66	47.53	-3.49	4.94
18	0.00	-0.76	50.41	-2.89	4.70
19	0.00	-0.87	53.21	-2.30	4.46
20	0.00	-0.98	55.92	-1.74	4.22
21	0.00	-1.10	58.53	-1.21	4.00
22	0.00	-1.23	61.05	-0.72	3.79
23	0.00	-1.35	63.45	-0.27	3.59
24	0.00	-1.48	65.75	0.13	3.40
25	0.00	-1.62	67.94	0.49	3.22
26	0.00	-1.75	70.01	0.82	3.06
27	0.00	-1.88	71.97	1.11	2.91
28	0.00	-2.01	73.82	1.38	2.78
29	0.00	-2.14	75.55	1.63	2.65
30	0.00	-2.26	77.19	1.86	2.54
31	0.00	-2.38	78.71	2.08	2.43
32	0.00	-2.50	80.14	2.28	2.33
33	0.00	-2.61	81.47	2.47	2.23
34	0.00	-2.72	82.71	2.64	2.13
35	0.00	-2.82	83.86	2.80	2.02
36	0.00	-2.92	84.93	2.95	1.90
37	0.00	-3.01	85.91	3.07	1.78
38	0.00	-3.10	86.83	3.18	1.63
39	0.00	-3.18	87.67	3.27	1.44
40	0.00	-3.26	88.45	3.36	1.18
41	0.00	-3.33	89.17	3.43	0.60

Table C.4: Blade Structural Properties (N=50) [9]

Section (-)	Rotor radius $[m]$	Structural Twist $[°]$	Mass / Length $[kg.m^{-1}]$	Flap.Bend. Stiff $[N.m2]$	Edge.Bend. Stiff $[N.m2]$	Flap.Shear Stiff. [N]	Edge.Shear Stiff $[N]$	Cross Section Area $[m^2]$
1	2.800	0.00	1189.51	6.19E+10	6.10E+10	2.51E+09	1.94E+09	1.41
2	4.815	0.00	1191.64	6.22E+10	6.11E+10	2.51E+09	1.95E+09	1.41
3	6.542	0.00	1202.77	6.30E+10	6.11E+10	2.49E+09	1.97E+09	1.45
4	8.269	0.00	1171.49	6.01E+10	5.81E+10	2.34E+09	1.95E+09	1.43
5	9.996	0.00	1113.62	5.46E+10	5.30E+10	2.08E+09	1.85E+09	1.47
6	11.724	-42.80	1049.31	4.41E+10	5.09E+10	1.78E+09	1.78E+09	1.46
7	13.450	-35.91	974.63	3.58E+10	4.39E+10	1.46E+09	1.65E+09	1.46
8	15.176	-25.74	908.74	2.84E+10	3.79E+10	1.17E+09	1.51E+09	1.43
9	16.904	-18.93	868.87	2.27E+10	3.38E+10	9.88E+08	1.45E+09	1.42
10	18.344	-14.28	845.51	1.91E+10	3.18E+10	8.70E+08	1.47E+09	1.38
11	20.498	-10.97	775.15	1.48E+10	2.75E+10	7.25E+08	1.25E+09	1.35
12	22.232	-8.87	735.79	1.27E+10	2.54E+10	6.80E+08	1.11E+09	1.31
13	23.959	-7.62	691.12	1.08E+10	2.29E+10	6.16E+08	9.46E+08	1.26
14	25.686	-6.79	654.85	9.33E+09	2.06E+10	5.70E+08	8.14E+08	1.23
15	27.413	-6.09	625.88	8.14E+09	1.88E+10	5.37E+08	7.18E+08	1.19
16	29.141	-4.89	593.32	6.88E+09	1.88E+10	5.02E+08	6.13E+08	1.13
17	30.868	-4.53	580.97	6.09E+09	1.77E+10	4.86E+08	6.02E+08	1.10
18	32.595	-4.25	566.23	5.40E+09	1.65E+10	4.66E+08	5.75E+08	1.07
19	34.323	-4.10	548.24	4.80E+09	1.50E+10	4.46E+08	5.65E+08	1.01
20	36.050	-3.93	529.65	4.26E+09	1.35E+10	4.20E+08	5.37E+08	0.97
21	37.778	-3.65	510.31	3.79E+09	1.24E+10	3.99E+08	5.26E+08	0.89
22	39.505	-3.35	494.68	3.35E+09	1.15E+10	3.77E+08	5.13E+08	0.86
23	41.233	-3.09	477.51	2.96E+09	1.04E+10	3.56E+08	4.84E+08	0.83
24	42.873	-2.89	460.93	2.62E+09	9.47E+09	3.38E+08	4.71E+08	0.79
25	44.601	-2.65	441.78	2.30E+09	8.50E+09	3.15E+08	4.59E+08	0.75
26	46.328	-2.41	425.33	2.01E+09	7.70E+09	2.99E+08	4.47E+08	0.71
27	48.055	-2.26	401.38	1.76E+09	6.64E+09	2.82E+08	4.18E+08	0.65
28	49.783	-2.05	385.14	1.53E+09	5.97E+09	2.64E+08	4.05E+08	0.63
29	51.510	-1.86	365.95	1.35E+09	5.33E+09	2.52E+08	3.93E+08	0.57
30	53.237	-1.70	346.94	1.17E+09	4.67E+09	2.33E+08	3.65E+08	0.54
31	55.051	-1.56	326.32	1.02E+09	3.99E+09	2.22E+08	3.51E+08	0.48
32	56.779	-1.42	310.27	8.85E+08	3.54E+09	2.09E+08	3.39E+08	0.46
33	58.506	-1.29	291.66	7.72E+08	3.05E+09	1.99E+08	3.14E+08	0.41
34	60.233	-1.19	272.43	6.68E+08	2.62E+09	1.86E+08	2.99E+08	0.37
35	61.961	-1.10	256.95	5.78E+08	2.27E+09	1.74E+08	2.88E+08	0.36
36	63.688	-1.00	237.77	5.00E+08	1.92E+09	1.63E+08	2.65E+08	0.31
37	65.354	-0.92	221.77	4.29E+08	1.67E+09	1.53E+08	2.54E+08	0.29
38	67.081	-0.87	203.15	3.63E+08	1.39E+09	1.45E+08	2.40E+08	0.25
39	68.808	-0.78	186.77	3.05E+08	1.18E+09	1.35E+08	2.20E+08	0.24
40	70.535	-0.74	171.66	2.54E+08	9.98E+08	1.26E+08	2.09E+08	0.22
41	72.324	-0.67	153.75	2.08E+08	8.15E+08	1.17E+08	1.90E+08	0.19
42	74.052	-0.65	140.05	1.71E+08	6.85E+08	1.09E+08	1.81E+08	0.17
43	75.779	-0.60	124.35	1.38E+08	5.54E+08	9.88E+07	1.75E+08	0.15
44	77.459	-0.57	108.93	1.09E+08	4.61E+08	9.09E+07	1.54E+08	0.13
45	79.186	-0.54	95.18	8.39E+07	3.59E+08	8.32E+07	1.43E+08	0.12
46	80.961	-0.57	82.34	6.31E+07	2.96E+08	7.43E+07	1.39E+08	0.10
47	82.688	-0.55	68.28	4.43E+07	2.17E+08	6.28E+07	1.23E+08	0.08
48	84.377	-0.59	54.47	2.83E+07	1.55E+08	4.96E+07	1.10E+08	0.07
49	86.143	-0.69	40.65	1.45E+07	1.00E+08	3.76E+07	9.39E+07	0.05
50	87.871	-0.79	25.20	4.50E+06	4.17E+07	2.30E+07	6.47E+07	0.04
51	89.166	-0.96	15.42	1.03E+06	1.27E+07	1.23E+07	3.86E+07	0.03

D

Appendix D : Deflections, Forces and Bending Moments Full Simulation Results

Full Simulation Results

Table D.1: Out-of-plane (OP) deflections (δ), Forces (F) and Bending Moments (M) for the Kaimal Spectrum simulations

Kaimal		Deflection δ [m]				Force F [kN]				Moment M [MNm]			
U_{10} [m/s]	T [years]	δ_y 5%	δ_y 50%	δ_y 95%	σ	F_y 5%	F_y 50%	F_y 95%	σ	M_x 5%	M_x 50%	M_x 95%	σ
11.4	Rated	0.002	0.003	0.004	0.001	0.210	0.314	0.418	0.063	0.004	0.007	0.009	0.00
30.6	[H1	0.016	0.023	0.030	0.004	1.556	2.239	2.922	0.415	0.033	0.047	0.061	0.01
36.5	10	0.022	0.032	0.043	0.006	2.154	3.198	4.242	0.635	0.045	0.067	0.089	0.01
40.1	[H2	0.026	0.039	0.051	0.007	2.606	3.812	5.019	0.733	0.055	0.080	0.105	0.02
44.9	25	0.032	0.049	0.065	0.010	3.159	4.804	6.449	1.000	0.066	0.101	0.135	0.02
46.8	[H3	0.035	0.053	0.071	0.011	3.452	5.226	6.999	1.078	0.072	0.109	0.146	0.02
50.1	50	0.038	0.061	0.084	0.014	3.782	6.023	8.265	1.363	0.079	0.126	0.173	0.03
54.5	100	0.047	0.072	0.096	0.015	4.684	7.092	9.500	1.464	0.098	0.148	0.199	0.03
55.4	[H4	0.048	0.074	0.101	0.016	4.719	7.322	9.925	1.583	0.099	0.153	0.208	0.03
58.2	200	0.051	0.082	0.112	0.019	5.047	8.070	11.093	1.838	0.106	0.169	0.232	0.04
66.9	[H5	0.067	0.109	0.152	0.026	6.569	10.764	14.960	2.551	0.137	0.225	0.313	0.05
69.5	1000	0.075	0.119	0.163	0.027	7.356	11.734	16.113	2.662	0.154	0.246	0.337	0.06
72.5	2000	0.080	0.128	0.176	0.029	7.880	12.598	17.316	2.868	0.165	0.264	0.362	0.06
78.7	10000	0.089	0.151	0.213	0.038	8.768	14.898	21.028	3.727	0.183	0.312	0.440	0.08

Table D.2: In-plane (IP) deflections (δ), Forces (F) and Bending Moments (M) for the Kaimal Spectrum simulations

Kaimal		Deflection δ [m]				Force F [kN]				Moment M [MNm]			
U_{10} [m/s]	T [years]	δ_x 5%	δ_x 50%	δ_x 95%	σ	F_x 5%	F_x 50%	F_x 95%	σ	M_y 5%	M_y 50%	M_y 95%	σ
11.40	Rated	0.004	0.017	0.031	0.008	-3.23	-5.05	-6.87	1.11	-0.47	-1.47	-2.46	0.61
30.60	[H1	0.040	0.125	0.211	0.052	-25.11	-35.99	-46.88	6.62	-4.36	-10.58	-16.80	3.78
36.50	10	0.064	0.176	0.289	0.068	-36.32	-51.62	-66.91	9.30	-6.72	-14.94	-23.16	5.00
40.10	[H2	0.085	0.211	0.338	0.077	-43.57	-61.32	-79.06	10.79	-8.64	-17.88	-27.13	5.62
44.90	25	0.099	0.266	0.434	0.102	-53.94	-77.33	-100.72	14.22	-10.21	-22.54	-34.88	7.50
46.80	[H3	0.128	0.289	0.449	0.098	-59.41	-84.14	-108.87	15.04	-12.56	-24.44	-36.32	7.22
50.10	50	0.144	0.334	0.524	0.116	-67.28	-96.93	-126.59	18.03	-14.11	-28.27	-42.44	8.61
54.50	100	0.170	0.396	0.623	0.138	-80.84	-113.92	-147.01	20.11	-16.88	-33.49	-50.10	10.10
55.40	[H4	0.176	0.403	0.630	0.138	-85.71	-117.91	-150.11	19.58	-17.51	-34.16	-50.81	10.12
58.20	200	0.205	0.444	0.684	0.146	-92.08	-130.03	-167.97	23.07	-19.90	-37.64	-55.38	10.79
66.90	[H5	0.294	0.596	0.898	0.184	-122.38	-173.21	-224.05	30.91	-28.02	-50.43	-72.84	13.62
69.50	1000	0.309	0.650	0.991	0.207	-134.53	-188.68	-242.83	32.92	-29.58	-55.00	-80.41	15.45
72.50	2000	0.326	0.695	1.063	0.224	-147.16	-203.43	-259.70	34.21	-31.66	-58.86	-86.05	16.53
78.70	10000	0.428	0.826	1.224	0.242	-172.95	-239.68	-306.42	40.57	-40.20	-69.91	-99.62	18.07

Table D.3: Out-of-plane deflections (δ) and Forces (F) and Bending Moments (M) for the Yu Spectrum simulations

Yu		Deflection δ [m]				Force F [kN]				Moment M [MNm]			
U_{10} [m/s]	T [years]	δ_y 5%	δ_y 50%	δ_y 95%	σ	F_y 5%	F_y 50%	F_y 95%	σ	M_x 5%	M_x 50%	M_x 95%	σ
11.4	Rated	0.003	0.004	0.005	0.001	0.248	0.376	0.505	0.078	0.005	0.008	0.011	0.002
30.6	[H1	0.017	0.027	0.037	0.006	1.725	2.677	3.629	0.579	0.036	0.056	0.076	0.012
36.5	10	0.026	0.039	0.051	0.008	2.575	3.810	5.044	0.751	0.054	0.080	0.106	0.016
40.1	[H2	0.032	0.047	0.063	0.010	3.131	4.677	6.222	0.940	0.066	0.098	0.130	0.020
44.9	25	0.040	0.059	0.078	0.012	3.914	5.819	7.723	1.158	0.082	0.122	0.162	0.024
46.8	[H3	0.045	0.064	0.084	0.012	4.457	6.359	8.261	1.156	0.093	0.133	0.173	0.024
50.1	50	0.047	0.072	0.097	0.015	4.663	7.140	9.617	1.506	0.098	0.149	0.201	0.032
54.5	100	0.059	0.088	0.116	0.018	5.802	8.643	11.484	1.727	0.121	0.181	0.240	0.036
55.4	[H4	0.062	0.091	0.120	0.018	6.080	8.981	11.883	1.764	0.127	0.188	0.249	0.037
58.2	200	0.067	0.100	0.133	0.020	6.574	9.831	13.088	1.980	0.138	0.206	0.274	0.041
66.9	[H5	0.085	0.130	0.176	0.028	8.369	12.858	17.348	2.729	0.175	0.269	0.363	0.057
69.5	1000	0.093	0.141	0.189	0.029	9.151	13.917	18.682	2.897	0.191	0.291	0.391	0.061
72.5	2000	0.103	0.156	0.209	0.032	10.168	15.371	20.575	3.163	0.213	0.322	0.430	0.066
78.7	10000	0.123	0.182	0.241	0.036	12.093	17.953	23.812	3.562	0.253	0.376	0.498	0.075

Table D.4: In-plane deflections (δ), Forces (F) and Bending Moments (M) for the Yu Spectrum simulations

Yu		Deflection δ [m]				Force F [kN]				Moment M [MNm]			
U_{10} [m/s]	T [years]	δ_x 5%	δ_x 50%	δ_x 95%	σ	F_x 5%	F_x 50%	F_x 95%	σ	M_y 5%	M_y 50%	M_y 95%	σ
11.400	Rated	0.006	0.020	0.034	0.009	-4.075	-6.082	-8.089	1.220	-0.657	-1.722	-2.787	0.647
30.600	[H1	0.059	0.143	0.228	0.051	-28.214	-43.302	-58.390	9.173	-5.767	-12.184	-18.600	3.901
36.500	10	0.104	0.204	0.304	0.061	-40.982	-61.681	-82.380	12.584	-9.728	-17.343	-24.958	4.630
40.100	[H2	0.106	0.251	0.395	0.088	-51.418	-75.641	-99.864	14.726	-10.353	-21.321	-32.288	6.668
44.900	25	0.154	0.314	0.475	0.097	-62.753	-94.117	-125.482	19.068	-14.481	-26.711	-38.941	7.435
46.800	[H3	0.166	0.339	0.513	0.105	-71.733	-103.232	-134.730	19.150	-15.793	-28.916	-42.039	7.978
50.100	50	0.188	0.383	0.579	0.119	-74.699	-115.511	-156.323	24.812	-17.642	-32.593	-47.544	9.089
54.500	100	0.207	0.461	0.715	0.154	-96.086	-139.971	-183.856	26.680	-19.783	-39.265	-58.748	11.845
55.400	[H4	0.236	0.482	0.727	0.149	-99.494	-145.268	-191.042	27.829	-22.142	-40.972	-59.802	11.448
58.200	200	0.276	0.520	0.765	0.149	-105.993	-159.372	-212.750	32.452	-25.653	-44.369	-63.084	11.378
66.900	[H5	0.368	0.687	1.005	0.194	-135.608	-208.181	-280.755	44.122	-33.882	-58.459	-83.036	14.942
69.500	1000	0.411	0.741	1.071	0.200	-148.656	-225.565	-302.473	46.757	-37.448	-63.127	-88.806	15.612
72.500	2000	0.414	0.823	1.233	0.249	-167.554	-249.062	-330.569	49.553	-38.430	-70.083	-101.736	19.244
78.700	10000	0.487	0.959	1.430	0.287	-199.227	-290.334	-381.441	55.389	-45.491	-81.601	-117.712	21.954

Table D.5: Out-of-plane deflections (δ), Forces (F) and Bending Moments (M) for the Li Spectrum simulations

Li		Deflection δ [m]				Force F [kN]				Moment M [MNm]			
U_{10} [m/s]	T [years]	δ_y 5%	δ_y 50%	δ_y 95%	σ	F_y 5%	F_y 50%	F_y 95%	σ	M_x 5%	M_x 50%	M_x 95%	σ
11.4	Rated	0.003	0.004	0.005	0.001	0.259	0.375	0.491	0.071	0.005	0.008	0.010	0.001
30.6	[H1	0.019	0.027	0.035	0.005	1.843	2.661	3.479	0.497	0.039	0.056	0.073	0.010
36.5	10	0.027	0.039	0.051	0.007	2.628	3.831	5.034	0.732	0.055	0.080	0.105	0.015
40.1	[H2	0.032	0.046	0.061	0.009	3.118	4.555	5.993	0.874	0.065	0.095	0.125	0.018
44.9	25	0.040	0.059	0.077	0.011	3.985	5.789	7.593	1.097	0.083	0.121	0.159	0.023
46.8	[H3	0.044	0.065	0.085	0.012	4.343	6.364	8.386	1.229	0.091	0.133	0.175	0.026
50.1	50	0.051	0.073	0.094	0.013	5.007	7.164	9.320	1.311	0.105	0.150	0.195	0.027
54.5	100	0.059	0.085	0.110	0.015	5.855	8.355	10.855	1.520	0.123	0.175	0.227	0.032
55.4	[H4	0.059	0.089	0.119	0.018	5.821	8.765	11.709	1.790	0.122	0.183	0.245	0.037
58.2	200	0.066	0.099	0.132	0.020	6.462	9.747	13.033	1.998	0.135	0.204	0.273	0.042
66.9	[H5	0.084	0.130	0.176	0.028	8.244	12.786	17.328	2.761	0.172	0.268	0.363	0.058
69.5	1000	0.093	0.140	0.187	0.029	9.142	13.776	18.410	2.817	0.191	0.288	0.385	0.059
72.5	2000	0.099	0.152	0.204	0.032	9.768	14.950	20.132	3.150	0.204	0.313	0.421	0.066
78.7	10000	0.115	0.180	0.246	0.040	11.301	17.761	24.221	3.927	0.236	0.372	0.507	0.082

Table D.6: In-plane deflections (δ), Forces (F) and Bending Moments (M) for the Li Spectrum simulations

Li		Deflection δ [m]				Force F [kN]				Moment M [MNm]			
U_{10} [m/s]	T [years]	δ_x 5%	δ_x 50%	δ_x 95%	σ	F_x 5%	F_x 50%	F_x 95%	σ	M_y 5%	M_y 50%	M_y 95%	σ
11.400	Rated	0.006	0.020	0.034	0.008	-3.874	-6.076	-8.278	1.339	-0.720	-1.706	-2.691	0.599
30.600	[H1	0.062	0.142	0.221	0.048	-30.298	-43.121	-55.944	7.796	-6.204	-12.061	-17.917	3.560
36.500	10	0.085	0.204	0.322	0.072	-43.598	-62.119	-80.639	11.260	-8.511	-17.351	-26.190	5.374
40.100	[H2	0.092	0.244	0.395	0.092	-52.643	-73.718	-94.793	12.813	-9.577	-20.752	-31.926	6.794
44.900	25	0.140	0.309	0.477	0.103	-67.250	-93.855	-120.460	16.175	-13.728	-26.298	-38.868	7.642
46.800	[H3	0.166	0.340	0.513	0.106	-73.903	-103.163	-132.423	17.789	-15.969	-28.920	-41.870	7.873
50.100	50	0.187	0.383	0.579	0.119	-84.060	-116.110	-148.160	19.485	-18.105	-32.624	-47.142	8.827
54.500	100	0.229	0.448	0.668	0.133	-101.404	-135.192	-168.980	20.541	-21.875	-38.150	-54.425	9.894
55.400	[H4	0.249	0.470	0.692	0.135	-98.629	-141.873	-185.117	26.290	-23.395	-40.028	-56.661	10.112
58.200	200	0.263	0.521	0.780	0.157	-111.626	-157.758	-203.889	28.046	-24.980	-44.377	-63.774	11.793
66.900	[H5	0.359	0.682	1.005	0.196	-148.362	-207.421	-266.481	35.906	-33.748	-58.070	-82.391	14.786
69.500	1000	0.383	0.732	1.080	0.212	-161.829	-223.394	-284.960	37.429	-36.341	-62.351	-88.361	15.813
72.500	2000	0.430	0.798	1.167	0.224	-176.331	-242.488	-308.645	40.220	-40.164	-67.994	-95.824	16.919
78.700	10000	0.566	0.945	1.324	0.230	-208.753	-288.204	-367.654	48.302	-51.895	-80.504	-109.114	17.393

Blade Response Ratios

Table D.7: Out-of-plane Yu Spectrum Blade Response Ratios

Yu	Deflection γ_δ [-]			Force γ_F [-]			Moment γ_M [-]		
$U_1 0$ [m/s]	$\gamma_{\delta y}$ 5%	$\gamma_{\delta y}$ 50%	γ_δ 95%	γ_{Fy} 5%	γ_{Fy} 50%	γ_{Fy} 95%	γ_{Mx} 5%	γ_{Mx} 50%	γ_{Mx} 95%
11.4	1.18	1.20	1.21	1.18	1.20	1.21	1.18	1.20	1.21
30.6	1.11	1.20	1.24	1.11	1.20	1.24	1.11	1.20	1.24
36.5	1.20	1.19	1.19	1.20	1.19	1.19	1.20	1.19	1.19
40.1	1.20	1.23	1.24	1.20	1.23	1.24	1.20	1.23	1.24
44.9	1.24	1.21	1.20	1.24	1.21	1.20	1.24	1.21	1.20
46.8	1.29	1.22	1.18	1.29	1.22	1.18	1.29	1.22	1.18
50.1	1.23	1.19	1.16	1.23	1.19	1.16	1.23	1.19	1.16
54.5	1.24	1.22	1.21	1.24	1.22	1.21	1.24	1.22	1.21
55.4	1.29	1.23	1.20	1.29	1.23	1.20	1.29	1.23	1.20
58.2	1.30	1.22	1.18	1.30	1.22	1.18	1.30	1.22	1.18
66.9	1.27	1.19	1.16	1.27	1.19	1.16	1.27	1.19	1.16
69.5	1.24	1.19	1.16	1.24	1.19	1.16	1.24	1.19	1.16
72.5	1.29	1.22	1.19	1.29	1.22	1.19	1.29	1.22	1.19
78.7	1.38	1.21	1.13	1.38	1.21	1.13	1.38	1.21	1.13

Table D.8: In-plane Yu Spectrum Blade Response Ratios

Yu	Deflection γ_δ [-]			Force γ_F [-]			Moment γ_M [-]		
U_{10} [m/s]	$\gamma_{\delta x}$ 5%	$\gamma_{\delta x}$ 50%	$\gamma_{\delta x}$ 95%	γ_{Fx} 5%	γ_{Fx} 50%	γ_{Fx} 95%	γ_{My} 5%	γ_{My} 50%	γ_{My} 95%
11.4	1.72	1.17	1.11	1.26	1.20	1.18	1.40	1.17	1.13
30.6	1.48	1.14	1.08	1.12	1.20	1.25	1.32	1.15	1.11
36.5	1.62	1.16	1.05	1.13	1.20	1.23	1.45	1.16	1.08
40.1	1.25	1.19	1.17	1.18	1.23	1.26	1.20	1.19	1.19
44.9	1.56	1.18	1.09	1.16	1.22	1.25	1.42	1.18	1.12
46.8	1.30	1.18	1.14	1.21	1.23	1.24	1.26	1.18	1.16
50.1	1.30	1.15	1.10	1.11	1.19	1.23	1.25	1.15	1.12
54.5	1.22	1.16	1.15	1.19	1.23	1.25	1.17	1.17	1.17
55.4	1.34	1.19	1.15	1.16	1.23	1.27	1.26	1.20	1.18
58.2	1.35	1.17	1.12	1.15	1.23	1.27	1.29	1.18	1.14
66.9	1.25	1.15	1.12	1.11	1.20	1.25	1.21	1.16	1.14
69.5	1.33	1.14	1.08	1.11	1.20	1.25	1.27	1.15	1.10
72.5	1.27	1.19	1.16	1.14	1.22	1.27	1.21	1.19	1.18
78.7	1.14	1.16	1.17	1.15	1.21	1.24	1.13	1.17	1.18

Table D.9: Out-of-plane Li Spectrum Blade Response Ratios

Li	Deflection γ_δ [-]			Force γ_F [-]			Moment γ_M [-]		
$U_1 0$ [m/s]	$\gamma_{\delta y}$ 5%	$\gamma_{\delta y}$ 50%	γ_δ 95%	γ_{Fy} 5%	γ_{Fy} 50%	γ_{Fy} 95%	γ_{Mx} 5%	γ_{Mx} 50%	γ_{Mx} 95%
11.4	1.23	1.19	1.18	1.23	1.19	1.18	1.23	1.19	1.18
30.6	1.18	1.19	1.19	1.18	1.19	1.19	1.18	1.19	1.19
36.5	1.22	1.20	1.19	1.22	1.20	1.19	1.22	1.20	1.19
40.1	1.20	1.19	1.19	1.20	1.19	1.19	1.20	1.19	1.19
44.9	1.26	1.21	1.18	1.26	1.21	1.18	1.26	1.21	1.18
46.8	1.26	1.22	1.20	1.26	1.22	1.20	1.26	1.22	1.20
50.1	1.32	1.19	1.13	1.32	1.19	1.13	1.32	1.19	1.13
54.5	1.25	1.18	1.14	1.25	1.18	1.14	1.25	1.18	1.14
55.4	1.23	1.20	1.18	1.23	1.20	1.18	1.23	1.20	1.18
58.2	1.28	1.21	1.17	1.28	1.21	1.17	1.28	1.21	1.17
66.9	1.26	1.19	1.16	1.26	1.19	1.16	1.26	1.19	1.16
69.5	1.24	1.17	1.14	1.24	1.17	1.14	1.24	1.17	1.14
72.5	1.24	1.19	1.16	1.24	1.19	1.16	1.24	1.19	1.16
78.7	1.29	1.19	1.15	1.29	1.19	1.15	1.29	1.19	1.15

Table D.10: In-plane Li Spectrum Blade Response Ratios

Li	Deflection γ_δ [-]			Force γ_F [-]			Moment γ_M [-]		
U_{10} [m/s]	$\gamma_{\delta x}$ 5%	$\gamma_{\delta x}$ 50%	$\gamma_{\delta x}$ 95%	γ_{Fx} 5%	γ_{Fx} 50%	γ_{Fx} 95%	γ_{My} 5%	γ_{My} 50%	γ_{My} 95%
11.4	1.77	1.16	1.09	1.20	1.20	1.20	1.53	1.16	1.09
30.6	1.56	1.13	1.05	1.21	1.20	1.19	1.42	1.14	1.07
36.5	1.33	1.15	1.12	1.20	1.20	1.21	1.27	1.16	1.13
40.1	1.09	1.15	1.17	1.21	1.20	1.20	1.11	1.16	1.18
44.9	1.42	1.16	1.10	1.25	1.21	1.20	1.35	1.17	1.11
46.8	1.30	1.18	1.14	1.24	1.23	1.22	1.27	1.18	1.15
50.1	1.30	1.15	1.11	1.25	1.20	1.17	1.28	1.15	1.11
54.5	1.35	1.13	1.07	1.25	1.19	1.15	1.30	1.14	1.09
55.4	1.41	1.17	1.10	1.15	1.20	1.23	1.34	1.17	1.12
58.2	1.28	1.17	1.14	1.21	1.21	1.21	1.26	1.18	1.15
66.9	1.22	1.14	1.12	1.21	1.20	1.19	1.20	1.15	1.13
69.5	1.24	1.13	1.09	1.20	1.18	1.17	1.23	1.13	1.10
72.5	1.32	1.15	1.10	1.20	1.19	1.19	1.27	1.16	1.11
78.7	1.32	1.14	1.08	1.21	1.20	1.20	1.29	1.15	1.10

Model Linearity Properties

Table D.11: Model Linearity Properties for Kaimal Spectrum OP simulations

Kaimal		Deflection γ_δ [-]			Force γ_F [-]			Moment γ_M [-]		
U_{10} [m/s]	γ [-]	$\gamma_{\delta y}$ 5%	$\gamma_{\delta y}$ 50%	$\gamma_{\delta y}$ 95%	γ_{Fy} 5%	γ_{Fy} 50%	γ_{Fy} 95%	γ_{Mx} 5%	γ_{Mx} 50%	γ_{Mx} 95%
11.4	1.00	1.00	1.00	1.00	1.00	1.00	1.00	1.00	1.00	1.00
30.6	2.68	2.72	2.67	2.65	2.72	2.67	2.65	2.72	2.67	2.65
36.5	3.20	3.20	3.19	3.19	3.20	3.19	3.19	3.20	3.19	3.19
40.1	3.52	3.52	3.48	3.47	3.52	3.48	3.47	3.52	3.48	3.47
44.9	3.94	3.87	3.91	3.93	3.87	3.91	3.93	3.87	3.91	3.93
46.8	4.11	4.05	4.08	4.09	4.05	4.08	4.09	4.05	4.08	4.09
50.1	4.39	4.24	4.38	4.45	4.24	4.38	4.45	4.24	4.38	4.45
54.5	4.78	4.72	4.75	4.77	4.72	4.75	4.77	4.72	4.75	4.77
55.4	4.86	4.74	4.83	4.88	4.74	4.83	4.88	4.74	4.83	4.88
58.2	5.11	4.90	5.07	5.15	4.90	5.07	5.15	4.90	5.07	5.15
66.9	5.87	5.59	5.86	5.99	5.59	5.86	5.99	5.59	5.86	5.99
69.5	6.10	5.91	6.11	6.21	5.91	6.11	6.21	5.91	6.11	6.21
72.5	6.36	6.12	6.33	6.44	6.12	6.33	6.44	6.12	6.33	6.44
78.7	6.90	6.46	6.89	7.10	6.46	6.89	7.10	6.46	6.89	7.10

Table D.12: Model Linearity Properties for Kaimal Spectrum IP simulations

Kaimal	Deflection γ_δ [-]			Force γ_F [-]			Moment γ_M [-]		
U_{10} [m/s]	$\gamma_{\delta x}$ 5%	$\gamma_{\delta x}$ 50%	$\gamma_{\delta x}$ 95%	γ_{Fx} 5%	γ_{Fx} 50%	γ_{Fx} 95%	γ_{My} 5%	γ_{My} 50%	γ_{My} 95%
11.4	1.00	1.00	1.00	1.00	1.00	1.00	1.00	1.00	1.00
30.6	3.33	2.69	2.61	2.79	2.67	2.61	3.04	2.69	2.61
36.5	4.24	3.19	3.05	3.35	3.20	3.12	3.78	3.19	3.07
40.1	4.89	3.49	3.30	3.67	3.48	3.39	4.28	3.49	3.32
44.9	5.27	3.92	3.74	4.08	3.91	3.83	4.66	3.92	3.76
46.8	6.00	4.08	3.80	4.29	4.08	3.98	5.17	4.08	3.84
50.1	6.36	4.39	4.11	4.56	4.38	4.29	5.48	4.39	4.15
54.5	6.91	4.79	4.48	5.00	4.75	4.63	5.99	4.78	4.51
55.4	7.03	4.83	4.51	5.15	4.83	4.67	6.10	4.83	4.54
58.2	7.59	5.07	4.69	5.34	5.07	4.94	6.50	5.07	4.74
66.9	9.08	5.87	5.38	6.15	5.85	5.71	7.72	5.87	5.44
69.5	9.32	6.13	5.65	6.45	6.11	5.94	7.93	6.13	5.72
72.5	9.57	6.34	5.85	6.75	6.34	6.15	8.20	6.34	5.91
78.7	10.97	6.91	6.28	7.31	6.89	6.68	9.24	6.91	6.36

Table D.13: Model Linearity Properties for Yu Spectrum OP simulations

Yu		Deflection γ_δ [-]			Force γ_F [-]			Moment γ_M [-]		
U_{10} [m/s]	γ [-]	$\gamma_{\delta y}$ 5%	$\gamma_{\delta y}$ 50%	$\gamma_{\delta y}$ 95%	γ_{Fy} 5%	γ_{Fy} 50%	γ_{Fy} 95%	γ_{Mx} 5%	γ_{Mx} 50%	γ_{Mx} 95%
11.4	1.00	1.00	1.00	1.00	1.00	1.00	1.00	1.00	1.00	1.00
30.6	2.68	2.64	2.67	2.68	2.64	2.67	2.68	2.64	2.67	2.68
36.5	3.20	3.22	3.18	3.16	3.22	3.18	3.16	3.22	3.18	3.16
40.1	3.52	3.56	3.52	3.51	3.56	3.52	3.51	3.56	3.52	3.51
44.9	3.94	3.97	3.93	3.91	3.97	3.93	3.91	3.97	3.93	3.91
46.8	4.11	4.24	4.11	4.04	4.24	4.11	4.04	4.24	4.11	4.04
50.1	4.39	4.34	4.36	4.36	4.34	4.36	4.36	4.34	4.36	4.36
54.5	4.78	4.84	4.79	4.77	4.84	4.79	4.77	4.84	4.79	4.77
55.4	4.86	4.95	4.88	4.85	4.95	4.88	4.85	4.95	4.88	4.85
58.2	5.11	5.15	5.11	5.09	5.15	5.11	5.09	5.15	5.11	5.09
66.9	5.87	5.81	5.84	5.86	5.81	5.84	5.86	5.81	5.84	5.86
69.5	6.10	6.08	6.08	6.08	6.08	6.08	6.08	6.08	6.08	6.08
72.5	6.36	6.41	6.39	6.38	6.41	6.39	6.38	6.41	6.39	6.38
78.7	6.90	6.99	6.91	6.87	6.99	6.91	6.87	6.99	6.91	6.87

Table D.14: Model Linearity Properties for Yu Spectrum IP simulations

Yu	Deflection γ_δ [-]			Force γ_F [-]			Moment γ_M [-]		
U_{10} [m/s]	$\gamma_{\delta x}$ 5%	$\gamma_{\delta x}$ 50%	$\gamma_{\delta x}$ 95%	γ_{Fx} 5%	γ_{Fx} 50%	γ_{Fx} 95%	γ_{My} 5%	γ_{My} 50%	γ_{My} 95%
11.4	1.00	1.00	1.00	1.00	1.00	1.00	1.00	1.00	1.00
30.6	3.09	2.66	2.57	2.63	2.67	2.69	2.96	2.66	2.58
36.5	4.11	3.17	2.97	3.17	3.18	3.19	3.85	3.17	2.99
40.1	4.16	3.52	3.39	3.55	3.53	3.51	3.97	3.52	3.40
44.9	5.01	3.94	3.72	3.92	3.93	3.94	4.69	3.94	3.74
46.8	5.20	4.09	3.86	4.20	4.12	4.08	4.90	4.10	3.88
50.1	5.53	4.35	4.10	4.28	4.36	4.40	5.18	4.35	4.13
54.5	5.81	4.77	4.56	4.86	4.80	4.77	5.49	4.78	4.59
55.4	6.20	4.88	4.60	4.94	4.89	4.86	5.81	4.88	4.63
58.2	6.70	5.07	4.72	5.10	5.12	5.13	6.25	5.08	4.76
66.9	7.74	5.82	5.41	5.77	5.85	5.89	7.18	5.83	5.46
69.5	8.18	6.05	5.58	6.04	6.09	6.12	7.55	6.05	5.64
72.5	8.21	6.38	5.99	6.41	6.40	6.39	7.65	6.38	6.04
78.7	8.91	6.88	6.45	6.99	6.91	6.87	8.32	6.88	6.50

Table D.15: Model Linearity Properties for Li Spectrum OP simulations

Li		Deflection γ_δ [-]			Force γ_F [-]			Moment γ_M [-]		
U_{10} [m/s]	γ [-]	$\gamma_{\delta y}$ 5%	$\gamma_{\delta y}$ 50%	$\gamma_{\delta y}$ 95%	γ_{Fy} 5%	γ_{Fy} 50%	γ_{Fy} 95%	γ_{Mx} 5%	γ_{Mx} 50%	γ_{Mx} 95%
11.4	1.00	1.00	1.00	1.00	1.00	1.00	1.00	1.00	1.00	1.00
30.6	2.68	2.67	2.66	2.66	2.67	2.66	2.66	2.67	2.66	2.66
36.5	3.20	3.19	3.20	3.20	3.19	3.20	3.20	3.19	3.20	3.20
40.1	3.52	3.47	3.48	3.49	3.47	3.48	3.49	3.47	3.48	3.49
44.9	3.94	3.92	3.93	3.93	3.92	3.93	3.93	3.92	3.93	3.93
46.8	4.11	4.10	4.12	4.13	4.10	4.12	4.13	4.10	4.12	4.13
50.1	4.39	4.40	4.37	4.36	4.40	4.37	4.36	4.40	4.37	4.36
54.5	4.78	4.76	4.72	4.70	4.76	4.72	4.70	4.76	4.72	4.70
55.4	4.86	4.74	4.83	4.88	4.74	4.83	4.88	4.74	4.83	4.88
58.2	5.11	5.00	5.10	5.15	5.00	5.10	5.15	5.00	5.10	5.15
66.9	5.87	5.64	5.84	5.94	5.64	5.84	5.94	5.64	5.84	5.94
69.5	6.10	5.94	6.06	6.12	5.94	6.06	6.12	5.94	6.06	6.12
72.5	6.36	6.14	6.31	6.40	6.14	6.31	6.40	6.14	6.31	6.40
78.7	6.90	6.61	6.88	7.02	6.61	6.88	7.02	6.61	6.88	7.02

Table D.16: Model Linearity Properties for Li IP Spectrum simulations

Li	Deflection γ_δ [-]			Force γ_F [-]			Moment γ_M [-]		
U_{10} [m/s]	$\gamma_{\delta x}$ 5%	$\gamma_{\delta x}$ 50%	$\gamma_{\delta x}$ 95%	γ_{Fx} 5%	γ_{Fx} 50%	γ_{Fx} 95%	γ_{My} 5%	γ_{My} 50%	γ_{My} 95%
11.4	1.00	1.00	1.00	1.00	1.00	1.00	1.00	1.00	1.00
30.6	3.13	2.66	2.56	2.80	2.66	2.60	2.94	2.66	2.58
36.5	3.67	3.19	3.09	3.35	3.20	3.12	3.44	3.19	3.12
40.1	3.82	3.49	3.42	3.69	3.48	3.38	3.65	3.49	3.44
44.9	4.71	3.93	3.76	4.17	3.93	3.81	4.37	3.93	3.80
46.8	5.13	4.12	3.90	4.37	4.12	4.00	4.71	4.12	3.94
50.1	5.44	4.37	4.14	4.66	4.37	4.23	5.01	4.37	4.19
54.5	6.03	4.73	4.45	5.12	4.72	4.52	5.51	4.73	4.50
55.4	6.28	4.85	4.53	5.05	4.83	4.73	5.70	4.84	4.59
58.2	6.46	5.10	4.81	5.37	5.10	4.96	5.89	5.10	4.87
66.9	7.54	5.83	5.46	6.19	5.84	5.67	6.85	5.83	5.53
69.5	7.79	6.04	5.66	6.46	6.06	5.87	7.10	6.05	5.73
72.5	8.25	6.31	5.88	6.75	6.32	6.11	7.47	6.31	5.97
78.7	9.47	6.87	6.26	7.34	6.89	6.66	8.49	6.87	6.37

E

Appendix E : Roughness Length Sensitivity - Full Simulation Results

Table E.1: Out-of-Plane deflections (δ), Forces (F) and Bending Moments for the Kaimal Spectrum simulations with varying Roughness Lengths z_0

Kaimal	Deflection δ [m]				Force F [kN]				Moment M [MNm]			
R.L. z_0 [m]	δ_y 5%	δ_y 50%	δ_y 95%	σ	F_y 5%	F_y 50%	F_y 95%	σ	M_x 5%	M_x 50%	M_x 95%	σ
0.0002	0.047	0.072	0.096	0.015	4.684	7.092	9.500	1.464	0.666	0.903	1.140	0.144
0.0004	0.047	0.073	0.099	0.016	4.612	7.210	9.808	1.580	0.664	0.920	1.175	0.155
0.0008	0.048	0.077	0.106	0.018	4.734	7.597	10.460	1.741	0.700	0.969	1.238	0.164
0.0016	0.049	0.079	0.109	0.018	4.882	7.830	10.778	1.792	0.740	0.999	1.259	0.158
0.0032	0.049	0.082	0.116	0.020	4.841	8.138	11.434	2.004	0.736	1.038	1.341	0.184
0.0064	0.054	0.086	0.117	0.019	5.374	8.475	11.575	1.885	0.790	1.083	1.377	0.179
0.0128	0.057	0.092	0.127	0.021	5.661	9.080	12.500	2.079	0.831	1.160	1.490	0.201

Table E.2: In-Plane deflections (δ), Forces (F) and Bending Moments for the Kaimal Spectrum simulations with varying Roughness Lengths z_0

Kaimal	Deflection δ [m]				Force F [kN]				Moment M [MNm]			
R.L. z_0 [m]	δ_x 5%	δ_x 50%	δ_x 95%	σ	F_x 5%	F_x 50%	F_x 95%	σ	M_y 5%	M_y 50%	M_y 95%	σ
0.0002	0.170	0.396	0.623	0.138	-80.840	-113.923	-147.006	20.113	-10.852	-15.435	-20.018	2.786
0.0004	0.170	0.395	0.619	0.137	-81.388	-116.463	-151.538	21.324	-10.981	-15.808	-20.636	2.935
0.0008	0.195	0.411	0.628	0.132	-85.425	-122.693	-159.962	22.658	-11.530	-16.662	-21.794	3.120
0.0016	0.187	0.424	0.661	0.144	-89.964	-126.559	-163.153	22.248	-12.030	-17.196	-22.362	3.141
0.0032	0.194	0.438	0.683	0.149	-91.602	-131.582	-171.562	24.306	-12.420	-17.879	-23.338	3.319
0.0064	0.188	0.442	0.696	0.154	-97.426	-137.837	-178.247	24.568	-13.209	-18.756	-24.303	3.372
0.0128	0.211	0.480	0.750	0.164	-103.328	-147.452	-191.577	26.826	-14.026	-20.062	-26.098	3.670

Table E.3: Out-of-Plane deflections (δ), Forces (F) and Bending Moments for the Yu Spectrum simulations with varying Roughness Lengths z_0

Yu	Deflection δ [m]				Force F [kN]				Moment M [MNm]			
R.L. z_0 [m]	δ_y 5%	δ_y 50%	δ_y 95%	σ	F_y 5%	F_y 50%	F_y 95%	σ	M_x 5%	M_x 50%	M_x 95%	σ
0.0002	0.046	0.072	0.097	0.016	4.545	7.063	9.581	1.531	0.587	0.900	1.213	0.191
0.0004	0.047	0.074	0.100	0.016	4.679	7.266	9.854	1.573	0.604	0.926	1.248	0.196
0.0008	0.049	0.076	0.103	0.016	4.837	7.507	10.177	1.623	0.625	0.957	1.289	0.202
0.0016	0.051	0.079	0.107	0.017	5.007	7.777	10.547	1.684	0.647	0.992	1.337	0.210
0.0032	0.053	0.082	0.111	0.018	5.206	8.099	10.992	1.759	0.674	1.033	1.393	0.219
0.006	*0.059*	*0.088*	*0.116*	*0.018*	*5.802*	*8.643*	*11.484*	*1.727*	*0.754*	*1.103*	*1.453*	*0.213*
0.0064	0.056	0.086	0.117	0.019	5.477	8.511	11.546	1.845	0.709	1.087	1.465	0.230
0.0128	0.059	0.091	0.124	0.020	5.776	9.009	12.242	1.965	0.750	1.152	1.554	0.244

Table E.4: In-Plane deflections (δ), Forces (F) and Bending Moments for the Yu Spectrum simulations with varying Roughness Lengths z_0

Yu	Deflection δ [m]				Force F [kN]				Moment M [MNm]			
R.L. z_0 [m]	δ_x 5%	δ_x 50%	δ_x 95%	σ	F_x 5%	F_x 50%	F_x 95%	σ	M_y 5%	M_y 50%	M_y 95%	σ
0.0002	0.170	0.390	0.609	0.134	-74.125	-113.710	-153.296	24.066	-9.972	-15.409	-20.846	3.306
0.0004	0.174	0.399	0.624	0.137	-76.380	-117.024	-157.667	24.710	-10.281	-15.862	-21.443	3.393
0.0008	0.178	0.409	0.639	0.140	-79.047	-121.085	-163.123	25.557	-10.647	-16.423	-22.198	3.511
0.0016	0.184	0.421	0.658	0.144	-81.929	-125.581	-169.232	26.538	-11.040	-17.041	-23.041	3.648
0.0032	0.189	0.435	0.682	0.150	-85.437	-130.988	-176.540	27.693	-11.521	-17.784	-24.048	3.808
0.006	*0.207*	*0.461*	*0.715*	*0.154*	*-96.086*	*-139.971*	*-183.856*	*26.680*	*-13.055*	*-19.035*	*-25.015*	*3.635*
0.0064	0.198	0.453	0.708	0.155	-89.989	-137.938	-185.886	29.151	-12.144	-18.742	-25.341	4.012
0.0128	0.205	0.473	0.741	0.163	-95.241	-146.337	-197.432	31.064	-12.866	-19.900	-26.935	4.277

Table E.5: Out-of-Plane -plane deflections (δ), Forces (F) and Bending Moments for the Li Spectrum simulations with varying Roughness Lengths z_0

Li	Deflection δ [m]				Force F [kN]				Moment M [MNm]			
R.L. z_0 [m]	δ_y 5%	δ_y 50%	δ_y 95%	σ	F_y 5%	F_y 50%	F_y 95%	σ	M_x 5%	M_x 50%	M_x 95%	σ
0.0002	0.048	0.071	0.095	0.014	4.744	7.047	9.350	1.400	0.648	0.897	1.147	0.152
0.0004	0.052	0.075	0.098	0.014	5.145	7.396	9.647	1.369	0.708	0.943	1.177	0.142
0.0008	0.051	0.076	0.100	0.015	5.062	7.472	9.882	1.465	0.686	0.952	1.219	0.162
0.0016	0.052	0.080	0.107	0.017	5.122	7.848	10.573	1.657	0.719	1.001	1.284	0.172
0.0032	0.055	0.082	0.109	0.016	5.444	8.101	10.758	1.615	0.750	1.034	1.318	0.173
0.006	*0.059*	*0.085*	*0.110*	*0.015*	*5.855*	*8.355*	*10.855*	*1.520*	*0.817*	*1.066*	*1.315*	*0.151*
0.0064	0.058	0.087	0.117	0.018	5.690	8.601	11.511	1.770	0.786	1.099	1.411	0.190
0.0128	0.061	0.092	0.123	0.019	6.024	9.081	12.137	1.858	0.840	1.159	1.479	0.194

Table E.6: In-Plane deflections (δ), Forces (F) and Bending Moments for the Li Spectrum simulations with varying Roughness Lengths z_0

Li	Deflection δ [m]				Force F [kN]				Moment M [MNm]			
R.L. z_0 [m]	δ_x 5%	δ_x 50%	δ_x 95%	σ	F_x 5%	F_x 50%	F_x 95%	σ	M_y 5%	M_y 50%	M_y 95%	σ
0.0002	0.200	0.391	0.583	0.116	-80.538	-113.247	-145.956	19.886	-10.901	-15.348	-19.794	2.703
0.0004	0.172	0.401	0.629	0.139	-86.998	-119.442	-151.887	19.725	-11.646	-16.218	-20.790	2.780
0.0008	0.218	0.411	0.605	0.118	-85.140	-120.356	-155.573	21.410	-11.520	-16.335	-21.150	2.927
0.0016	0.194	0.419	0.644	0.137	-89.028	-127.006	-164.984	23.089	-12.061	-17.263	-22.466	3.163
0.0032	0.215	0.438	0.660	0.135	-93.000	-131.031	-169.063	23.121	-12.524	-17.807	-23.090	3.212
0.006	*0.229*	*0.448*	*0.668*	*0.133*	*-101.404*	*-135.192*	*-168.980*	*20.541*	*-13.701*	*-18.378*	*-23.055*	*2.843*
0.0064	0.247	0.460	0.672	0.129	-96.661	-139.309	-181.957	25.928	-12.969	-18.927	-24.885	3.622
0.0128	0.242	0.481	0.720	0.145	-103.988	-147.245	-190.502	26.298	-14.023	-20.038	-26.052	3.657

Roughness Length Ratios

Table E.7: Out-of-Plane Roughness Length Ratios for Yu($z_0(n)$) vs. Kaimal($z_0(n)$)

Yu	Deflection γ_δ [-]			Force γ_F [-]			Moment γ_M [-]		
R.L. z_0 [m]	$\gamma_{\delta y}$ 5%	$\gamma_{\delta y}$ 50%	$\gamma_{\delta y}$ 95%	γ_{Fy} 5%	γ_{Fy} 50%	γ_{Fy} 95%	γ_{Mx} 5%	γ_{Mx} 50%	γ_{Mx} 95%
0.0002	0.97	1.00	1.01	0.97	1.00	1.01	0.88	1.00	1.06
0.0004	1.01	1.01	1.00	1.01	1.01	1.00	0.91	1.01	1.06
0.0008	1.02	0.99	0.97	1.02	0.99	0.97	0.89	0.99	1.04
0.0016	1.03	0.99	0.98	1.03	0.99	0.98	0.87	0.99	1.06
0.0032	1.08	1.00	0.96	1.08	1.00	0.96	0.92	1.00	1.04
0.006	*1.08*	*1.02*	*0.99*	*1.08*	*1.02*	*0.99*	*0.95*	*1.02*	*1.06*
0.0064	1.02	1.00	1.00	1.02	1.00	1.00	0.90	1.00	1.06
0.0128	1.02	0.99	0.98	1.02	0.99	0.98	0.90	0.99	1.04

Table E.8: In-Plane Roughness Length Ratios for Yu($z_0(n)$) vs. Kaimal($z_0(n)$)

Yu	Deflection γ_δ [-]			Force γ_F [-]			Moment γ_M [-]		
R.L. z_0 [m]	$\gamma_{\delta x}$ 5%	$\gamma_{\delta x}$ 50%	$\gamma_{\delta x}$ 95%	γ_{Fx} 5%	γ_{Fx} 50%	γ_{Fx} 95%	γ_{My} 5%	γ_{My} 50%	γ_{My} 95%
0.0002	1.00	0.98	0.98	0.92	1.00	1.04	0.92	1.00	1.04
0.0004	1.02	1.01	1.01	0.94	1.00	1.04	0.94	1.00	1.04
0.0008	0.92	0.99	1.02	0.93	0.99	1.02	0.92	0.99	1.02
0.0016	0.98	0.99	1.00	0.91	0.99	1.04	0.92	0.99	1.03
0.0032	0.98	0.99	1.00	0.93	1.00	1.03	0.93	0.99	1.03
0.006	*1.10*	*1.04*	*1.03*	*0.99*	*1.02*	*1.03*	*0.99*	*1.01*	*1.03*
0.0064	1.05	1.03	1.02	0.92	1.00	1.04	0.92	1.00	1.04
0.0128	0.97	0.99	0.99	0.92	0.99	1.03	0.92	0.99	1.03

Table E.9: Out-of-Plane Roughness Length Ratios for Li($z_0(n)$) vs. Kaimal($z_0(n)$)

Li	Deflection γ_δ [-]			Force γ_F [-]			Moment γ_M [-]		
R.L. z_0 [m]	$\gamma_{\delta y}$ 5%	$\gamma_{\delta y}$ 50%	$\gamma_{\delta y}$ 95%	γ_{Fy} 5%	γ_{Fy} 50%	γ_{Fy} 95%	γ_{Mx} 5%	γ_{Mx} 50%	γ_{Mx} 95%
0.0002	1.01	0.99	0.98	0.96	1.01	0.99	0.98	0.96	0.97
0.0004	1.12	1.03	0.98	0.87	1.12	1.03	0.98	0.87	1.07
0.0008	1.07	0.98	0.94	0.84	1.07	0.98	0.94	0.84	0.98
0.0016	1.05	1.00	0.98	0.92	1.05	1.00	0.98	0.92	0.97
0.0032	1.12	1.00	0.94	0.81	1.12	1.00	0.94	0.81	1.02
0.006	*1.09*	*0.99*	*0.94*	*0.81*	*1.09*	*0.99*	*0.94*	*0.81*	*1.04*
0.0064	1.06	1.01	0.99	0.94	1.06	1.01	0.99	0.94	1.00
0.0128	1.06	1.00	0.97	0.89	1.06	1.00	0.97	0.89	1.01

Table E.10: In-Plane Roughness Length Ratios for Li($z_0(n)$) vs. Kaimal($z_0(n)$)

Li	Deflection γ_δ [-]			Force γ_F [-]			Moment γ_M [-]		
R.L. z_0 [m]	$\gamma_{\delta x}$ 5%	$\gamma_{\delta x}$ 50%	$\gamma_{\delta x}$ 95%	γ_{Fx} 5%	γ_{Fx} 50%	γ_{Fx} 95%	γ_{My} 5%	γ_{My} 50%	γ_{My} 95%
0.0002	0.99	1.01	1.05	1.18	0.99	0.94	0.85	1.00	0.99
0.0004	1.03	1.00	0.92	1.01	1.02	1.02	1.02	1.07	1.03
0.0008	0.98	0.98	0.99	1.12	1.00	0.96	0.89	1.00	0.98
0.0016	1.00	1.02	1.09	1.04	0.99	0.97	0.95	0.99	1.00
0.0032	1.00	0.98	0.94	1.11	1.00	0.97	0.91	1.02	1.00
0.006	*0.98*	*0.95*	*0.85*	*1.22*	*1.02*	*0.96*	*0.86*	*1.04*	*0.98*
0.0064	1.01	1.02	1.06	1.32	1.04	0.97	0.84	0.99	1.01
0.0128	1.00	0.99	0.97	1.15	1.00	0.96	0.89	1.01	1.00

Roughness Length Sensitivity

Table E.11: Out-of-Plane Roughness Length Sensitivity for Kaimal($z_0(n)$) vs. Kaimal($z_0(0.0002)$)

Kaimal	Deflection γ_δ [-]			Force γ_F [-]			Moment γ_M [-]		
R.L. z_0 [m]	$\gamma_{\delta y}$ 5%	$\gamma_{\delta y}$ 50%	$\gamma_{\delta y}$ 95%	γ_{Fy} 5%	γ_{Fy} 50%	γ_{Fy} 95%	γ_{Mx} 5%	γ_{Mx} 50%	γ_{Mx} 95%
0.0002	1.00	1.00	1.00	1.00	1.00	1.00	1.00	1.00	1.00
0.0004	0.98	1.02	1.03	1.08	0.98	1.02	1.03	1.08	1.00
0.0008	1.01	1.07	1.10	1.19	1.01	1.07	1.10	1.19	1.05
0.0016	1.04	1.10	1.13	1.22	1.04	1.10	1.13	1.22	1.11
0.0032	1.03	1.15	1.20	1.37	1.03	1.15	1.20	1.37	1.10
0.0060	*1.15*	*1.20*	*1.22*	*1.29*	*1.15*	*1.20*	*1.22*	*1.29*	*1.19*
0.0064	1.21	1.28	1.32	1.42	1.21	1.28	1.32	1.42	1.25
0.0128	1.21	1.28	1.32	1.42	1.21	1.28	1.32	1.42	1.25

Table E.12: In-Plane Roughness Length Sensitivity for Kaimal($z_0(n)$) vs. Kaimal($z_0(0.0002)$)

Kaimal	Deflection γ_δ [-]			Force γ_F [-]			Moment γ_M [-]		
R.L. z_0 [m]	$\gamma_{\delta x}$ 5%	$\gamma_{\delta x}$ 50%	$\gamma_{\delta x}$ 95%	γ_{Fx} 5%	γ_{Fx} 50%	γ_{Fx} 95%	γ_{My} 5%	γ_{My} 50%	γ_{My} 95%
0.0002	1.00	1.00	1.00	1.00	1.00	1.00	1.00	1.00	1.00
0.0004	1.02	1.03	1.08	1.00	1.00	0.99	0.99	1.01	1.02
0.0008	1.07	1.09	1.14	1.15	1.04	1.01	0.96	1.06	1.08
0.0016	1.11	1.10	1.09	1.10	1.07	1.06	1.05	1.11	1.11
0.0032	1.15	1.18	1.28	1.14	1.11	1.10	1.08	1.13	1.16
0.0060	*1.20*	*1.21*	*1.24*	*1.11*	*1.11*	*1.12*	*1.12*	*1.21*	*1.21*
0.0064	1.28	1.31	1.39	1.24	1.21	1.20	1.19	1.28	1.29
0.0128	1.28	1.31	1.39	1.24	1.21	1.20	1.19	1.28	1.29

Table E.13: Out-of-Plane Roughness Length Sensitivity for Yu($z_0(n)$) vs. Kaimal($z_0(0.0002)$)

Yu	Deflection γ_δ [-]			Force γ_F [-]			Moment γ_M [-]		
R.L. z_0 [m]	$\gamma_{\delta y}$ 5%	$\gamma_{\delta y}$ 50%	$\gamma_{\delta y}$ 95%	γ_{Fy} 5%	γ_{Fy} 50%	γ_{Fy} 95%	γ_{Mx} 5%	γ_{Mx} 50%	γ_{Mx} 95%
0.0002	0.78	0.82	0.83	0.78	0.82	0.83	0.78	0.82	0.83
0.0004	0.81	0.84	0.86	0.81	0.84	0.86	0.80	0.84	0.86
0.0008	0.83	0.87	0.89	0.83	0.87	0.89	0.83	0.87	0.89
0.0016	0.86	0.90	0.92	0.86	0.90	0.92	0.86	0.90	0.92
0.0032	0.90	0.94	0.96	0.90	0.94	0.96	0.89	0.94	0.96
0.0060	*1.00*	*1.00*	*1.00*	*1.00*	*1.00*	*1.00*	*1.00*	*1.00*	*1.00*
0.0064	0.94	0.98	1.01	0.94	0.98	1.01	0.94	0.99	1.01
0.0128	1.00	1.04	1.07	1.00	1.04	1.07	0.99	1.04	1.07

Table E.14: In-Plane Roughness Length Sensitivity for Yu($z_0(n)$) vs. Kaimal($z_0(0.0002)$)

Yu	Deflection γ_δ [-]			Force γ_F [-]			Moment γ_M [-]		
R.L. z_0 [m]	$\gamma_{\delta x}$ 5%	$\gamma_{\delta x}$ 50%	$\gamma_{\delta x}$ 95%	γ_{Fx} 5%	γ_{Fx} 50%	γ_{Fx} 95%	γ_{My} 5%	γ_{My} 50%	γ_{My} 95%
0.0002	0.82	0.85	0.85	0.77	0.81	0.83	0.76	0.81	0.83
0.0004	0.84	0.87	0.87	0.79	0.84	0.86	0.79	0.83	0.86
0.0008	0.86	0.89	0.89	0.82	0.87	0.89	0.82	0.86	0.89
0.0016	0.89	0.91	0.92	0.85	0.90	0.92	0.85	0.90	0.92
0.0032	0.91	0.94	0.95	0.89	0.94	0.96	0.88	0.93	0.96
0.0060	*1.00*	*1.00*	*1.00*	*1.00*	*1.00*	*1.00*	*1.00*	*1.00*	*1.00*
0.0064	0.95	0.98	0.99	0.94	0.99	1.01	0.93	0.98	1.01
0.0128	0.99	1.03	1.04	0.99	1.05	1.07	0.99	1.05	1.08

Table E.15: Out-of-Plane Roughness Length Sensitivity for Li($z_0(n)$) vs. Kaimal($z_0(0.0002)$)

Li	Deflection γ_δ [-]			Force γ_F [-]			Moment γ_M [-]		
R.L. z_0 [m]	$\gamma_{\delta y}$ 5%	$\gamma_{\delta y}$ 50%	$\gamma_{\delta y}$ 95%	γ_{Fy} 5%	γ_{Fy} 50%	γ_{Fy} 95%	γ_{Mx} 5%	γ_{Mx} 50%	γ_{Mx} 95%
0.0002	0.81	0.84	0.86	0.81	0.84	0.86	0.79	0.84	0.87
0.0004	0.88	0.89	0.89	0.88	0.89	0.89	0.87	0.88	0.90
0.0008	0.86	0.89	0.91	0.86	0.89	0.91	0.84	0.89	0.93
0.0016	0.87	0.94	0.97	0.87	0.94	0.97	0.88	0.94	0.98
0.0032	0.93	0.97	0.99	0.93	0.97	0.99	0.92	0.97	1.00
0.0060	*1.00*	*1.00*	*1.00*	*1.00*	*1.00*	*1.00*	*1.00*	*1.00*	*1.00*
0.0064	0.97	1.03	1.06	0.97	1.03	1.06	0.96	1.03	1.07
0.0128	1.03	1.09	1.12	1.03	1.09	1.12	1.03	1.09	1.12

Table E.16: In-Plane Roughness Length Sensitivity for Li($z_0(n)$) vs. Kaimal($z_0(0.0002)$)

Li	Deflection γ_δ [-]			Force γ_F [-]			Moment γ_M [-]		
R.L. z_0 [m]	$\gamma_{\delta x}$ 5%	$\gamma_{\delta x}$ 50%	$\gamma_{\delta x}$ 95%	γ_{Fx} 5%	γ_{Fx} 50%	γ_{Fx} 95%	γ_{My} 5%	γ_{My} 50%	γ_{My} 95%
0.0002	0.87	0.87	0.87	0.79	0.84	0.86	0.80	0.84	0.86
0.0004	0.75	0.89	0.94	0.86	0.88	0.90	0.85	0.88	0.90
0.0008	0.95	0.92	0.91	0.84	0.89	0.92	0.84	0.89	0.92
0.0016	0.85	0.94	0.97	0.88	0.94	0.98	0.88	0.94	0.97
0.0032	0.94	0.98	0.99	0.92	0.97	1.00	0.91	0.97	1.00
0.0060	*1.00*	*1.00*	*1.00*	*1.00*	*1.00*	*1.00*	*1.00*	*1.00*	*1.00*
0.0064	1.08	1.02	1.01	0.95	1.03	1.08	0.95	1.03	1.08
0.0128	1.06	1.07	1.08	1.03	1.09	1.13	1.02	1.09	1.13

Appendix F : Coherence Sensitivity - Full Simulation Results

Table F.1: Out-of-Plane deflections (δ), Forces (F) and Bending Moments for the Kaimal Spectrum simulations for varying Coherence Decay Coefficients C_{ii}

Kaimal	Deflection δ [m]				Force F [kN]				Moment M [MNm]			
C_{ii} [-]	δ_y 5%	δ_y 50%	δ_y 95%	σ	F_y 5%	F_y 50%	F_y 95%	σ	M_x 5%	M_x 50%	M_x 95%	σ
5	0.041	0.071	0.102	0.018	4.033	7.031	10.028	1.823	0.642	0.898	1.155	0.156
10	0.046	0.072	0.098	0.016	4.535	7.112	9.689	1.567	0.662	0.907	1.153	0.149
15	0.048	0.072	0.097	0.015	4.749	7.147	9.545	1.458	0.662	0.910	1.159	0.151
25	0.050	0.072	0.094	0.013	4.947	7.103	9.260	1.311	0.668	0.904	1.139	0.143
50	0.052	0.071	0.090	0.011	5.141	6.998	8.854	1.129	0.680	0.891	1.101	0.128

Table F.2: In-Plane deflections (δ), Forces (F) and Bending Moments for the Kaimal Spectrum simulations for varying Coherence Decay Coefficients C_{ii}

Kaimal	Deflection δ [m]				Force F [kN]				Moment M [MNm]			
C_{ii} [-]	δ_x 5%	δ_x 50%	δ_x 95%	σ	F_x 5%	F_x 50%	F_x 95%	σ	M_y 5%	M_y 50%	M_y 95%	σ
5	0.193	0.390	0.586	0.119	-79.481	-113.437	-147.393	20.644	-10.780	-15.381	-19.982	2.797
10	0.179	0.395	0.612	0.132	-81.641	-114.626	-147.611	20.054	-11.021	-15.557	-20.092	2.757
15	0.152	0.396	0.641	0.149	-80.375	-114.915	-149.455	20.999	-10.805	-15.581	-20.358	2.904
25	0.142	0.400	0.658	0.157	-80.739	-113.887	-147.036	20.153	-10.714	-15.418	-20.121	2.859
50	0.139	0.386	0.633	0.150	-82.442	-112.562	-142.682	18.312	-11.010	-15.265	-19.519	2.587

Table F.3: Out-of-Plane deflections (δ), Forces (F) and Bending Moments for the Yu Spectrum simulations for varying Coherence Decay Coefficients C_{ii}

Yu	Deflection δ [m]				Force F [kN]				Moment M [MNm]			
C_{ii} [-]	δ_y 5%	δ_y 50%	δ_y 95%	σ	F_y 5%	F_y 50%	F_y 95%	σ	M_x 5%	M_x 50%	M_x 95%	σ
5	0.056	0.085	0.115	0.018	5.500	8.410	11.321	1.770	0.713	1.073	1.432	0.218
10	0.056	0.086	0.115	0.018	5.566	8.478	11.391	1.771	0.720	1.083	1.446	0.221
15	0.055	0.087	0.118	0.019	5.461	8.566	11.670	1.887	0.705	1.094	1.484	0.237
25	0.062	0.088	0.114	0.016	6.150	8.684	11.217	1.540	0.789	1.107	1.425	0.193
50	0.057	0.086	0.115	0.017	5.666	8.504	11.342	1.725	0.722	1.084	1.446	0.220

Table F.4: In-Plane deflections (δ), Forces (F) and Bending Moments for the Yu Spectrum simulations for varying Coherence Decay Coefficients C_{ii}

Yu	Deflection δ [m]				Force F [kN]				Moment M [MNm]			
C_{ii} [-]	δ_x 5%	δ_x 50%	δ_x 95%	σ	F_x 5%	F_x 50%	F_x 95%	σ	M_y 5%	M_y 50%	M_y 95%	σ
5	0.228	0.457	0.686	0.139	-89.931	-135.760	-181.590	27.862	-12.163	-18.433	-24.703	3.812
10	0.210	0.454	0.699	0.149	-90.730	-137.330	-183.929	28.330	-12.260	-18.676	-25.092	3.901
15	0.171	0.450	0.729	0.170	-88.705	-138.946	-189.186	30.544	-12.010	-18.897	-25.783	4.187
25	0.205	0.472	0.740	0.163	-98.242	-139.836	-181.429	25.287	-13.201	-18.975	-24.750	3.510
50	0.165	0.472	0.778	0.186	-87.559	-136.956	-186.354	30.032	-11.779	-18.607	-25.435	4.151

Table F.5: Out-of-Plane deflections (δ), Forces (F) and Bending Moments for the Li Spectrum simulations for varying Coherence Decay Coefficients C_{ii}

Li	Deflection δ [m]				Force F [kN]				Moment M [MNm]			
C_{ii} [-]	δ_y 5%	δ_y 50%	δ_y 95%	σ	F_y 5%	F_y 50%	F_y 95%	σ	M_x 5%	M_x 50%	M_x 95%	σ
5	0.053	0.087	0.121	0.021	5.267	8.600	11.932	2.026	0.782	1.098	1.414	0.192
10	0.061	0.088	0.115	0.017	5.977	8.683	11.388	1.645	0.826	1.108	1.390	0.172
15	0.059	0.086	0.113	0.016	5.818	8.490	11.162	1.624	0.788	1.083	1.377	0.179
25	0.064	0.086	0.107	0.013	6.351	8.467	10.582	1.286	0.840	1.082	1.323	0.147
50	0.066	0.086	0.106	0.012	6.550	8.523	10.496	1.200	0.855	1.088	1.320	0.141

Table F.6: In-Plane deflections (δ), Forces (F) and Bending Moments for the Li Spectrum simulations for varying Coherence Decay Coefficients C_{ii}

Li	Deflection δ [m]				Force F [kN]				Moment M [MNm]			
C_{ii} [-]	δ_x 5%	δ_x 50%	δ_x 95%	σ	F_x 5%	F_x 50%	F_x 95%	σ	M_y 5%	M_y 50%	M_y 95%	σ
5	0.257	0.463	0.669	0.125	-98.413	-139.086	-179.758	24.727	-13.364	-18.895	-24.427	3.363
10	0.240	0.466	0.692	0.137	-102.840	-140.478	-178.115	22.882	-13.922	-19.098	-24.273	3.146
15	0.209	0.454	0.700	0.150	-96.542	-137.288	-178.035	24.772	-12.963	-18.685	-24.406	3.479
25	0.185	0.450	0.714	0.161	-101.496	-137.426	-173.355	21.844	-13.439	-18.705	-23.970	3.201
50	0.170	0.453	0.735	0.172	-104.514	-137.831	-171.149	20.256	-13.898	-18.708	-23.517	2.924

Coherence Ratios

Table F.7: Out-of-Plane Coherence Ratios for Yu($C_{ii}(n)$) vs. Kaimal($C_{ii}(n)$)

Yu	Deflection γ [-]			Force γ_F [-]			Moment γ_M [-]		
C_{ii} [-]	$\gamma_{\delta y}$ 5%	$\gamma_{\delta y}$ 50%	$\gamma_{\delta y}$ 95%	γ_{Fy} 5%	γ_{Fy} 50%	γ_{Fy} 95%	γ_{Mx} 5%	γ_{Mx} 50%	γ_{Mx} 95%
5	1.36	1.20	1.13	1.36	1.20	1.13	1.11	1.19	1.24
10	1.23	1.19	1.18	1.23	1.19	1.18	1.09	1.19	1.25
15	1.15	1.20	1.22	1.15	1.20	1.22	1.07	1.20	1.28
25	1. .22	1.21	1.18	1.22	1.25				
50	1.10	1.22	1.28	1.10	1.22	1.28	1.06	1.22	1.31

Table F.8: In-Plane Coherence Ratios for Yu($C_{ii}(n)$) vs. Kaimal($C_{ii}(n)$)

Yu	Deflection γ [-]			Force γ_F [-]			Moment γ_M [-]		
C_{ii} [-]	$\gamma_{\delta x}$ 5%	$\gamma_{\delta x}$ 50%	$\gamma_{\delta x}$ 95%	γ_{Fx} 5%	γ_{Fx} 50%	γ_{Fx} 95%	γ_{My} 5%	γ_{My} 50%	γ_{My} 95%
5	1.18	1.17	1.17	1.13	1.20	1.23	1.13	1.20	1.24
10	1.17	1.15	1.14	1.11	1.20	1.25	1.11	1.20	1.25
15	1.13	1.14	1.14	1.10	1.21	1.27	1.11	1.21	1.27
25	1.44	1.18	1.12	1.22	1.23	1.23	1.23	1.23	1.23
50	1.19	1.22	1.23	1.06	1.22	1.31	1.07	1.22	1.30

Table F.9: Out-of-Plane Coherence Ratios for Li($C_{ii}(n)$) vs. Kaimal($C_{ii}(n)$)

Li	Deflection γ [-]			Force γ_F [-]			Moment γ_M [-]		
C_{ii} [-]	$\gamma_{\delta y}$ 5%	$\gamma_{\delta y}$ 50%	$\gamma_{\delta y}$ 95%	γ_{Fy} 5%	γ_{Fy} 50%	γ_{Fy} 95%	γ_{Mx} 5%	γ_{Mx} 50%	γ_{Mx} 95%
5	1.31	1.22	1.19	1.31	1.22	1.19	1.22	1.22	1.22
10	1.32	1.22	1.18	1.32	1.22	1.18	1.25	1.22	1.21
15	1.23	1.19	1.17	1.23	1.19	1.17	1.19	1.19	1.19
25	1.28	1.19	1.14	1.28	1.19	1.14	1.26	1.20	1.16
50	1.27	1.22	1.19	1.27	1.22	1.19	1.26	1.22	1.20

Table F.10: In-Plane Coherence Ratios for Yu($C_{ii}(n)$) vs. Kaimal($C_{ii}(n)$)

Li	Deflection γ [-]			Force γ_F [-]			Moment γ_M [-]		
C_{ii} [-]	$\gamma_{\delta x}$ 5%	$\gamma_{\delta x}$ 50%	$\gamma_{\delta x}$ 95%	γ_{Fx} 5%	γ_{Fx} 50%	γ_{Fx} 95%	γ_{My} 5%	γ_{My} 50%	γ_{My} 95%
5	1.33	1.19	1.14	1.24	1.23	1.22	1.24	1.23	1.22
10	1.34	1.18	1.13	1.26	1.23	1.21	1.26	1.23	1.21
15	1.37	1.15	1.09	1.20	1.19	1.19	1.20	1.20	1.20
25	1.30	1.12	1.09	1.26	1.21	1.18	1.25	1.21	1.19
50	1.22	1.17	1.16	1.27	1.22	1.20	1.26	1.23	1.20

Coherence Sensitivity

Table F.11: Out-of-Plane Coherence Sensitivity for Kaimal($C_{ii}(n)$) vs. Kaimal($C_{ii}(10)$)

Kaimal	Deflection γ [-]			Force γ_F [-]			Moment γ_M [-]		
C_{ii} [-]	$\gamma_{\delta y}$ 5%	$\gamma_{\delta y}$ 50%	$\gamma_{\delta y}$ 95%	γ_{Fy} 5%	γ_{Fy} 50%	γ_{Fy} 95%	γ_{Mx} 5%	γ_{Mx} 50%	γ_{Mx} 95%
5	0.89	0.99	1.04	0.89	0.99	1.04	0.97	0.99	1.00
10	1.00	1.00	1.00	1.00	1.00	1.00	1.00	1.00	1.00
15	1.05	1.00	0.99	1.05	1.00	0.99	1.00	1.00	1.01
25	1.09	1.00	0.96	1.09	1.00	0.96	1.01	1.00	0.99
50	1.13	0.98	0.91	1.13	0.98	0.91	1.03	0.98	0.96

Table F.12: In-Plane Coherence Sensitivity for Kaimal($C_{ii}(n)$) vs. Kaimal($C_{ii}(10)$)

Kaimal	Deflection γ [-]			Force γ_F [-]			Moment γ_M [-]		
C_{ii} [-]	$\gamma_{\delta x}$ 5%	$\gamma_{\delta x}$ 50%	$\gamma_{\delta x}$ 95%	γ_{Fx} 5%	γ_{Fx} 50%	γ_{Fx} 95%	γ_{My} 5%	γ_{My} 50%	γ_{My} 95%
5	1.08	0.99	0.96	0.97	0.99	1.00	0.98	0.99	0.99
10	1.00	1.00	1.00	1.00	1.00	1.00	1.00	1.00	1.00
15	0.85	1.00	1.05	0.98	1.00	1.01	0.98	1.00	1.01
25	0.80	1.01	1.07	0.99	0.99	1.00	0.97	0.99	1.00
50	0.78	0.98	1.03	1.01	0.98	0.97	1.00	0.98	0.97

Table F.13: Out-of-Plane Coherence Sensitivity for Yu($C_{ii}(n)$) vs. Yu($C_{ii}(10)$)

Yu	Deflection γ [-]			Force γ_F [-]			Moment γ_M [-]		
C_{ii} [-]	$\gamma_{\delta y}$ 5%	$\gamma_{\delta y}$ 50%	$\gamma_{\delta y}$ 95%	γ_{Fy} 5%	γ_{Fy} 50%	γ_{Fy} 95%	γ_{Mx} 5%	γ_{Mx} 50%	γ_{Mx} 95%
5	0.99	0.99	0.99	0.99	0.99	0.99	0.99	0.99	0.99
10	1.00	1.00	1.00	1.00	1.00	1.00	1.00	1.00	1.00
15	0.98	1.01	1.02	0.98	1.01	1.02	0.98	1.01	1.03
25	1.10	1.02	0.98	1.10	1.02	0.98	1.10	1.02	0.99
50	1.02	1.00	1.00	1.02	1.00	1.00	1.00	1.00	1.00

Table F.14: In-Plane Coherence Sensitivity for Yu($C_{ii}(n)$) vs. Yu($C_{ii}(10)$)

Yu	Deflection γ [-]			Force γ_F [-]			Moment γ_M [-]		
C_{ii} [-]	$\gamma_{\delta x}$ 5%	$\gamma_{\delta x}$ 50%	$\gamma_{\delta x}$ 95%	γ_{Fx} 5%	γ_{Fx} 50%	γ_{Fx} 95%	γ_{My} 5%	γ_{My} 50%	γ_{My} 95%
5	1.09	1.01	0.98	0.99	0.99	0.99	0.99	0.99	0.98
10	1.00	1.00	1.00	1.00	1.00	1.00	1.00	1.00	1.00
15	0.82	0.99	1.04	0.98	1.01	1.03	0.98	1.01	1.03
25	0.98	1.04	1.06	1.08	1.02	0.99	1.08	1.02	0.99
50	0.79	1.04	1.11	0.97	1.00	1.01	0.96	1.00	1.01

Table F.15: Out-of-Plane Coherence Sensitivity for Li($C_{ii}(n)$) vs. Li($C_{ii}(10)$)

Li	Deflection γ [-]			Force γ_F [-]			Moment γ_M [-]		
C_{ii} [-]	$\gamma_{\delta y}$ 5%	$\gamma_{\delta y}$ 50%	$\gamma_{\delta y}$ 95%	γ_{Fy} 5%	γ_{Fy} 50%	γ_{Fy} 95%	γ_{Mx} 5%	γ_{Mx} 50%	γ_{Mx} 95%
5	0.88	0.99	1.05	0.88	0.99	1.05	0.95	0.99	1.02
10	1.00	1.00	1.00	1.00	1.00	1.00	1.00	1.00	1.00
15	0.97	0.98	0.98	0.97	0.98	0.98	0.95	0.98	0.99
25	1.06	0.98	0.93	1.06	0.98	0.93	1.02	0.98	0.95
50	1.10	0.98	0.92	1.10	0.98	0.92	1.04	0.98	0.95

Table F.16: In-Plane Coherence Sensitivity for Li($C_{ii}(n)$) vs. Li($C_{ii}(10)$)

Li	Deflection γ [-]			Force γ_F [-]			Moment γ_M [-]		
C_{ii} [-]	$\gamma_{\delta x}$ 5%	$\gamma_{\delta x}$ 50%	$\gamma_{\delta x}$ 95%	γ_{Fx} 5%	γ_{Fx} 50%	γ_{Fx} 95%	γ_{My} 5%	γ_{My} 50%	γ_{My} 95%
5	1.07	0.99	0.97	0.96	0.99	1.01	0.96	0.99	1.01
10	1.00	1.00	1.00	1.00	1.00	1.00	1.00	1.00	1.00
15	0.87	0.98	1.01	0.94	0.98	1.00	0.93	0.98	1.01
25	0.77	0.97	1.03	0.99	0.98	0.97	0.97	0.98	0.99
50	0.71	0.97	1.06	1.02	0.98	0.96	1.00	0.98	0.97

G

Appendix G : Orientation Sensitivity - Full Simulation Results

Table G.1: Out-of-plane and In-plane Deflections (δ) and Forces (F) for the Kaimal Spectrum simulations for varying Azimuth Angle ϵ [°]

Kaimal	Deflection δ [m]				Force F [kN]				Moment M [MNm]			
AA ϵ [°]	δ_y 5%	δ_y 50%	δ_y 95%	σ	F_y 5%	F_y 50%	F_y 95%	σ	M_x 5%	M_x 50%	M_x 95%	σ
0	0.048	0.073	0.097	0.015	4.778	7.177	9.576	1.458	0.685	0.915	1.145	0.140
15	0.047	0.072	0.097	0.015	4.675	7.134	9.593	1.495	0.669	0.908	1.147	0.145
30	0.045	0.072	0.098	0.016	4.409	7.056	9.704	1.610	0.646	0.899	1.151	0.154
45	0.045	0.072	0.098	0.016	4.454	7.065	9.676	1.587	0.657	0.899	1.141	0.147
60	0.046	0.070	0.095	0.015	4.529	6.947	9.366	1.470	0.642	0.881	1.120	0.145
75	0.044	0.069	0.094	0.015	4.372	6.820	9.269	1.489	0.624	0.865	1.106	0.147
90	0.045	0.069	0.093	0.015	4.456	6.832	9.207	1.444	0.648	0.864	1.080	0.131
105	0.044	0.067	0.090	0.014	4.347	6.611	8.875	1.376	0.614	0.832	1.051	0.133
120	0.043	0.066	0.089	0.014	4.254	6.494	8.733	1.362	0.593	0.816	1.039	0.136
135	0.042	0.064	0.086	0.013	4.156	6.314	8.473	1.312	0.574	0.789	1.004	0.131
150	0.040	0.064	0.087	0.014	3.974	6.270	8.566	1.396	0.556	0.779	1.001	0.135
165	0.040	0.063	0.085	0.014	3.975	6.199	8.423	1.352	0.554	0.766	0.979	0.129
180	0.041	0.063	0.084	0.013	4.082	6.188	8.295	1.281	0.569	0.765	0.960	0.119

Table G.2: Out-of-plane and In-plane Deflections (δ) and Forces (F) for the Kaimal Spectrum simulations for varying Azimuth Angle ϵ [°]

Kaimal	Deflection δ [m]				Force F [kN]				Moment M [MNm]			
AA ϵ [°]	δ_x 5%	δ_x 50%	δ_x 95%	σ	F_x 5%	F_x 50%	F_x 95%	σ	M_y 5%	M_y 50%	M_y 95%	σ
0	0.168	0.394	0.619	0.137	-83.711	-115.743	-147.774	19.474	-11.217	-15.702	-20.187	2.727
15	0.191	0.397	0.604	0.126	-81.285	-114.770	-148.254	20.357	-10.900	-15.559	-20.218	2.832
30	0.163	0.395	0.627	0.141	-79.806	-113.434	-147.063	20.444	-10.839	-15.361	-19.884	2.750
45	0.179	0.404	0.629	0.137	-80.784	-113.196	-145.608	19.705	-10.877	-15.318	-19.760	2.700
60	0.182	0.403	0.623	0.134	-77.559	-110.693	-143.828	20.144	-10.372	-14.943	-19.513	2.779
75	0.167	0.403	0.639	0.143	-75.323	-108.394	-141.465	20.106	-10.063	-14.616	-19.169	2.768
90	0.203	0.417	0.631	0.130	-78.365	-107.775	-137.186	17.881	-10.499	-14.499	-18.499	2.432
105	0.222	0.425	0.628	0.123	-73.329	-103.126	-132.923	18.115	-9.700	-13.816	-17.933	2.503
120	0.218	0.430	0.641	0.128	-70.455	-100.341	-130.228	18.169	-9.318	-13.384	-17.450	2.472
135	0.221	0.438	0.655	0.132	-67.297	-96.298	-125.298	17.631	-8.819	-12.782	-16.746	2.410
150	0.242	0.456	0.669	0.130	-65.593	-94.112	-122.631	17.338	-8.560	-12.394	-16.228	2.331
165	0.257	0.471	0.686	0.130	-63.696	-91.620	-119.544	16.976	-8.245	-11.968	-15.690	2.263
180	0.256	0.475	0.694	0.133	-65.434	-91.206	-116.979	15.669	-8.416	-11.895	-15.374	2.115

Table G.3: Out-of-plane and In-plane Deflections (δ) and Forces (F) for the Yu Spectrum simulations for varying Azimuth Angle ϵ [°]

Yu	Deflection δ [m]				Force F [kN]				Moment M [MNm]			
AA ϵ [°]	δ_y 5%	δ_y 50%	δ_y 95%	σ	F_y 5%	F_y 50%	F_y 95%	σ	M_x 5%	M_x 50%	M_x 95%	σ
0	0.060	0.088	0.116	0.017	5.923	8.664	11.405	1.666	0.760	1.107	1.453	0.210
15	0.057	0.084	0.111	0.017	5.578	8.257	10.935	1.628	0.722	1.055	1.388	0.203
30	0.053	0.085	0.117	0.019	5.207	8.358	11.509	1.916	0.674	1.066	1.458	0.238
45	0.055	0.085	0.114	0.018	5.462	8.355	11.249	1.759	0.707	1.063	1.420	0.217
60	0.053	0.084	0.114	0.019	5.246	8.254	11.262	1.829	0.682	1.049	1.416	0.223
75	0.055	0.081	0.107	0.016	5.415	7.967	10.520	1.552	0.698	1.010	1.323	0.190
90	0.053	0.079	0.106	0.016	5.181	7.841	10.501	1.617	0.666	0.992	1.318	0.198
105	0.050	0.079	0.109	0.018	4.905	7.814	10.723	1.768	0.629	0.983	1.337	0.215
120	0.047	0.077	0.107	0.018	4.605	7.573	10.541	1.804	0.590	0.948	1.307	0.218
135	0.046	0.075	0.105	0.018	4.516	7.422	10.328	1.767	0.575	0.922	1.270	0.211
150	0.046	0.073	0.101	0.017	4.559	7.244	9.928	1.632	0.582	0.894	1.206	0.190
165	0.045	0.073	0.100	0.017	4.432	7.170	9.908	1.664	0.564	0.880	1.196	0.192
180	0.042	0.072	0.101	0.018	4.192	7.086	9.981	1.760	0.531	0.868	1.206	0.205

Table G.4: Out-of-plane and In-plane Deflections (δ) and Forces (F) for the Yu Spectrum simulations for varying Azimuth Angle ϵ [°]

Yu	Deflection δ [m]				Force F [kN]				Moment M [MNm]			
AA ϵ [°]	δ_x 5%	δ_x 50%	δ_x 95%	σ	F_x 5%	F_x 50%	F_x 95%	σ	M_y 5%	M_y 50%	M_y 95%	σ
0	0.227	0.463	0.698	0.143	-94.531	-140.423	-186.314	27.900	-12.682	-19.099	-25.516	3.901
15	0.217	0.433	0.649	0.131	-90.995	-134.018	-177.041	26.156	-12.337	-18.229	-24.121	3.582
30	0.216	0.452	0.688	0.144	-85.430	-135.060	-184.690	30.173	-11.602	-18.331	-25.060	4.091
45	0.223	0.468	0.713	0.149	-89.772	-134.072	-178.373	26.933	-12.115	-18.178	-24.241	3.686
60	0.200	0.474	0.748	0.167	-85.830	-131.828	-177.826	27.965	-11.615	-17.827	-24.039	3.777
75	0.255	0.469	0.683	0.130	-85.641	-126.618	-167.594	24.912	-11.478	-17.077	-22.677	3.404
90	0.243	0.477	0.710	0.142	-81.257	-123.786	-166.316	25.856	-10.812	-16.663	-22.514	3.557
105	0.250	0.505	0.760	0.155	-76.098	-121.407	-166.715	27.546	-10.042	-16.234	-22.426	3.765
120	0.255	0.513	0.771	0.157	-71.383	-116.164	-160.944	27.224	-9.437	-15.451	-21.465	3.656
135	0.271	0.545	0.819	0.166	-68.190	-111.322	-154.454	26.222	-8.942	-14.661	-20.379	3.476
150	0.287	0.561	0.836	0.167	-66.762	-106.531	-146.299	24.178	-8.548	-13.888	-19.228	3.246
165	0.314	0.579	0.845	0.161	-64.288	-103.806	-143.325	24.026	-8.148	-13.422	-18.696	3.206
180	0.298	0.580	0.862	0.171	-60.150	-101.994	-143.837	25.439	-7.666	-13.132	-18.599	3.323

Table G.5: Out-of-plane and In-plane Deflections (δ) and Forces (F) for the Li Spectrum simulations for varying Azimuth Angle ϵ [°]

Li	Deflection δ [m]				Force F [kN]				Moment M [MNm]			
AA ϵ [°]	δ_y 5%	δ_y 50%	δ_y 95%	σ	F_y 5%	F_y 50%	F_y 95%	σ	M_x 5%	M_x 50%	M_x 95%	σ
0	0.058	0.087	0.115	0.017	5.694	8.534	11.373	1.726	0.773	1.090	1.408	0.193
15	0.057	0.086	0.116	0.018	5.639	8.527	11.415	1.756	0.787	1.087	1.386	0.182
30	0.058	0.085	0.113	0.017	5.689	8.423	11.156	1.662	0.780	1.075	1.370	0.179
45	0.055	0.084	0.114	0.018	5.399	8.332	11.265	1.783	0.751	1.060	1.369	0.188
60	0.057	0.084	0.111	0.016	5.628	8.274	10.919	1.608	0.770	1.053	1.336	0.172
75	0.055	0.082	0.110	0.017	5.413	8.116	10.818	1.643	0.755	1.029	1.302	0.166
90	0.052	0.081	0.110	0.018	5.099	7.979	10.858	1.751	0.724	1.008	1.292	0.172
105	0.052	0.079	0.106	0.017	5.091	7.786	10.481	1.639	0.717	0.979	1.241	0.159
120	0.050	0.077	0.104	0.016	4.925	7.589	10.252	1.619	0.698	0.950	1.202	0.153
135	0.050	0.074	0.098	0.015	4.932	7.322	9.711	1.453	0.676	0.911	1.147	0.143
150	0.048	0.073	0.097	0.015	4.693	7.153	9.613	1.496	0.658	0.884	1.110	0.137
165	0.046	0.072	0.098	0.016	4.516	7.083	9.649	1.560	0.652	0.869	1.085	0.132
180	0.045	0.070	0.095	0.015	4.487	6.910	9.333	1.473	0.651	0.847	1.043	0.119

Table G.6: Out-of-plane and In-plane Deflections (δ) and Forces (F) for the Li Spectrum simulations for varying Azimuth Angle ϵ [°]

Li	Deflection δ [m]				Force F [kN]				Moment M [MNm]			
AA ϵ [°]	δ_x 5%	δ_x 50%	δ_x 95%	σ	F_x 5%	F_x 50%	F_x 95%	σ	M_y 5%	M_y 50%	M_y 95%	σ
0	0.245	0.454	0.662	0.127	-95.488	-138.428	-181.367	26.105	-12.945	-18.820	-24.695	3.572
15	0.233	0.457	0.682	0.137	-97.561	-137.703	-177.844	24.404	-13.228	-18.718	-24.207	3.337
30	0.211	0.452	0.693	0.147	-96.304	-136.368	-176.431	24.357	-12.973	-18.527	-24.081	3.377
45	0.238	0.462	0.686	0.136	-94.243	-133.972	-173.702	24.154	-12.820	-18.174	-23.528	3.255
60	0.246	0.470	0.693	0.136	-94.236	-132.739	-171.242	23.408	-12.599	-17.979	-23.360	3.271
75	0.243	0.475	0.708	0.141	-91.678	-129.051	-166.424	22.721	-12.291	-17.430	-22.569	3.124
90	0.250	0.485	0.720	0.143	-88.092	-125.858	-163.624	22.960	-11.775	-16.937	-22.100	3.139
105	0.255	0.505	0.755	0.152	-85.829	-120.980	-156.131	21.370	-11.332	-16.192	-21.051	2.954
120	0.276	0.521	0.766	0.149	-83.879	-116.324	-148.769	19.725	-11.059	-15.461	-19.863	2.676
135	0.273	0.531	0.789	0.157	-79.272	-110.315	-141.357	18.872	-10.364	-14.545	-18.726	2.542
150	0.304	0.557	0.809	0.153	-76.445	-105.417	-134.390	17.614	-9.907	-13.754	-17.601	2.339
165	0.311	0.577	0.843	0.162	-74.591	-102.243	-129.896	16.812	-9.542	-13.206	-16.869	2.227
180	0.314	0.563	0.812	0.151	-72.937	-99.693	-126.449	16.266	-9.258	-12.868	-16.478	2.195

Orientation Ratios

Table G.7: Out-of-Plane Orientation Ratios for Yu($\epsilon(ii)$) vs. Kaimal($\epsilon(ii)$)

Yu	Deflection γ_δ [-]			Force γ_F [-]			Moment γ_M [-]		
AA ϵ [°]	$\gamma_{\delta y}$ 5%	$\gamma_{\delta y}$ 50%	$\gamma_{\delta y}$ 95%	γ_{Fy} 5%	γ_{Fy} 50%	γ_{Fy} 95%	γ_{Mx} 5%	γ_{Mx} 50%	γ_{Mx} 95%
0	1.24	1.21	1.19	1.24	1.21	1.19	1.11	1.21	1.27
15	1.19	1.16	1.14	1.19	1.16	1.14	1.08	1.16	1.21
30	1.18	1.18	1.19	1.18	1.18	1.19	1.04	1.19	1.27
45	1.23	1.18	1.16	1.23	1.18	1.16	1.08	1.18	1.24
60	1.16	1.19	1.20	1.16	1.19	1.20	1.06	1.19	1.26
75	1.24	1.17	1.13	1.24	1.17	1.13	1.12	1.17	1.20
90	1.16	1.15	1.14	1.16	1.15	1.14	1.03	1.15	1.22
105	1.13	1.18	1.21	1.13	1.18	1.21	1.02	1.18	1.27
120	1.08	1.17	1.21	1.08	1.17	1.21	0.99	1.16	1.26
135	1.09	1.18	1.22	1.09	1.18	1.22	1.00	1.17	1.26
150	1.15	1.16	1.16	1.15	1.16	1.16	1.05	1.15	1.20
165	1.11	1.16	1.18	1.11	1.16	1.18	1.02	1.15	1.22
180	1.03	1.15	1.20	1.03	1.15	1.20	0.93	1.14	1.26

Table G.8: In-Plane Orientation Ratios for Yu($\epsilon(ii)$) vs. Kaimal($\epsilon(ii)$)

Yu	Deflection γ_δ [-]			Force γ_F [-]			Moment γ_M [-]		
AA ϵ [°]	$\gamma_{\delta x}$ 5%	$\gamma_{\delta x}$ 50%	$\gamma_{\delta x}$ 95%	γ_{Fx} 5%	γ_{Fx} 50%	γ_{Fx} 95%	γ_{My} 5%	γ_{My} 50%	γ_{My} 95%
0	1.35	1.18	1.13	1.13	1.21	1.26	1.13	1.22	1.26
15	1.14	1.09	1.07	1.12	1.17	1.19	1.13	1.17	1.19
30	1.33	1.15	1.10	1.07	1.19	1.26	1.07	1.19	1.26
45	1.25	1.16	1.13	1.11	1.18	1.23	1.11	1.19	1.23
60	1.10	1.18	1.20	1.11	1.19	1.24	1.12	1.19	1.23
75	1.52	1.16	1.07	1.14	1.17	1.18	1.14	1.17	1.18
90	1.20	1.14	1.13	1.04	1.15	1.21	1.03	1.15	1.22
105	1.13	1.19	1.21	1.04	1.18	1.25	1.04	1.17	1.25
120	1.17	1.19	1.20	1.01	1.16	1.24	1.01	1.15	1.23
135	1.23	1.24	1.25	1.01	1.16	1.23	1.01	1.15	1.22
150	1.18	1.23	1.25	1.02	1.13	1.19	1.00	1.12	1.18
165	1.22	1.23	1.23	1.01	1.13	1.20	0.99	1.12	1.19
180	1.17	1.22	1.24	0.92	1.12	1.23	0.91	1.10	1.21

Table G.9: Out-of-Plane Orientation Ratios for Li($\epsilon(ii)$) vs. Kaimal($\epsilon(ii)$)

Li	Deflection γ_δ [-]			Force γ_F [-]			Moment γ_M [-]		
AA ϵ [°]	$\gamma_{\delta y}$ 5%	$\gamma_{\delta y}$ 50%	$\gamma_{\delta y}$ 95%	γ_{Fy} 5%	γ_{Fy} 50%	γ_{Fy} 95%	γ_{Mx} 5%	γ_{Mx} 50%	γ_{Mx} 95%
0	1.19	1.19	1.19	1.18	1.19	1.19	1.19	1.18	1.13
15	1.21	1.20	1.19	1.17	1.21	1.20	1.19	1.17	1.18
30	1.29	1.19	1.15	1.03	1.29	1.19	1.15	1.03	1.21
45	1.21	1.18	1.16	1.12	1.21	1.18	1.16	1.12	1.14
60	1.24	1.19	1.17	1.09	1.24	1.19	1.17	1.09	1.20
75	1.24	1.19	1.17	1.10	1.24	1.19	1.17	1.10	1.21
90	1.14	1.17	1.18	1.21	1.14	1.17	1.18	1.21	1.12
105	1.17	1.18	1.18	1.19	1.17	1.18	1.18	1.19	1.17
120	1.16	1.17	1.17	1.19	1.16	1.17	1.17	1.19	1.18
135	1.19	1.16	1.15	1.11	1.19	1.16	1.15	1.11	1.18
150	1.18	1.14	1.12	1.07	1.18	1.14	1.12	1.07	1.18
165	1.14	1.14	1.15	1.15	1.14	1.14	1.15	1.15	1.18
180	1.10	1.12	1.13	1.15	1.10	1.12	1.13	1.15	1.14

Table G.10: In-Plane Orientation Ratios for Li($\epsilon(ii)$) vs. Kaimal($\epsilon(ii)$)

Li	Deflection γ_δ [-]			Force γ_F [-]			Moment γ_M [-]		
AA ϵ [°]	$\gamma_{\delta x}$ 5%	$\gamma_{\delta x}$ 50%	$\gamma_{\delta x}$ 95%	γ_{Fx} 5%	γ_{Fx} 50%	γ_{Fx} 95%	γ_{My} 5%	γ_{My} 50%	γ_{My} 95%
0	1.19	1.23	1.38	1.46	1.15	1.07	0.93	1.14	1.20
15	1.20	1.21	1.25	1.22	1.15	1.13	1.09	1.20	1.20
30	1.20	1.19	1.17	1.30	1.15	1.11	1.04	1.21	1.20
45	1.18	1.20	1.28	1.33	1.14	1.09	0.99	1.17	1.18
60	1.19	1.19	1.19	1.35	1.17	1.11	1.01	1.22	1.20
75	1.19	1.18	1.13	1.45	1.18	1.11	0.99	1.22	1.19
90	1.17	1.20	1.31	1.24	1.16	1.14	1.10	1.12	1.17
105	1.18	1.18	1.20	1.15	1.19	1.20	1.23	1.17	1.17
120	1.16	1.16	1.13	1.26	1.21	1.20	1.16	1.19	1.16
135	1.15	1.14	1.10	1.24	1.21	1.21	1.19	1.18	1.15
150	1.14	1.11	1.02	1.25	1.22	1.21	1.18	1.17	1.12
165	1.13	1.11	1.02	1.21	1.22	1.23	1.24	1.17	1.12
180	1.11	1.09	1.00	1.23	1.18	1.17	1.14	1.11	1.09

Blade Orientation Sensitivity

Table G.11: Out-of-plane Orientation Sensitivity for Kaimal($\epsilon(n)$ vs. Kaimal(ϵ = 0[°])

Kaimal	Deflection γ_δ [-]			Force γ_F [-]			Moment γ_M [-]		
AA ϵ [°]	$\gamma_{\delta y}$ 5%	$\gamma_{\delta y}$ 50%	$\gamma_{\delta y}$ 95%	γ_{Fy} 5%	γ_{Fy} 50%	γ_{Fy} 95%	γ_{Mx} 5%	γ_{Mx} 50%	γ_{Mx} 95%
0	1.00	1.00	1.00	1.00	1.00	1.00	1.00	1.00	1.00
15	0.98	0.99	1.00	0.98	0.99	1.00	1.03	0.98	1.00
30	0.92	0.98	1.01	0.92	0.98	1.01	1.10	0.94	1.01
45	0.93	0.98	1.01	0.93	0.98	1.01	1.09	0.96	1.00
60	0.95	0.97	0.98	0.95	0.97	0.98	1.01	0.94	0.98
75	0.91	0.95	0.97	0.91	0.95	0.97	1.02	0.91	0.97
90	0.93	0.95	0.96	0.93	0.95	0.96	0.99	0.95	0.94
105	0.91	0.92	0.93	0.91	0.92	0.93	0.94	0.90	0.92
120	0.89	0.90	0.91	0.89	0.90	0.91	0.93	0.87	0.91
135	0.87	0.88	0.88	0.87	0.88	0.88	0.90	0.84	0.88
150	0.83	0.87	0.89	0.83	0.87	0.89	0.96	0.81	0.87
165	0.83	0.86	0.88	0.83	0.86	0.88	0.93	0.81	0.85
180	0.85	0.86	0.87	0.85	0.86	0.87	0.88	0.83	0.84

Table G.12: In-plane Orientation Sensitivity for Kaimal($\epsilon(n)$ vs. Kaimal(ϵ = 0[°])

Kaimal	Deflection γ_δ [-]			Force γ_F [-]			Moment γ_M [-]		
AA ϵ [°]	$\gamma_{\delta x}$ 5%	$\gamma_{\delta x}$ 50%	$\gamma_{\delta x}$ 95%	γ_{Fx} 5%	γ_{Fx} 50%	γ_{Fx} 95%	γ_{My} 5%	γ_{My} 50%	γ_{My} 95%
0	1.00	1.00	1.00	1.00	1.00	1.00	1.00	1.00	1.00
15	1.13	1.01	0.98	0.97	0.99	1.00	0.97	0.99	1.00
30	0.97	1.00	1.01	0.95	0.98	1.00	0.97	0.98	0.98
45	1.06	1.03	1.02	0.97	0.98	0.99	0.97	0.98	0.98
60	1.08	1.02	1.01	0.93	0.96	0.97	0.92	0.95	0.97
75	0.99	1.02	1.03	0.90	0.94	0.96	0.90	0.93	0.95
90	1.20	1.06	1.02	0.94	0.93	0.93	0.94	0.92	0.92
105	1.32	1.08	1.01	0.88	0.89	0.90	0.86	0.88	0.89
120	1.30	1.09	1.04	0.84	0.87	0.88	0.83	0.85	0.86
135	1.31	1.11	1.06	0.80	0.83	0.85	0.79	0.81	0.83
150	1.44	1.16	1.08	0.78	0.81	0.83	0.76	0.79	0.80
165	1.53	1.20	1.11	0.76	0.79	0.81	0.74	0.76	0.78
180	1.52	1.21	1.12	0.78	0.79	0.79	0.75	0.76	0.76

Table G.13: Out-of-plane Orientation Sensitivity for Yu($\epsilon(n)$ vs. Yu(ϵ = 0[°])

Yu	Deflection γ_δ [-]			Force γ_F [-]			Moment γ_M [-]		
AA ϵ [°]	$\gamma_{\delta y}$ 5%	$\gamma_{\delta y}$ 50%	$\gamma_{\delta y}$ 95%	γ_{Fy} 5%	γ_{Fy} 50%	γ_{Fy} 95%	γ_{Mx} 5%	γ_{Mx} 50%	γ_{Mx} 95%
0	1.00	1.00	1.00	1.00	1.00	1.00	1.00	1.00	1.00
15	0.94	0.95	0.96	0.94	0.95	0.96	0.95	0.95	0.96
30	0.88	0.96	1.01	0.88	0.96	1.01	0.89	0.96	1.00
45	0.92	0.96	0.99	0.92	0.96	0.99	0.93	0.96	0.98
60	0.89	0.95	0.99	0.89	0.95	0.99	0.90	0.95	0.97
75	0.91	0.92	0.92	0.91	0.92	0.92	0.92	0.91	0.91
90	0.87	0.91	0.92	0.87	0.91	0.92	0.88	0.90	0.91
105	0.83	0.90	0.94	0.83	0.90	0.94	0.83	0.89	0.92
120	0.78	0.87	0.92	0.78	0.87	0.92	0.78	0.86	0.90
135	0.76	0.86	0.91	0.76	0.86	0.91	0.76	0.83	0.87
150	0.77	0.84	0.87	0.77	0.84	0.87	0.76	0.81	0.83
165	0.75	0.83	0.87	0.75	0.83	0.87	0.74	0.80	0.82
180	0.71	0.82	0.88	0.71	0.82	0.88	0.70	0.78	0.83

Table G.14: In-plane Orientation Sensitivity for Yu($\epsilon(n)$ vs. Yu(ϵ = 0[°])

Yu	Deflection γ_δ [-]			Force γ_F [-]			Moment γ_M [-]		
AA ϵ [°]	$\gamma_{\delta x}$ 5%	$\gamma_{\delta x}$ 50%	$\gamma_{\delta x}$ 95%	γ_{Fx} 5%	γ_{Fx} 50%	γ_{Fx} 95%	γ_{My} 5%	γ_{My} 50%	γ_{Mx} 95%
0	1.00	1.00	1.00	1.00	1.00	1.00	1.00	1.00	1.00
15	0.95	0.93	0.93	0.96	0.95	0.95	0.97	0.95	0.95
30	0.95	0.98	0.99	0.90	0.96	0.99	0.91	0.96	0.98
45	0.98	1.01	1.02	0.95	0.95	0.96	0.96	0.95	0.95
60	0.88	1.02	1.07	0.91	0.94	0.95	0.92	0.93	0.94
75	1.12	1.01	0.98	0.91	0.90	0.90	0.91	0.89	0.89
90	1.07	1.03	1.02	0.86	0.88	0.89	0.85	0.87	0.88
105	1.10	1.09	1.09	0.81	0.86	0.89	0.79	0.85	0.88
120	1.12	1.11	1.10	0.76	0.83	0.86	0.74	0.81	0.84
135	1.19	1.18	1.17	0.72	0.79	0.83	0.71	0.77	0.80
150	1.26	1.21	1.20	0.71	0.76	0.79	0.67	0.73	0.75
165	1.38	1.25	1.21	0.68	0.74	0.77	0.64	0.70	0.73
180	1.31	1.25	1.23	0.64	0.73	0.77	0.60	0.69	0.73

Table G.15: Out-of-plane Orientation Sensitivity for Li($\epsilon(n)$ vs. Li(ϵ = 0[°])

Li	Deflection γ_δ [-]			Force γ_F [-]			Moment γ_M [-]		
AA ϵ [°]	$\gamma_{\delta y}$ 5%	$\gamma_{\delta y}$ 50%	$\gamma_{\delta y}$ 95%	γ_{Fy} 5%	γ_{Fy} 50%	γ_{Fy} 95%	γ_{Mx} 5%	γ_{Mx} 50%	γ_{Mx} 95%
0	1.00	1.00	1.00	1.00	1.00	1.00	1.00	1.00	1.00
15	0.99	1.00	1.00	0.99	1.00	1.00	1.02	1.00	0.98
30	1.00	0.99	0.98	1.00	0.99	0.98	1.01	0.99	0.97
45	0.95	0.98	0.99	0.95	0.98	0.99	0.97	0.97	0.97
60	0.99	0.97	0.96	0.99	0.97	0.96	1.00	0.97	0.95
75	0.95	0.95	0.95	0.95	0.95	0.95	0.98	0.94	0.92
90	0.90	0.93	0.95	0.90	0.93	0.95	0.94	0.92	0.92
105	0.89	0.91	0.92	0.89	0.91	0.92	0.93	0.90	0.88
120	0.86	0.89	0.90	0.86	0.89	0.90	0.90	0.87	0.85
135	0.87	0.86	0.85	0.87	0.86	0.85	0.87	0.84	0.81
150	0.82	0.84	0.85	0.82	0.84	0.85	0.85	0.81	0.79
165	0.79	0.83	0.85	0.79	0.83	0.85	0.84	0.80	0.77
180	0.79	0.81	0.82	0.79	0.81	0.82	0.84	0.78	0.74

Table G.16: In-plane Orientation Sensitivity for Li($\epsilon(n)$ vs. Li(ϵ = 0[°])

Li	Deflection γ_δ [-]			Force γ_F [-]			Moment γ_M [-]		
AA ϵ [°]	$\gamma_{\delta x}$ 5%	$\gamma_{\delta x}$ 50%	$\gamma_{\delta x}$ 95%	γ_{Fx} 5%	γ_{Fx} 50%	γ_{Fx} 95%	γ_{My} 5%	γ_{My} 50%	γ_{My} 95%
0	1.00	1.00	1.00	1.00	1.00	1.00	1.00	1.00	1.00
15	0.95	1.01	1.03	1.02	0.99	0.98	1.02	0.99	0.98
30	0.86	1.00	1.05	1.01	0.99	0.97	1.00	0.98	0.98
45	0.97	1.02	1.04	0.99	0.97	0.96	0.99	0.97	0.95
60	1.01	1.04	1.05	0.99	0.96	0.94	0.97	0.96	0.95
75	0.99	1.05	1.07	0.96	0.93	0.92	0.95	0.93	0.91
90	1.02	1.07	1.09	0.92	0.91	0.90	0.91	0.90	0.89
105	1.04	1.11	1.14	0.90	0.87	0.86	0.88	0.86	0.85
120	1.12	1.15	1.16	0.88	0.84	0.82	0.85	0.82	0.80
135	1.12	1.17	1.19	0.83	0.80	0.78	0.80	0.77	0.76
150	1.24	1.23	1.22	0.80	0.76	0.74	0.77	0.73	0.71
165	1.27	1.27	1.27	0.78	0.74	0.72	0.74	0.70	0.68
180	1.28	1.24	1.23	0.76	0.72	0.70	0.72	0.68	0.67

3-Bladed Rotor Thrust Force

Table G.17: 3-Bladed, stationary Rotor Thrust Force F_t for Kaimal($z_0(0.0002)$), Yu($z_0(0.006)$) and Li($z_0(0.006)$)

Spectrum	Kaimal			Yu			Li		
	Force F_t [kN]			Force F_t [kN]			Force F_t [kN]		
AA [°]	F_y 5%	F_y 50%	F_y 95%	F_y 5%	F_y 50%	F_y 95%	F_y 5%	F_y 50%	F_y 95%
0	13.29	20.16	27.04	15.13	23.81	32.49	15.54	23.71	31.88
15	13.18	20.06	26.94	15.00	23.49	31.99	15.66	23.63	31.61
30	12.84	20.16	27.48	14.95	23.44	31.94	15.48	23.55	31.63
45	12.80	20.08	27.37	15.31	23.49	31.68	15.33	23.53	31.73
60	13.31	20.39	27.47	14.68	23.59	32.50	15.74	23.46	31.17

Table G.18

Spectrum	Yu			Li		
	Force γ_{Ft} [-]			Force γ_{Ft} [-]		
AA [°]	γ_{Fy} 5%	γ_{Fy} 50%	γ_{Fy} 95%	γ_{Fy} 5%	γ_{Fy} 50%	γ_{Fy} 95%
0	1.14	1.18	1.20	1.17	1.18	1.18
15	1.14	1.17	1.19	1.19	1.18	1.17
30	1.16	1.16	1.16	1.21	1.17	1.15
45	1.20	1.17	1.16	1.20	1.17	1.16
60	1.10	1.16	1.18	1.18	1.15	1.13

H

Appendix H : Constant Wind Speed - Full Simulation Results

Table H.1: External Blade Forces and Bending Moments for a constant acting wind speed i.e. zero turbulence intensity ($T.I. = 0\%$)

		Out-of-Plane			In-Plane		
		δ [m]	F [kN]	M [MNm]	δ [m]	F [kN]	M [MNm]
U10 [m/s]	T [years]	δ_y 50%	F_y 50%	M_x 50%	δ_x 50%	F_x 50%	M_y 50%
11.4	Rated	0.00	0.99	0.04	0.02	-33.19	-0.62
30.6	[H1	0.02	7.15	0.27	0.13	-239.15	-4.46
36.5	10	0.03	10.17	0.38	0.18	-340.27	-6.35
40.1	[H2	0.04	12.27	0.46	0.22	-410.70	-7.67
44.9	25	0.05	15.38	0.57	0.28	-514.90	-9.61
46.8	[H3	0.05	16.71	0.62	0.30	-559.40	-10.44
50.1	50	0.06	19.15	0.71	0.35	-641.07	-11.97
54.5	100	0.07	22.67	0.84	0.41	-758.62	-14.16
55.4	[H4	0.07	23.42	0.87	0.42	-783.88	-14.63
58.2	200	0.08	25.85	0.96	0.47	-865.12	-16.15
66.9	[H5	0.10	34.15	1.27	0.62	-1143.10	-21.34
69.5	1000	0.11	36.86	1.37	0.67	-1233.68	-23.03
72.5	2000	0.12	40.11	1.49	0.73	-1342.48	-25.06
78.7	10000	0.14	47.26	1.76	0.85	-1581.91	-29.53

Table H.2: Internal Blade Forces and Bending Moments for a constant acting wind speed i.e. zero turbulence intensity ($T.I. = 0\%$)

		Out-of-Plane			In-Plane		
		δ [m]	F [kN]	M [MNm]	δ [m]	F [kN]	M [MNm]
U10 [m/s]	T [years]	δ_y 50%	F_y 50%	M_x 50%	δ_x 50%	F_x 50%	M_y 50%
11.4	Rated	0.00	0.29	0.01	0.02	-4.61	-1.49
30.6	[H1	0.02	2.11	0.04	0.13	-33.20	-10.76
36.5	10	0.03	3.00	0.06	0.18	-47.23	-15.31
40.1	[H2	0.04	3.62	0.08	0.22	-57.01	-18.47
44.9	25	0.05	4.54	0.09	0.28	-71.47	-23.16
46.8	[H3	0.05	4.93	0.10	0.30	-77.65	-25.16
50.1	50	0.06	5.65	0.12	0.35	-88.98	-28.84
54.5	100	0.07	6.68	0.14	0.41	-105.30	-34.13
55.4	[H4	0.07	6.90	0.14	0.42	-108.81	-35.26
58.2	200	0.08	7.62	0.16	0.47	-120.08	-38.92
66.9	[H5	0.10	10.07	0.21	0.62	-158.67	-51.42
69.5	1000	0.10	10.07	0.21	0.62	-158.67	-51.42
72.5	2000	0.12	11.83	0.25	0.73	-186.34	-60.39
78.7	10000	0.14	13.93	0.29	0.85	-219.58	-71.16

Appendix I : Failure Probability - Full Calculation Results

Kaimal Spectrum - Shear Failure Probabilities

Table I.1: Probability of Failure Calculation Rated Wind Kaimal Spectrum

		Iteration			
Rated	Initial Values	1	2	3	4
σ_Z	3600888	3600888	3600888	3600888	3600888
μ_Z	31726732	13414605	18312127	13414605	18312127
β	8.81	3.73	5.09	3.73	5.09
a1	0.58	1.00	1.00	1.00	1.00
a2	-0.58	0.00	0.00	0.00	0.00
a5	-0.58	0.00	0.00	0.00	0.00
X1*	35.25	14.90	20.35	14.91	20.35
X2*	376.46	774.54	376.46	376.46	376.46
X3*	-6082.06	123.58	-6081.82	-6084.16	-6083.60
Pf	0.00E+00	9.75E-05	1.83E-07	9.75E-05	1.83E-07

Table I.2: Probability of Failure Calculation H1 Wind Kaimal Spectrum

		Iteration			
H1	Initial Values	1	2	3	4
σ_Z	3600900	3600891	3600900	3600900	3600900
μ_Z	31689440	13430461	18259046	13430394	18259046
β	8.80	3.73	5.07	3.73	5.07
a1	0.58	1.00	1.00	1.00	1.00
a2	-0.58	0.00	0.00	0.00	0.00
a5	-0.58	0.00	0.00	0.00	0.00
X1*	35.25	14.93	20.33	14.97	20.33
X2*	2676.58	5617.31	2676.88	2676.61	2676.60
X3*	-43302.37	3304.12	-43258.19	-43420.63	-43389.36
Pf	0.00E+00	9.58E-05	1.98E-07	9.58E-05	1.98E-07

Table I.3: Probability of Failure Calculation T10 Wind Kaimal Spectrum

		Iteration			
T10	Initial Values	1	2	3	4
σ_Z	3600910	3600890	3600910	3600910	3600910
μ_Z	31671027	13439723	18231363	13439663	18231363
β	8.80	3.73	5.06	3.73	5.06
a1	0.58	1.00	1.00	1.00	1.00
a2	-0.58	0.00	0.00	0.00	0.00
a5	-0.58	0.00	0.00	0.00	0.00
X1*	35.25	14.94	20.32	15.00	20.32
X2*	3809.67	7621.17	3810.24	3809.72	3809.71
X3*	-61681.00	2220.78	-61635.08	-61903.23	-61844.83
Pf	0.00E+00	9.49E-05	2.06E-07	9.49E-05	2.06E-07

Table I.4: Probability of Failure Calculation H2 Wind Kaimal Spectrum

		Iteration			
H2	Initial Values	1	2	3	4
σ_Z	3600918	3600888	3600918	3600918	3600918
μ_Z	31657040	13446289	18210733	13446307	18210733
β	8.79	3.73	5.06	3.73	5.06
a1	0.58	1.00	1.00	1.00	1.00
a2	-0.58	0.00	0.00	0.00	0.00
a5	-0.58	0.00	0.00	0.00	0.00
X1*	35.25	14.95	20.31	15.02	20.31
X2*	4676.73	9446.22	4677.65	4676.81	4676.79
X3*	-75640.87	-894.18	-75662.06	-75944.86	-75865.33
Pf	0.00E+00	9.42E-05	2.13E-07	9.42E-05	2.13E-07

Table I.5: Probability of Failure Calculation T25 Wind Kaimal Spectrum

		Iteration			
T25	Initial Values	1	2	3	4
σ_Z	3600938	3600891	3600938	3600938	3600938
μ_Z	31638528	13454588	18184041	13454487	18184041
β	8.79	3.74	5.05	3.74	5.05
a1	0.58	1.00	1.00	1.00	1.00
a2	-0.58	0.00	0.00	0.00	0.00
a5	-0.58	0.00	0.01	0.01	0.01
X1*	35.25	14.96	20.30	15.05	20.30
X2*	5818.53	11691.38	5819.89	5818.65	5818.62
X3*	-94117.45	2610.94	-94035.21	-94626.37	-94494.01
Pf	0.00E+00	9.33E-05	2.21E-07	9.33E-05	2.21E-07

Table I.6: Probability of Failure Calculation H3 Wind Kaimal Spectrum

		Iteration			
H3	Initial Values	1	2	3	4
σ_Z	3600939	3600898	3600939	3600939	3600939
μ_Z	31629398	13458173	18171133	13458265	18171133
β	8.78	3.74	5.05	3.74	5.05
a1	0.58	1.00	1.00	1.00	1.00
a2	-0.58	0.00	0.00	0.00	0.00
a5	-0.58	0.00	0.01	0.01	0.01
X1*	35.25	14.97	20.30	15.07	20.30
X2*	6358.63	12222.68	6359.87	6358.74	6358.71
X3*	-103231.61	-6118.25	-103401.98	-103744.54	-103611.51
Pf	0.00E+00	9.29E-05	2.25E-07	9.30E-05	2.25E-07

Table I.7: Probability of Failure Calculation T50 Wind Kaimal Spectrum

		Iteration			
T50	Initial Values	1	2	3	4
σ_Z	3600973	3600916	3600973	3600973	3600973
μ_Z	31617094	13461129	18156538	13460556	18156538
β	8.78	3.74	5.04	3.74	5.04
a1	0.58	1.00	1.00	1.00	1.00
a2	-0.58	0.00	0.00	0.00	0.00
a5	-0.58	0.00	0.01	0.01	0.01
X1*	35.25	14.97	20.30	15.08	20.30
X2*	7140.12	14773.99	7142.05	7140.32	7140.27
X3*	-115511.14	10265.16	-115146.47	-116371.49	-116149.00
Pf	0.00E+00	9.27E-05	2.30E-07	9.27E-05	2.30E-07

Table I.8: Probability of Failure Calculation T100 Wind Kaimal Spectrum

		Iteration			
T100	Initial Values	1	2	3	4
σ_Z	3600986	3600895	3600986	3600986	3600986
μ_Z	31592587	13475286	18117160	13475427	18117160
β	8.77	3.74	5.03	3.74	5.03
a1	0.58	1.00	1.00	1.00	1.00
a2	-0.58	0.00	0.00	0.00	0.00
a5	-0.58	0.00	0.01	0.01	0.01
X1*	35.25	14.99	20.28	15.13	20.28
X2*	8642.81	17391.89	8645.80	8643.07	8643.00
X3*	-139971.28	-4828.26	-140169.17	-140963.95	-140709.64
Pf	0.00E+00	9.12E-05	2.44E-07	9.12E-05	2.44E-07

Table I.9: Probability of Failure Calculation H4 Wind Kaimal Spectrum

		Iteration			
H4	Initial Values	1	2	3	4
σ_Z	3600995	3600894	3600995	3600995	3600995
μ_Z	31587280	13478011	18109127	13478152	18109127
β	8.77	3.74	5.03	3.74	5.03
a1	0.58	1.00	1.00	1.00	1.00
a2	-0.58	0.00	0.00	0.00	0.00
a5	-0.58	0.00	0.01	0.01	0.01
X1*	35.25	14.99	20.28	15.13	20.28
X2*	8981.48	17916.20	8984.62	8981.74	8981.67
X3*	-145268.20	-4332.33	-145457.40	-146347.67	-146071.64
Pf	0.00E+00	9.09E-05	2.47E-07	9.10E-05	2.47E-07

Table I.10: Probability of Failure Calculation T200 Wind Kaimal Spectrum

		Iteration			
T200	Initial Values	1	2	3	4
σ_Z	3601034	3600897	3601034	3601034	3601034
μ_Z	31573151	13484345	18089134	13484016	18089134
β	8.77	3.74	5.02	3.74	5.02
a1	0.58	1.00	1.00	1.00	1.00
a2	-0.58	0.00	0.00	0.00	0.00
a5	-0.58	0.00	0.01	0.01	0.01
X1*	35.25	15.00	20.27	15.16	20.27
X2*	9830.89	19854.76	9834.85	9831.23	9831.14
X3*	-159371.79	4901.75	-159109.29	-160838.04	-160464.81
Pf	0.00E+00	9.03E-05	2.54E-07	9.04E-05	2.54E-07

Table I.11: Probability of Failure Calculation H5 Wind Kaimal Spectrum

		Iteration			
H5	Initial Values	1	2	3	4
σ_Z	3601157	3600953	3601157	3601157	3601157
μ_Z	31524247	13503161	18022553	13501694	18022553
β	8.75	3.75	5.00	3.75	5.00
a1	0.58	1.00	1.00	1.00	1.00
a2	-0.58	0.00	0.00	0.00	0.00
a5	-0.58	-0.01	0.01	0.01	0.01
X1*	35.25	15.03	20.25	15.23	20.25
X2*	12858.47	26652.71	12865.25	12859.11	12858.94
X3*	-208181.22	14812.60	-207196.44	-210881.44	-210204.24
Pf	0.00E+00	8.85E-05	2.80E-07	8.87E-05	2.80E-07

Table I.12: Probability of Failure Calculation T1000 Wind Kaimal Spectrum

		Iteration			
T1000	Initial Values	1	2	3	4
σ_Z	3601190	3600926	3601190	3601190	3601190
μ_Z	31506832	13513413	17994495	13512337	17994495
β	8.75	3.75	5.00	3.75	5.00
a1	0.58	1.00	1.00	1.00	1.00
a2	-0.58	0.00	0.00	0.00	0.00
a5	-0.58	0.00	0.01	0.01	0.01
X1*	35.25	15.05	20.24	15.26	20.24
X2*	13916.62	28551.91	13924.82	13917.34	13917.15
X3*	-225564.63	10616.10	-224770.59	-228592.30	-227838.30
Pf	0.00E+00	8.74E-05	2.91E-07	8.76E-05	2.91E-07

Table I.13: Probability of Failure Calculation T2000 Wind Kaimal Spectrum

		Iteration			
T2000	Initial Values	1	2	3	4
σ_Z	3601228	3600890	3601228	3601228	3601228
μ_Z	31483290	13526298	17957091	13526199	17957091
β	8.74	3.76	4.99	3.76	4.99
a1	0.58	1.00	1.00	1.00	1.00
a2	-0.58	0.00	0.00	0.00	0.00
a5	-0.58	0.00	0.01	0.01	0.01
X1*	35.25	15.06	20.22	15.31	20.23
X2*	15371.42	31338.50	15381.85	15372.27	15372.05
X3*	-249061.69	1052.72	-248975.69	-252455.18	-251617.98
Pf	0.00E+00	8.62E-05	3.08E-07	8.63E-05	3.08E-07

Table I.14: Probability of Failure Calculation T10000 Wind Kaimal Spectrum

		Iteration			
T10000	Initial Values	1	2	3	4
σ_Z	3601312	3600927	3601312	3601312	3601312
μ_Z	31441937	13544357	17896924	13545012	17896925
β	8.73	3.76	4.97	3.76	4.97
a1	0.58	1.00	1.00	1.00	1.00
a2	-0.58	0.00	0.00	0.00	0.00
a5	-0.58	0.00	0.02	0.02	0.02
X1*	35.25	15.09	20.20	15.37	20.21
X2*	17952.79	35909.15	17965.45	17953.87	17953.60
X3*	-290334.02	-11136.37	-291283.26	-294559.54	-293532.18
Pf	0.00E+00	8.45E-05	3.36E-07	8.46E-05	3.36E-07

Yu Spectrum - Shear Failure Probabilities

Table I.15: Probability of Shear Failure Calculation Rated Wind Yu Spectrum

		Iteration			
Rated	Initial Values	1	2	3	4
σ_Z	3600888	3600888	3600888	3600888	3600888
μ_Z	31726732	13414605	18312127	13414605	18312127
β	8.81	3.73	5.09	3.73	5.09
a1	0.58	1.00	1.00	1.00	1.00
a2	-0.58	0.00	0.00	0.00	0.00
a5	-0.58	0.00	0.00	0.00	0.00
X1*	35.25	14.90	20.35	14.91	20.35
X2*	376.46	774.54	376.46	376.46	376.46
X3*	-6082.06	123.58	-6081.82	-6084.16	-6083.60
Pf	0.00E+00	9.75E-05	1.83E-07	9.75E-05	1.83E-07

Table I.16: Probability of Shear Failure Calculation H1 Wind Yu Spectrum

H1	Initial Values	1	2	3	4
σ_Z	3600900	3600891	3600900	3600900	3600900
μ_Z	31689440	13430461	18259046	13430394	18259046
β	8.80	3.73	5.07	3.73	5.07
a1	0.58	1.00	1.00	1.00	1.00
a2	-0.58	0.00	0.00	0.00	0.00
a5	-0.58	0.00	0.00	0.00	0.00
X1*	35.25	14.93	20.33	14.97	20.33
X2*	2676.58	5617.31	2676.88	2676.61	2676.60
X3*	-43302.37	3304.12	-43258.19	-43420.63	-43389.36
Pf	0.00E+00	9.58E-05	1.98E-07	9.58E-05	1.98E-07

Table I.17: Probability of Failure Calculation T10 Wind Yu Spectrum

		Iteration			
T10	Initial Values	1	2	3	4
σ_Z	3600910	3600890	3600910	3600910	3600910
μ_Z	31671027	13439723	18231363	13439663	18231363
β	8.80	3.73	5.06	3.73	5.06
a1	0.58	1.00	1.00	1.00	1.00
a2	-0.58	0.00	0.00	0.00	0.00
a5	-0.58	0.00	0.00	0.00	0.00
X1*	35.25	14.94	20.32	15.00	20.32
X2*	3809.67	7621.17	3810.24	3809.72	3809.71
X3*	-61681.00	2220.78	-61635.08	-61903.23	-61844.83
Pf	0.00E+00	9.49E-05	2.06E-07	9.49E-05	2.06E-07

Table I.18: Probability of Failure Calculation H2 Wind Yu Spectrum

		Iteration			
H2	Initial Values	1	2	3	4
σ_Z	3600918	3600888	3600918	3600918	3600918
μ_Z	31657040	13446289	18210733	13446307	18210733
β	8.79	3.73	5.06	3.73	5.06
a1	0.58	1.00	1.00	1.00	1.00
a2	-0.58	0.00	0.00	0.00	0.00
a5	-0.58	0.00	0.00	0.00	0.00
X1*	35.25	14.95	20.31	15.02	20.31
X2*	4676.73	9446.22	4677.65	4676.81	4676.79
X3*	-75640.87	-894.18	-75662.06	-75944.86	-75865.33
Pf	0.00E+00	9.42E-05	2.13E-07	9.42E-05	2.13E-07

Table I.19: Probability of Failure Calculation T25 Wind Yu Spectrum

		Iteration			
T25	Initial Values	1	2	3	4
σ_Z	3600938	3600891	3600938	3600938	3600938
μ_Z	31638528	13454588	18184041	13454487	18184041
β	8.79	3.74	5.05	3.74	5.05
a1	0.58	1.00	1.00	1.00	1.00
a2	-0.58	0.00	0.00	0.00	0.00
a5	-0.58	0.00	0.01	0.01	0.01
X1*	35.25	14.96	20.30	15.05	20.30
X2*	5818.53	11691.38	5819.89	5818.65	5818.62
X3*	-94117.45	2610.94	-94035.21	-94626.37	-94494.01
Pf	0.00E+00	9.33E-05	2.21E-07	9.33E-05	2.21E-07

Table I.20: Probability of Failure Calculation H3 Wind Yu Spectrum

		Iteration			
H3	Initial Values	1	2	3	4
σ_Z	3600939	3600898	3600939	3600939	3600939
μ_Z	31629398	13458173	18171133	13458265	18171133
β	8.78	3.74	5.05	3.74	5.05
a1	0.58	1.00	1.00	1.00	1.00
a2	-0.58	0.00	0.00	0.00	0.00
a5	-0.58	0.00	0.01	0.01	0.01
X1*	35.25	14.97	20.30	15.07	20.30
X2*	6358.63	12222.68	6359.87	6358.74	6358.71
X3*	-103231.61	-6118.25	-103401.98	-103744.54	-103611.51
Pf	0.00E+00	9.29E-05	2.25E-07	9.30E-05	2.25E-07

Table I.21: Probability of Failure Calculation T50 Wind Yu Spectrum

		Iteration			
T50	Initial Values	1	2	3	4
σ_Z	3600973	3600916	3600973	3600973	3600973
μ_Z	31617094	13461129	18156538	13460556	18156538
β	8.78	3.74	5.04	3.74	5.04
a1	0.58	1.00	1.00	1.00	1.00
a2	-0.58	0.00	0.00	0.00	0.00
a5	-0.58	0.00	0.01	0.01	0.01
X1*	35.25	14.97	20.30	15.08	20.30
X2*	7140.12	14773.99	7142.05	7140.32	7140.27
X3*	-115511.14	10265.16	-115146.47	-116371.49	-116149.00
Pf	0.00E+00	9.27E-05	2.30E-07	9.27E-05	2.30E-07

Table I.22: Probability of Failure Calculation T100 Wind Yu Spectrum

		Iteration			
T100	Initial Values	1	2	3	4
σ_Z	3600986	3600895	3600986	3600986	3600986
μ_Z	31592587	13475286	18117160	13475427	18117160
β	8.77	3.74	5.03	3.74	5.03
a1	0.58	1.00	1.00	1.00	1.00
a2	-0.58	0.00	0.00	0.00	0.00
a5	-0.58	0.00	0.01	0.01	0.01
X1*	35.25	14.99	20.28	15.13	20.28
X2*	8642.81	17391.89	8645.80	8643.07	8643.00
X3*	-139971.28	-4828.26	-140169.17	-140963.95	-140709.64
Pf	0.00E+00	9.12E-05	2.44E-07	9.12E-05	2.44E-07

Table I.23: Probability of Failure Calculation H4 Wind Yu Spectrum

		Iteration			
H4	Initial Values	1	2	3	4
σ_Z	3600995	3600894	3600995	3600995	3600995
μ_Z	31587280	13478011	18109127	13478152	18109127
β	8.77	3.74	5.03	3.74	5.03
a1	0.58	1.00	1.00	1.00	1.00
a2	-0.58	0.00	0.00	0.00	0.00
a5	-0.58	0.00	0.01	0.01	0.01
X1*	35.25	14.99	20.28	15.13	20.28
X2*	8981.48	17916.20	8984.62	8981.74	8981.67
X3*	-145268.20	-4332.33	-145457.40	-146347.67	-146071.64
Pf	0.00E+00	9.09E-05	2.47E-07	9.10E-05	2.47E-07

Table I.24: Probability of Failure Calculation T200 Wind Yu Spectrum

		Iteration			
T200	Initial Values	1	2	3	4
σ_Z	3601034	3600897	3601034	3601034	3601034
μ_Z	31573151	13484345	18089134	13484016	18089134
β	8.77	3.74	5.02	3.74	5.02
a1	0.58	1.00	1.00	1.00	1.00
a2	-0.58	0.00	0.00	0.00	0.00
a5	-0.58	0.00	0.01	0.01	0.01
X1*	35.25	15.00	20.27	15.16	20.27
X2*	9830.89	19854.76	9834.85	9831.23	9831.14
X3*	-159371.79	4901.75	-159109.29	-160838.04	-160464.81
Pf	0.00E+00	9.03E-05	2.54E-07	9.04E-05	2.54E-07

Table I.25: Probability of Failure Calculation H5 Wind Yu Spectrum

		Iteration			
H5	Initial Values	1	2	3	4
σ_Z	3601157	3600953	3601157	3601157	3601157
μ_Z	31524247	13503161	18022553	13501694	18022553
β	8.75	3.75	5.00	3.75	5.00
a1	0.58	1.00	1.00	1.00	1.00
a2	-0.58	0.00	0.00	0.00	0.00
a5	-0.58	-0.01	0.01	0.01	0.01
X1*	35.25	15.03	20.25	15.23	20.25
X2*	12858.47	26652.71	12865.25	12859.11	12858.94
X3*	-208181.22	14812.60	-207196.44	-210881.44	-210204.24
Pf	0.00E+00	8.85E-05	2.80E-07	8.87E-05	2.80E-07

Table I.26: Probability of Failure Calculation T1000 Wind Yu Spectrum

		Iteration			
T1000	Initial Values	1	2	3	4
σ_Z	3601190	3600926	3601190	3601190	3601190
μ_Z	31506832	13513413	17994495	13512337	17994495
β	8.75	3.75	5.00	3.75	5.00
a1	0.58	1.00	1.00	1.00	1.00
a2	-0.58	0.00	0.00	0.00	0.00
a5	-0.58	0.00	0.01	0.01	0.01
X1*	35.25	15.05	20.24	15.26	20.24
X2*	13916.62	28551.91	13924.82	13917.34	13917.15
X3*	-225564.63	10616.10	-224770.59	-228592.30	-227838.30
Pf	0.00E+00	8.74E-05	2.91E-07	8.76E-05	2.91E-07

Table I.27: Probability of Failure Calculation T2000 Wind Yu Spectrum

		Iteration			
T2000	Initial Values	1	2	3	4
σ_Z	3601228	3600890	3601228	3601228	3601228
μ_Z	31483290	13526298	17957091	13526199	17957091
β	8.74	3.76	4.99	3.76	4.99
a1	0.58	1.00	1.00	1.00	1.00
a2	-0.58	0.00	0.00	0.00	0.00
a5	-0.58	0.00	0.01	0.01	0.01
X1*	35.25	15.06	20.22	15.31	20.23
X2*	15371.42	31338.50	15381.85	15372.27	15372.05
X3*	-249061.69	1052.72	-248975.69	-252455.18	-251617.98
Pf	0.00E+00	8.62E-05	3.08E-07	8.63E-05	3.08E-07

Table I.28: Probability of Failure Calculation T10000 Wind Yu Spectrum

		Iteration			
T10000	Initial Values	1	2	3	4
σ_Z	3601312	3600927	3601312	3601312	3601312
μ_Z	31441937	13544357	17896924	13545012	17896925
β	8.73	3.76	4.97	3.76	4.97
a1	0.58	1.00	1.00	1.00	1.00
a2	-0.58	0.00	0.00	0.00	0.00
a5	-0.58	0.00	0.02	0.02	0.02
X1*	35.25	15.09	20.20	15.37	20.21
X2*	17952.79	35909.15	17965.45	17953.87	17953.60
X3*	-290334.02	-11136.37	-291283.26	-294559.54	-293532.18
Pf	0.00E+00	8.45E-05	3.36E-07	8.46E-05	3.36E-07

Li Spectrum - Shear Failure Probabilities

Table I.29: Probability of Failure Calculation Rated Wind Li Spectrum

		Iteration			
Rated	Initial Values	1	2	3	4
σ_Z	3600888	3600888	3600888	3600888	3600888
μ_Z	31726738	13414348	18312392	13414345	18312392
β	8.81	3.73	5.09	3.73	5.09
a1	0.58	1.00	1.00	1.00	1.00
a2	-0.58	0.00	0.00	0.00	0.00
a5	-0.58	0.00	0.00	0.00	0.00
X1*	35.25	14.90	20.35	14.91	20.35
X2*	375.09	734.33	375.09	375.09	375.09
X3*	-6075.92	734.05	-6074.61	-6078.44	-6077.77
Pf	0.00E+00	9.75E-05	1.83E-07	9.75E-05	1.83E-07

Table I.30: Probability of Failure Calculation H1 Wind Li Spectrum

		Iteration			
H1	Initial Values	1	2	3	4
σ_Z	3600896	3600891	3600896	3600896	3600896
μ_Z	31689622	13430592	18259015	13430607	18259015
β	8.80	3.73	5.07	3.73	5.07
a1	0.58	1.00	1.00	1.00	1.00
a2	-0.58	0.00	0.00	0.00	0.00
a5	-0.58	0.00	0.00	0.00	0.00
X1*	35.25	14.93	20.33	14.97	20.33
X2*	2660.87	5188.44	2661.09	2660.90	2660.89
X3*	-43120.88	-3510.12	-43156.16	-43206.30	-43183.72
Pf	0.00E+00	9.58E-05	1.98E-07	9.58E-05	1.98E-07

Table I.31: Probability of Failure Calculation T10 Wind Li Spectrum

		Iteration			
T10	Initial Values	1	2	3	4
σ_Z	3600906	3600893	3600906	3600906	3600906
μ_Z	31670589	13438870	18231686	13438902	18231686
β	8.80	3.73	5.06	3.73	5.06
a1	0.58	1.00	1.00	1.00	1.00
a2	-0.58	0.00	0.00	0.00	0.00
a5	-0.58	0.00	0.00	0.00	0.00
X1*	35.25	14.94	20.32	15.00	20.32
X2*	3831.00	7546.00	3831.46	3831.04	3831.03
X3*	-62118.56	-4943.53	-62190.57	-62296.48	-62249.71
Pf	0.00E+00	9.49E-05	2.06E-07	9.49E-05	2.06E-07

Table I.32: Probability of Failure Calculation H2 Wind Li Spectrum

		Iteration			
H2	Initial Values	1	2	3	4
σ_Z	3600911	3600899	3600911	3600911	3600911
μ_Z	31658967	13442130	18216801	13442166	18216801
β	8.79	3.73	5.06	3.73	5.06
a1	0.58	1.00	1.00	1.00	1.00
a2	-0.58	0.00	0.00	0.00	0.00
a5	-0.58	0.00	0.00	0.00	0.00
X1*	35.25	14.95	20.32	15.01	20.32
X2*	4555.44	8990.76	4556.01	4555.51	4555.49
X3*	-73717.68	-8679.86	-73835.89	-73947.88	-73887.55
Pf	0.00E+00	9.46E-05	2.11E-07	9.46E-05	2.11E-07

Table I.33: Probability of Failure Calculation T25 Wind Li Spectrum

		Iteration			
T25	Initial Values	1	2	3	4
σ_Z	3600924	3600907	3600924	3600924	3600924
μ_Z	31638792	13449967	18188772	13450020	18188772
β	8.79	3.74	5.05	3.74	5.05
a1	0.58	1.00	1.00	1.00	1.00
a2	-0.58	0.00	0.00	0.00	0.00
a5	-0.58	0.00	0.00	0.00	0.00
X1*	35.25	14.96	20.31	15.05	20.31
X2*	5788.98	11352.34	5789.85	5789.08	5789.06
X3*	-93855.02	-11804.09	-94050.61	-94221.31	-94125.88
Pf	0.00E+00	9.38E-05	2.20E-07	9.38E-05	2.20E-07

Table I.34: Probability of Failure Calculation H3 Wind Li Spectrum

		Iteration			
H3	Initial Values	1	2	3	4
σ_Z	3600932	3600911	3600932	3600932	3600932
μ_Z	31629466	13453701	18175700	13453766	18175700
β	8.78	3.74	5.05	3.74	5.05
a1	0.58	1.00	1.00	1.00	1.00
a2	-0.58	0.00	0.00	0.00	0.00
a5	-0.58	0.00	0.00	0.00	0.00
X1*	35.25	14.96	20.31	15.06	20.31
X2*	6364.48	12595.67	6365.57	6364.61	6364.57
X3*	-103162.75	-12950.73	-103398.12	-103605.48	-103490.47
Pf	0.00E+00	9.34E-05	2.24E-07	9.34E-05	2.24E-07

Table I.35: Probability of Failure Calculation T50 Wind Li Spectrum

		Iteration			
T50	Initial Values	1	2	3	4
σ_Z	3600940	3600920	3600940	3600940	3600940
μ_Z	31616495	13457135	18159294	13457201	18159294
β	8.78	3.74	5.04	3.74	5.04
a1	0.58	1.00	1.00	1.00	1.00
a2	-0.58	0.00	0.00	0.00	0.00
a5	-0.58	0.00	0.01	0.01	0.01
X1*	35.25	14.97	20.30	15.08	20.30
X2*	7163.94	13810.02	7165.06	7164.09	7164.05
X3*	-116109.65	-17336.37	-116417.85	-116640.35	-116502.94
Pf	0.00E+00	9.31E-05	2.29E-07	9.31E-05	2.29E-07

Table I.36: Probability of Failure Calculation T100 Wind Li Spectrum

		Iteration			
T100	Initial Values	1	2	3	4
σ_Z	3600946	3600934	3600946	3600946	3600946
μ_Z	31597375	13455345	18141988	13455387	18141988
β	8.77	3.74	5.04	3.74	5.04
a1	0.58	1.00	1.00	1.00	1.00
a2	-0.58	0.00	0.00	0.00	0.00
a5	-0.58	0.01	0.01	0.01	0.01
X1*	35.25	14.99	20.30	15.10	20.30
X2*	8354.82	16054.11	8355.92	8355.02	8354.97
X3*	-135192.14	-31126.99	-135581.28	-135781.38	-135629.17
Pf	0.00E+00	9.33E-05	2.35E-07	9.33E-05	2.35E-07

Table I.37: Probability of Failure Calculation H4 Wind Li Spectrum

		Iteration			
H4	Initial Values	1	2	3	4
σ_Z	3600984	3600907	3600984	3600984	3600984
μ_Z	31590682	13474576	18115932	13474750	18115932
β	8.77	3.74	5.03	3.74	5.03
a1	0.58	1.00	1.00	1.00	1.00
a2	-0.58	0.00	0.00	0.00	0.00
a5	-0.58	0.00	0.01	0.01	0.01
X1*	35.25	14.99	20.28	15.13	20.28
X2*	8764.69	17830.07	8767.68	8764.96	8764.89
X3*	-141872.99	-8712.63	-142188.34	-142836.80	-142589.89
Pf	0.00E+00	9.13E-05	2.44E-07	9.13E-05	2.44E-07

Table I.38: Probability of Failure Calculation T200 Wind Li Spectrum

		Iteration			
T200	Initial Values	1	2	3	4
σ_Z	3600997	3600931	3600997	3600997	3600997
μ_Z	31574767	13478312	18096266	13478501	18096266
β	8.77	3.74	5.03	3.74	5.03
a1	0.58	1.00	1.00	1.00	1.00
a2	-0.58	0.00	0.00	0.00	0.00
a5	-0.58	0.00	0.01	0.01	0.01
X1*	35.25	15.00	20.28	15.15	20.28
X2*	9747.35	19860.20	9750.60	9747.69	9747.61
X3*	-157757.75	-15777.24	-158266.33	-158853.38	-158573.81
Pf	0.00E+00	9.09E-05	2.51E-07	9.09E-05	2.51E-07

Table I.39: Probability of Failure Calculation H5 Wind Li Spectrum

		Iteration			
H5	Initial Values	1	2	3	4
σ_Z	3601066	3600975	3601066	3601066	3601066
μ_Z	31525010	13495495	18029237	13495773	18029237
β	8.75	3.75	5.01	3.75	5.01
a1	0.58	1.00	1.00	1.00	1.00
a2	-0.58	0.00	0.00	0.00	0.00
a5	-0.58	0.01	0.01	0.01	0.01
X1*	35.25	15.03	20.26	15.22	20.26
X2*	12786.00	26741.97	12791.69	12786.65	12786.48
X3*	-207421.46	-25943.22	-208355.73	-209210.50	-208760.67
Pf	0.00E+00	8.92E-05	2.77E-07	8.92E-05	2.77E-07

Table I.40: Probability of Failure Calculation T1000 Wind Li Spectrum

		Iteration			
T1000	Initial Values	1	2	3	4
σ_Z	3601082	3601005	3601082	3601082	3601082
μ_Z	31509007	13497778	18010979	13498028	18010979
β	8.75	3.75	5.00	3.75	5.00
a1	0.58	1.00	1.00	1.00	1.00
a2	-0.58	0.00	0.00	0.00	0.00
a5	-0.58	0.01	0.01	0.01	0.01
X1*	35.25	15.04	20.26	15.24	20.26
X2*	13776.20	28008.59	13781.42	13776.87	13776.70
X3*	-223394.33	-34312.26	-224524.00	-225336.43	-224849.83
Pf	0.00E+00	8.90E-05	2.84E-07	8.90E-05	2.84E-07

Table I.41: Probability of Failure Calculation T2000 Wind Li Spectrum

		Iteration			
T2000	Initial Values	1	2	3	4
σ_Z	3601112	3601028	3601112	3601112	3601112
μ_Z	31489877	13503199	17986402	13503474	17986402
β	8.74	3.75	4.99	3.75	4.99
a1	0.58	1.00	1.00	1.00	1.00
a2	-0.58	0.00	0.00	0.00	0.00
a5	-0.58	0.01	0.01	0.01	0.01
X1*	35.25	15.06	20.25	15.27	20.25
X2*	14949.87	30855.42	14956.24	14950.71	14950.50
X3*	-242487.95	-39429.61	-243814.56	-244727.44	-244169.30
Pf	0.00E+00	8.85E-05	2.95E-07	8.85E-05	2.95E-07

Table I.42: Probability of Failure Calculation T10000 Wind Li Spectrum

		Iteration			
T10000	Initial Values	1	2	3	4
σ_Z	3601211	3601079	3601211	3601211	3601211
μ_Z	31444075	13521819	17921829	13522246	17921829
β	8.73	3.75	4.98	3.75	4.98
a1	0.58	1.00	1.00	1.00	1.00
a2	-0.58	0.00	0.00	0.00	0.00
a5	-0.58	0.01	0.01	0.01	0.01
X1*	35.25	15.09	20.23	15.35	20.23
X2*	17760.69	37558.75	17771.03	17761.99	17761.66
X3*	-288203.67	-44704.56	-290066.33	-291421.83	-290631.86
Pf	0.00E+00	8.67E-05	3.24E-07	8.67E-05	3.24E-07

Kaimal Spectrum - Bending Failure Probabilities

Table I.43: Probability of Bending Failure Calculation Rated Wind Kaimal Spectrum

		Iteration				
Rated	Initial Values	1	2	3	4	5
σ_Z	605226	605181	605182	605182	605182	605182
μ_Z	68260081	14364805	39989052	14364843	39989056	14364840
β	112.78	23.74	66.08	23.74	66.08	23.74
a1	0.58	0.01	0.01	0.01	0.01	0.01
a2	-0.58	0.00	0.00	0.00	0.00	0.00
a3	-0.58	-1.00	-1.00	-1.00	-1.00	-1.00
X1*	58750000.00	58098838.46	58746469.15	58740170.80	58746469.16	58740170.80
X2*	6569.82	92366.94	6569.98	6569.91	6569.83	6569.91
X3*	-1465859.25	37936934.69	12895809.76	38514349.56	12895805.90	38514353.42
Pf	0.00E+00	0.00E+00	0.00E+00	0.00E+00	0.00E+00	0.00E+00

Table I.44: Probability of Failure Calculation H1 Wind Kaimal Spectrum

		Iteration				
H1	Initial Values	1	2	3	4	5
σ_Z	3782355	3782330	3782372	3782376	3782372	3782376
μ_Z	59146358	29237596	34229468	29237914	34229506	29237875
β	15.64	7.73	9.05	7.73	9.05	7.73
a1	0.58	0.00	0.00	0.00	0.00	0.00
a2	-0.58	0.00	0.00	0.00	0.00	0.00
a3	-0.58	-1.00	-1.00	-1.00	-1.00	-1.00
X1*	58750000.00	58659717.17	58749816.02	58749784.61	58749816.02	58749784.61
X2*	46847.95	125273.80	46848.77	46848.41	46848.26	46848.41
X3*	-10579493.73	23568838.48	18658349.71	23649888.18	18658311.60	23649926.30
Pf	0.00E+00	5.33E-15	0.00E+00	5.33E-15	0.00E+00	5.33E-15

Table I.45: Probability of Failure Calculation T10 Wind Kaimal Spectrum

		Iteration				
T10	Initial Values	1	2	3	4	5
σ_Z	4998260	4998100	4998280	4998265	4998280	4998265
μ_Z	54782711	36144446	31685105	36145739	31685002	36145842
β	10.96	7.23	6.34	7.23	6.34	7.23
a1	0.58	0.00	0.00	0.00	0.00	0.00
a2	-0.58	0.00	0.00	0.00	0.00	0.00
a3	-0.58	-1.00	-1.00	-1.00	-1.00	-1.00
X1*	58750000.00	58686720.36	58749869.75	58749885.83	58749869.75	58749885.83
X2*	66905.65	150938.49	66907.95	66906.35	66906.66	66906.35
X3*	-14943093.87	16685947.21	21202714.08	16742066.27	21202816.83	16741963.52
Pf	0.00E+00	2.39E-13	1.15E-10	2.39E-13	1.15E-10	2.38E-13

Table I.46: Probability of Failure Calculation H2 Wind Kaimal Spectrum

		Iteration				
H2	Initial Values	1	2	3	4	5
σ_Z	5620805	5620350	5620821	5620733	5620821	5620733
μ_Z	51842725	40790432	29976860	40793790	29976279	40794371
β	9.22	7.26	5.33	7.26	5.33	7.26
a1	0.58	0.00	0.00	0.00	0.00	0.00
a2	-0.58	0.00	0.00	0.00	0.00	0.00
a3	-0.58	-1.00	-1.00	-1.00	-1.00	-1.00
X1*	58750000.00	58696748.88	58749883.75	58749914.58	58749883.76	58749914.59
X2*	79764.42	161485.63	79768.49	79765.19	79766.42	79765.19
X3*	-17883052.15	12048590.14	22910938.66	12093912.53	22911520.05	12093331.14
Pf	0.00E+00	1.97E-13	4.83E-08	1.97E-13	4.83E-08	1.97E-13

Table I.47: Probability of Failure Calculation T25 Wind Kaimal Spectrum

		Iteration				
T25	Initial Values	1	2	3	4	5
σ_Z	7500146	7494930	7500159	7498503	7500159	7498495
μ_Z	47183136	48153193	27243282	48186071	27233355	48195996
β	6.29	6.42	3.63	6.43	3.63	6.43
a1	0.58	0.00	0.00	0.00	0.00	0.00
a2	-0.58	0.00	0.00	0.00	0.00	0.00
a3	-0.58	-1.00	-1.00	-1.00	-1.00	-1.00
X1*	58750000.00	58713679.11	58749922.83	58749956.40	58749922.85	58749956.42
X2*	100516.63	176517.28	100530.72	100517.46	100524.65	100517.46
X3*	-22542594.98	4698838.03	25644493.08	4700857.57	25654420.74	4690929.79
Pf	1.58E-10	6.60E-11	1.40E-04	6.55E-11	1.41E-04	6.49E-11

Table I.48: Probability of Failure Calculation H3 Wind Kaimal Spectrum

		Iteration				
H3	Initial Values	1	2	3	4	5
σ_Z	7222158	7177669	7222167	7201419	7222168	7196533
μ_Z	45289250	51133299	25873565	51446573	25729062	51590617
β	6.27	7.12	3.58	7.14	3.56	7.17
a1	0.58	0.00	0.00	0.00	0.00	0.00
a2	-0.58	0.00	0.00	0.00	0.00	0.00
a3	-0.58	-1.00	-1.00	-1.00	-1.00	-1.00
X1*	58750000.00	58713795.09	58749910.65	58749955.34	58749910.70	58749955.59
X2*	109337.60	191002.88	109393.61	109338.62	109375.89	109338.61
X3*	-24436460.86	1711526.05	27014175.40	1437275.81	27158679.29	1292769.94
Pf	1.80E-10	5.24E-13	1.70E-04	4.53E-13	1.84E-04	3.78E-13

Table I.49: Probability of Failure Calculation T50 Wind Kaimal Spectrum

		Iteration				
T50	Initial Values	1	2	3	4	5
σ_Z	8613094	8603564	8613165	8609508	8613165	8609475
μ_Z	41452117	48517228	-23957054	48569732	-23976048	48588718
β	4.81	5.64	-2.78	5.64	-2.78	5.64
a1	0.58	0.00	0.00	0.00	0.00	0.00
a2	-0.58	0.00	0.00	0.00	0.00	0.00
a3	-0.58	1.00	1.00	1.00	1.00	1.00
X1*	58750000.00	58722213.95	58749940.99	58750029.07	58749941.01	58750029.09
X2*	126031.80	205263.16	126056.97	126031.37	126047.35	126031.37
X3*	-28273556.82	-4340950.63	-76844939.56	-4316496.76	-76863933.65	-4297502.74
Pf	7.45E-07	8.54E-09	9.97E-01	8.43E-09	9.97E-01	8.32E-09

Table I.50: Probability of Failure Calculation T100 Wind Kaimal Spectrum

		Iteration				
T100	Initial Values	1	2	3	4	5
σ_Z	10097330	10095993	10097406	10096725	10097406	10096725
μ_Z	36233423	40294971	-20905001	40300007	-20907118	40302124
β	3.59	3.99	-2.07	3.99	-2.07	3.99
a1	0.58	0.00	0.00	0.00	0.00	0.00
a2	-0.58	0.00	0.00	0.00	0.00	0.00
a3	-0.58	1.00	1.00	1.00	1.00	1.00
X1*	58750000.00	58729282.27	58749964.41	58750018.46	58749964.41	58750018.46
X2*	148384.87	211847.77	148391.12	148384.48	148389.24	148384.48
X3*	-33492203.56	-12572636.26	-73792861.84	-12587176.90	-73794978.81	-12585059.94
Pf	1.66E-04	3.29E-05	9.81E-01	3.28E-05	9.81E-01	3.28E-05

Table I.51: Probability of Failure Calculation H4 Wind Kaimal Spectrum

		Iteration				
H4	Initial Values	1	2	3	4	5
σ_Z	10122642	10121417	10122719	10122102	10122719	10122102
μ_Z	35567573	39245099	-20520391	39249578	-20522211	39251399
β	3.51	3.88	-2.03	3.88	-2.03	3.88
a1	0.58	0.00	0.00	0.00	0.00	0.00
a2	-0.58	0.00	0.00	0.00	0.00	0.00
a3	-0.58	1.00	1.00	1.00	1.00	1.00
X1*	58750000.00	58729713.85	58749965.51	58750018.03	58749965.51	58750018.03
X2*	153206.87	220385.79	153213.67	153206.41	153211.59	153206.41
X3*	-34158038.74	-13622898.57	-73408241.67	-13637619.74	-73410062.32	-13635799.09
Pf	2.21E-04	5.28E-05	9.79E-01	5.27E-05	9.79E-01	5.27E-05

Table I.52: Probability of Failure Calculation T200 Wind Kaimal Spectrum

		Iteration				
T200	Initial Values	1	2	3	4	5
σ_Z	10785207	10784498	10785283	10784892	10785283	10784892
μ_Z	32086514	33757407	-18511176	33759462	-18511997	33760284
β	2.98	3.13	-1.72	3.13	-1.72	3.13
a1	0.58	0.00	0.00	0.00	0.00	0.00
a2	-0.58	0.00	0.00	0.00	0.00	0.00
a3	-0.58	1.00	1.00	1.00	1.00	1.00
X1*	58750000.00	58732823.55	58749973.87	58750014.33	58749973.87	58750014.33
X2*	168854.09	234910.71	168859.36	168853.53	168857.87	168853.53
X3*	-37639061.97	-19113729.04	-71398994.69	-19127847.27	-71399816.19	-19127025.78
Pf	1.46E-03	8.73E-04	9.57E-01	8.73E-04	9.57E-01	8.73E-04

Table I.53: Probability of Failure Calculation H5 Wind Kaimal Spectrum

		Iteration				
H5	Initial Values	1	2	3	4	5
σ_Z	13623601	13623415	13623650	13623511	13623650	13623511
μ_Z	19298385	13594726	-11134467	13594864	-11134509	13594907
β	1.42	1.00	-0.82	1.00	-0.82	1.00
a1	0.58	0.00	0.00	0.00	0.00	0.00
a2	-0.58	0.00	0.00	0.00	0.00	0.00
a3	-0.58	1.00	1.00	1.00	1.00	1.00
X1*	58750000.00	58741821.60	58749993.41	58750005.40	58749993.41	58750005.40
X2*	225227.40	268875.38	225228.83	225226.80	225228.60	225226.80
X3*	-50427067.60	-39285033.17	-64022106.46	-39292537.05	-64022149.36	-39292494.15
Pf	7.83E-02	1.59E-01	7.93E-01	1.59E-01	7.93E-01	1.59E-01

Table I.54: Probability of Failure Calculation T1000 Wind Kaimal Spectrum

		Iteration				
T1000	Initial Values	1	2	3	4	5
σ_Z	15452459	15452338	15452487	15452396	15452487	15452396
μ_Z	14729750	6390917	-8499136	6390941	-8499136	6390940
β	0.95	0.41	-0.55	0.41	-0.55	0.41
a1	0.58	0.00	0.00	0.00	0.00	0.00
a2	-0.58	0.00	0.00	0.00	0.00	0.00
a3	-0.58	1.00	1.00	1.00	1.00	1.00
X1*	58750000.00	58744496.52	58749997.59	58750003.20	58749997.59	58750003.20
X2*	245520.23	276172.86	245520.72	245519.79	245520.67	245519.79
X3*	-54995657.50	-46491350.38	-61386685.15	-46496456.16	-61386685.00	-46496456.32
Pf	1.70E-01	3.40E-01	7.09E-01	3.40E-01	7.09E-01	3.40E-01

Table I.55: Probability of Failure Calculation T2000 Wind Kaimal Spectrum

		Iteration				
T2000	Initial Values	1	2	3	4	5
σ_Z	16532963	16532882	16532963	16532919	16532963	16532919
μ_Z	10866156	298276	-6270035	298269	-6270028	298262
β	0.66	0.02	-0.38	0.02	-0.38	0.02
a1	0.58	0.00	0.00	0.00	0.00	0.00
a2	-0.58	0.00	0.00	0.00	0.00	0.00
a3	-0.58	1.00	1.00	1.00	1.00	1.00
X1*	58750000.00	58746205.41	58749999.90	58750002.06	58749999.90	58750002.06
X2*	263597.51	286371.00	263597.54	263597.15	263597.53	263597.15
X3*	-58859209.37	-52585570.27	-59157489.77	-52589113.92	-59157482.42	-52589121.27
Pf	2.56E-01	4.93E-01	6.48E-01	4.93E-01	6.48E-01	4.93E-01

Table I.56: Probability of Failure Calculation T10000 Wind Kaimal Spectrum

		Iteration				
T10000	Initial Values	1	2	3	4	5
σ_Z	18064921	18064921	18064784	18064920	18064784	18064920
μ_Z	-185286	-17130118	106863	-17130063	106808	-17130008
β	-0.01	-0.95	0.01	-0.95	0.01	-0.95
a1	0.58	0.00	0.00	0.00	0.00	0.00
a2	-0.58	0.00	0.00	0.00	0.00	0.00
a5	-0.58	1.00	1.00	1.00	1.00	1.00
X1*	58750000.00	58750059.22	58750004.73	58749999.97	58750004.73	58749999.97
X2*	311723.52	311261.78	311722.10	311723.53	311722.10	311723.53
X3*	-69910545.80	-70017521.56	-52780262.76	-70017410.69	-52780317.74	-70017355.71
Pf	5.04E-01	8.28E-01	4.98E-01	8.28E-01	4.98E-01	8.28E-01

Yu Spectrum - Bending Failure Probabilities

Table I.57: Probability of Failure Calculation Rated Wind Yu Spectrum

		Iteration				
Rated	Initial Values	1	2	3	4	5
σ_Z	647555	647513	647515	647515	647515	647515
μ_Z	68003939	14808162	39801815	14808217	39801820	14808212
β	105.02	22.87	61.47	22.87	61.47	22.87
a1	0.58	0.01	0.01	0.01	0.01	0.01
a2	-0.58	0.00	0.00	0.00	0.00	0.00
a5	-0.58	-1.00	-1.00	-1.00	-1.00	-1.00
X1*	58750000.00	58143687.07	58746820.54	58741454.21	58746820.55	58741454.21
X2*	7876.80	107155.71	7877.07	7876.95	7876.82	7876.95
X3*	-1721998.05	37533910.38	13083362.55	38072130.97	13083357.22	38072136.31
Pf	0.00E+00	0.00E+00	0.00E+00	0.00E+00	0.00E+00	0.00E+00

Table I.58: Probability of Failure Calculation H1 Wind Yu Spectrum

		Iteration				
H1	Initial Values	1	2	3	4	5
σ_Z	3900905	3900827	3900923	3900925	3900923	3900925
μ_Z	57541965	31772568	33298346	31773347	33298365	31773328
β	14.75	8.15	8.54	8.15	8.54	8.15
a1	0.58	0.00	0.00	0.00	0.00	0.00
a2	-0.58	0.00	0.00	0.00	0.00	0.00
a5	-0.58	-1.00	-1.00	-1.00	-1.00	-1.00
X1*	58750000.00	58664835.48	58749812.03	58749803.01	58749812.03	58749803.01
X2*	56003.76	159138.87	56006.07	56004.68	56004.57	56004.68
X3*	-12183861.05	21038205.34	19589446.56	21114443.93	19589428.03	21114462.46
Pf	0.00E+00	0.00E+00	0.00E+00	0.00E+00	0.00E+00	0.00E+00

Table I.59: Probability of Failure Calculation T10 Wind Yu Spectrum

		Iteration				
T10	Initial Values	1	2	3	4	5
σ_Z	4629659	4629239	4629672	4629614	4629672	4629614
μ_Z	52382580	39927822	30299284	39931516	30298822	39931978
β	11.31	8.63	6.54	8.63	6.54	8.63
a1	0.58	0.00	0.00	0.00	0.00	0.00
a2	-0.58	0.00	0.00	0.00	0.00	0.00
a5	-0.58	-1.00	-1.00	-1.00	-1.00	-1.00
X1*	58750000.00	58684675.32	58749832.27	58749872.74	58749832.28	58749872.75
X2*	79712.14	182305.67	79718.64	79713.37	79714.97	79713.37
X3*	-17343191.84	12900124.95	22588466.27	12956166.43	22588928.80	12955703.89
Pf	0.00E+00	0.00E+00	2.98E-11	0.00E+00	2.99E-11	0.00E+00

Table I.60: Probability of Failure Calculation H2 Wind Yu Spectrum

		Iteration				
H2	Initial Values	1	2	3	4	5
σ_Z	6667576	6665176	6667591	6666920	6667591	6666919
μ_Z	48404992	46221712	27969776	46238069	27965512	46242332
β	7.26	6.93	4.19	6.94	4.19	6.94
a1	0.58	0.00	0.00	0.00	0.00	0.00
a2	-0.58	0.00	0.00	0.00	0.00	0.00
a5	-0.58	-1.00	-1.00	-1.00	-1.00	-1.00
X1*	58750000.00	58708085.77	58749906.34	58749943.36	58749906.35	58749943.37
X2*	97854.16	180262.82	97865.10	97855.12	97860.08	97855.12
X3*	-21320738.76	6626146.36	24917989.81	6649201.72	24922253.14	6644938.34
Pf	1.94E-13	2.03E-12	1.37E-05	2.02E-12	1.37E-05	2.02E-12

Table I.61: Probability of Failure Calculation T25 Wind Yu Spectrum

		Iteration				
T25	Initial Values	1	2	3	4	5
σ_Z	7435316	7392375	7435380	7414485	7435380	7410362
μ_Z	43014932	50971221	-25090605	51263363	-25230687	51403015
β	5.79	6.90	-3.37	6.91	-3.39	6.94
a1	0.58	0.00	0.00	0.00	0.00	0.00
a2	-0.58	0.00	0.00	0.00	0.00	0.00
a5	-0.58	1.00	1.00	1.00	1.00	1.00
X1*	58750000.00	58716599.02	58749916.03	58750040.86	58749916.06	58750041.08
X2*	121744.68	202655.10	121803.47	121744.26	121785.68	121744.26
X3*	-26710746.15	-1875837.53	-77978475.89	-1620147.77	-78118558.98	-1480065.05
Pf	3.62E-09	2.69E-12	1.00E+00	2.36E-12	1.00E+00	2.01E-12

Table I.62: Probability of Failure Calculation H3 Wind Yu Spectrum

		Iteration				
H3	Initial Values	1	2	3	4	5
σ_Z μ_Z	7978021 40809920	7972288 47503665	7978089 -23566107	7975635 47536802	7978089 -23579303	7975623 47549994
β	5.12	5.96	-2.95	5.96	-2.96	5.96
a1 a2 a5	0.58 -0.58 -0.58	0.00 0.00 1.00	0.00 0.00 1.00	0.00 0.00 1.00	0.00 0.00 1.00	0.00 0.00 1.00
X1* X2* X3*	58750000.00 133045.47 -28915728.72	58720466.84 204500.04 -5353886.91	58749932.72 133062.17 -76453972.79	58750033.33 133045.09 -5349615.94	58749932.73 133056.34 -76467168.75	58750033.35 133045.09 -5336420.04
Pf	1.57E-07	1.27E-09	9.98E-01	1.26E-09	9.98E-01	1.25E-09

Table I.63: Probability of Failure Calculation T50 Wind Yu Spectrum

		Iteration				
T50	Initial Values	1	2	3	4	5
σ_Z μ_Z	9089250 37132532	9087515 41710169	9089324 -21423746	9088530 41717752	9089324 -21426672	9088529 41720677
β	4.09	4.59	-2.36	4.59	-2.36	4.59
a1 a2 a5	0.58 -0.58 -0.58	0.00 0.00 1.00	0.00 0.00 1.00	0.00 0.00 1.00	0.00 0.00 1.00	0.00 0.00 1.00
X1* X2* X3*	58750000.00 149397.11 -32593080.64	58726413.37 223717.15 -11154396.30	58749954.53 149407.16 -74311597.12	58750023.34 149396.59 -11169312.18	58749954.53 149403.81 -74314523.07	58750023.35 149396.59 -11166386.24
Pf	2.20E-05	2.22E-06	9.91E-01	2.21E-06	9.91E-01	2.21E-06

Table I.64: Probability of Failure Calculation T100 Wind Yu Spectrum

		Iteration				
T100	Initial Values	1	2	3	4	5
σ_Z μ_Z	11844433 30460105	11843863 31194301	11844517 -17573750	11844145 31195662	11844517 -17574370	11844145 31196282
β	2.57	2.63	-1.48	2.63	-1.48	2.63
a1 a2 a5	0.58 -0.58 -0.58	0.00 0.00 1.00	0.00 0.00 1.00	0.00 0.00 1.00	0.00 0.00 1.00	0.00 0.00 1.00
X1* X2* X3*	58750000.00 180838.79 -39265433.91	58735152.39 234498.99 -21679106.53	58749979.98 180841.93 -70461541.88	58750011.28 180838.37 -21691636.28	58749979.98 180841.21 -70462162.08	58750011.28 180838.37 -21691016.08
Pf	5.06E-03	4.22E-03	9.31E-01	4.22E-03	9.31E-01	4.22E-03

Table I.65: Probability of Failure Calculation H4 Wind Yu Spectrum

		Iteration				
H4	Initial Values	1	2	3	4	5
σ_Z	11447809	11447365	11447885	11447587	11447885	11447587
μ_Z	28753518	28502802	-16588420	28503792	-16588857	28504229
β	2.51	2.49	-1.45	2.49	-1.45	2.49
a1	0.58	0.00	0.00	0.00	0.00	0.00
a2	-0.58	0.00	0.00	0.00	0.00	0.00
a5	-0.58	1.00	1.00	1.00	1.00	1.00
X1*	58750000.00	58735498.67	58749980.42	58750011.39	58749980.42	58750011.40
X2*	187924.90	241454.81	187927.83	187924.43	187927.18	187924.43
X3*	-40972006.16	-24370989.11	-69476189.82	-24383536.19	-69476627.01	-24383099.00
Pf	6.01E-03	6.39E-03	9.26E-01	6.39E-03	9.26E-01	6.39E-03

Table I.66: Probability of Failure Calculation T200 Wind Yu Spectrum

		Iteration				
T200	Initial Values	1	2	3	4	5
σ_Z	11378174	11377862	11378241	11378022	11378241	11378022
μ_Z	25356799	23146555	-14628385	23147104	-14628608	23147327
β	2.23	2.03	-1.29	2.03	-1.29	2.03
a1	0.58	0.00	0.00	0.00	0.00	0.00
a2	-0.58	0.00	0.00	0.00	0.00	0.00
a5	-0.58	1.00	1.00	1.00	1.00	1.00
X1*	58750000.00	58737133.48	58749983.90	58750010.17	58749983.90	58750010.17
X2*	205697.79	259007.08	205700.47	205697.20	205699.92	205697.20
X3*	-44368679.65	-29728775.75	-67516098.91	-29740236.22	-67516322.44	-29740012.70
Pf	1.29E-02	2.10E-02	9.01E-01	2.10E-02	9.01E-01	2.10E-02

Table I.67: Probability of Failure Calculation H5 Wind Yu Spectrum

		Iteration				
H5	Initial Values	1	2	3	4	5
σ_Z	14941451	14941368	14941454	14941407	14941454	14941407
μ_Z	11266540	929303	-6500681	929297	-6500673	929289
β	0.75	0.06	-0.44	0.06	-0.44	0.06
a1	0.58	0.00	0.00	0.00	0.00	0.00
a2	-0.58	0.00	0.00	0.00	0.00	0.00
a5	-0.58	1.00	1.00	1.00	1.00	1.00
X1*	58750000.00	58745646.51	58749999.63	58750002.62	58749999.63	58750002.62
X2*	269045.56	293907.19	269045.64	269045.13	269045.63	269045.13
X3*	-58458795.69	-51953988.77	-59388113.10	-51958050.55	-59388105.12	-51958058.53
Pf	2.25E-01	4.75E-01	6.68E-01	4.75E-01	6.68E-01	4.75E-01

Table I.68: Probability of Failure Calculation T1000 Wind Yu Spectrum

		Iteration				
T1000	Initial Values	1	2	3	4	5
σ_Z	15611408	15611364	15611366	15611384	15611366	15611384
μ_Z	6598347	-6432283	-3807273	-6432286	-3807279	-6432280
β	0.42	-0.41	-0.24	-0.41	-0.24	-0.41
a1	0.58	0.00	0.00	0.00	0.00	0.00
a2	-0.58	0.00	0.00	0.00	0.00	0.00
a5	-0.58	1.00	1.00	1.00	1.00	1.00
X1*	58750000.00	58747559.76	58750002.38	58750001.41	58750002.38	58750001.41
X2*	291185.81	305979.37	291185.31	291185.52	291185.34	291185.52
X3*	-63126936.50	-59317339.62	-56694569.58	-59319614.41	-56694575.39	-59319608.60
Pf	3.36E-01	6.60E-01	5.96E-01	6.60E-01	5.96E-01	6.60E-01

Table I.69: Probability of Failure Calculation T2000 Wind Yu Spectrum

		Iteration				
T2000	Initial Values	1	2	3	4	5
σ_Z	19243538	19243539	19243381	19243538	19243381	19243538
μ_Z	-357834	-17402242	206433	-17402181	206373	-17402121
β	-0.02	-0.90	0.01	-0.90	0.01	-0.90
a1	0.58	0.00	0.00	0.00	0.00	0.00
a2	-0.58	0.00	0.00	0.00	0.00	0.00
a5	-0.58	1.00	1.00	1.00	1.00	1.00
X1*	58750000.00	58750107.36	58750004.23	58749999.95	58750004.23	58749999.95
X2*	321625.57	320914.97	321624.63	321625.59	321624.63	321625.59
X3*	-70083050.75	-70289648.23	-52680631.09	-70289487.56	-52680691.02	-70289427.63
Pf	5.07E-01	8.17E-01	4.96E-01	8.17E-01	4.96E-01	8.17E-01

Table I.70: Probability of Failure Calculation T10000 Wind Yu Spectrum

		Iteration				
T10000	Initial Values	1	2	3	4	5
σ_Z	21953393	21953450	21952894	21953426	21952894	21953426
μ_Z	-11876384	-35568228	6853545	-35568004	6853359	-35567818
β	-0.54	-1.62	0.31	-1.62	0.31	-1.62
a1	0.58	0.00	0.00	0.00	0.00	0.00
a2	-0.58	0.00	0.00	0.00	0.00	0.00
a5	-0.58	1.00	1.00	1.00	1.00	1.00
X1*	58750000.00	58753123.36	58750006.64	58749998.72	58750006.64	58749998.72
X2*	375637.21	352356.89	375635.58	375637.85	375635.47	375637.85
X3*	-81601474.93	-88458380.29	-46032970.46	-88455246.94	-46033156.57	-88455060.82
Pf	7.06E-01	9.47E-01	3.77E-01	9.47E-01	3.77E-01	9.47E-01

Li Spectrum - Bending Failure Probabilities

Table I.71: Probability of Bending Failure Calculation Rated Wind Li Spectrum

		Iteration				
Rated	Initial values	1	2	3	4	5
σ_Z	599341	599295	599298	599298	599298	599298
μ_Z	68020357	14739323	39854239	14739375	39854245	14739369
β	113.49	24.59	66.50	24.59	66.50	24.59
a1	0.58	0.02	0.02	0.02	0.02	0.02
a2	-0.58	0.00	0.00	0.00	0.00	0.00
a5	-0.58	-1.00	-1.00	-1.00	-1.00	-1.00
X1*	58750000.00	58094754.44	58746305.59	58740010.61	58746305.60	58740010.61
X2*	7848.19	104670.95	7848.44	7848.33	7848.21	7848.33
X3*	-1705580.10	37558706.54	13030474.55	38139673.82	13030469.20	38139679.18
Pf	0.00E+00	0.00E+00	0.00E+00	0.00E+00	0.00E+00	0.00E+00

Table I.72: Probability of Failure Calculation H1 Wind Li Spectrum

		Iteration				
H1	Initial values	1	2	3	4	5
σ_Z	3560304	3560241	3560319	3560321	3560319	3560321
μ_Z	57665285	31570613	33377071	31571303	33377093	31571282
β	16.20	8.87	9.37	8.87	9.37	8.87
a1	0.58	0.00	0.00	0.00	0.00	0.00
a2	-0.58	0.00	0.00	0.00	0.00	0.00
a5	-0.58	-1.00	-1.00	-1.00	-1.00	-1.00
X1*	58750000.00	58656488.12	58749775.78	58749762.96	58749775.79	58749762.96
X2*	55675.09	153007.95	55677.04	55675.91	55675.80	55675.91
X3*	-12060541.21	21232696.60	19510689.36	21316452.72	19510667.88	21316474.20
Pf	0.00E+00	0.00E+00	0.00E+00	0.00E+00	0.00E+00	0.00E+00

Table I.73: Probability of Failure Calculation T10 Wind Li Spectrum

		Iteration				
T10	Initial values	1	2	3	4	5
σ_Z	5373792	5373396	5373809	5373740	5373809	5373740
μ_Z	52375114	39947934	30287297	39950962	30286827	39951433
β	9.75	7.43	5.64	7.43	5.64	7.43
a1	0.58	0.00	0.00	0.00	0.00	0.00
a2	-0.58	0.00	0.00	0.00	0.00	0.00
a5	-0.58	-1.00	-1.00	-1.00	-1.00	-1.00
X1*	58750000.00	58693729.14	58749875.45	58749905.58	58749875.46	58749905.59
X2*	80158.31	166296.32	80162.49	80159.18	80160.32	80159.18
X3*	-17350655.98	12888379.13	22600490.88	12936746.44	22600961.10	12936276.21
Pf	0.00E+00	5.25E-14	8.70E-09	5.25E-14	8.70E-09	5.24E-14

Table I.74: Probability of Failure Calculation H2 Wind Li Spectrum

		Iteration				
H2	Initial values	1	2	3	4	5
σ_Z	6793541	6791846	6793557	6793067	6793557	6793067
μ_Z	48973967	45325003	28302862	45336135	28299880	45339117
β	7.21	6.67	4.17	6.67	4.17	6.67
a1	0.58	0.00	0.00	0.00	0.00	0.00
a2	-0.58	0.00	0.00	0.00	0.00	0.00
a5	-0.58	-1.00	-1.00	-1.00	-1.00	-1.00
X1*	58750000.00	58708379.39	58749911.55	58749944.79	58749911.56	58749944.80
X2*	95316.24	171409.47	95323.72	95317.03	95320.38	95317.03
X3*	-20751769.27	7523618.85	24584915.63	7551255.79	24587897.68	7548273.69
Pf	2.82E-13	1.25E-11	1.55E-05	1.25E-11	1.55E-05	1.24E-11

Table I.75: Probability of Failure Calculation T25 Wind Li Spectrum

		Iteration				
T25	Initial values	1	2	3	4	5
σ_Z	7642039	7545660	7642107	7495657	7642108	7313660
μ_Z	43427863	51618364	-25688065	52266410	-26697512	52470436
β	5.68	6.84	-3.36	6.97	-3.49	7.17
a1	0.58	0.00	0.00	0.00	0.00	0.00
a2	-0.58	0.00	0.00	0.00	0.00	0.00
a5	-0.58	1.00	1.00	1.00	1.00	-1.00
X1*	58750000.00	58717190.58	58749918.39	58750039.60	58749916.26	58750041.15
X2*	121126.38	196414.56	121201.98	121126.02	121221.82	121126.01
X3*	-26297813.40	-1224489.41	-78575939.76	-609753.85	-79585386.65	399692.81
Pf	6.63E-09	3.94E-12	1.00E+00	1.55E-12	1.00E+00	3.63E-13

Table I.76: Probability of Failure Calculation H3 Wind Li Spectrum

		Iteration				
H3	Initial values	1	2	3	4	5
σ_Z	7873024	7867062	7873092	7870670	7873092	7870658
μ_Z	40806143	47497142	-23565198	47532114	-23578393	47545305
β	5.18	6.04	-2.99	6.04	-2.99	6.04
a1	0.58	0.00	0.00	0.00	0.00	0.00
a2	-0.58	0.00	0.00	0.00	0.00	0.00
a5	-0.58	1.00	1.00	1.00	1.00	1.00
X1*	58750000.00	58720075.75	58749930.91	58750034.22	58749930.93	58750034.24
X2*	133167.81	210101.23	133187.68	133167.37	133180.42	133167.37
X3*	-28919505.86	-5359845.40	-76453062.08	-5354302.69	-76466256.50	-5341108.32
Pf	1.09E-07	7.83E-10	9.99E-01	7.75E-10	9.99E-01	7.67E-10

Table I.77: Probability of Failure Calculation T50 Wind Li Spectrum

		Iteration				
T50	Initial values	1	2	3	4	5
σ_Z	8826429	8824872	8826501	8825731	8826501	8825731
μ_Z	37101809	41661247	-21404935	41668217	-21407848	41671130
β	4.20	4.72	-2.43	4.72	-2.43	4.72
a1	0.58	0.00	0.00	0.00	0.00	0.00
a2	-0.58	0.00	0.00	0.00	0.00	0.00
a5	-0.58	1.00	1.00	1.00	1.00	1.00
X1*	58750000.00	58725731.14	58749951.84	58750024.73	58749951.84	58750024.74
X2*	149895.58	216471.01	149903.36	149895.16	149900.96	149895.16
X3*	-32623802.15	-11202856.21	-74292782.75	-11218845.57	-74295695.22	-11215933.11
Pf	1.31E-05	1.17E-06	9.92E-01	1.17E-06	9.92E-01	1.17E-06

Table I.78: Probability of Failure Calculation T100 Wind Li Spectrum

		Iteration				
T100	Initial values	1	2	3	4	5
σ_Z	9894282	9893703	9894353	9894002	9894353	9894002
μ_Z	31575741	32950716	-18214964	32952481	-18215734	32953252
β	3.19	3.33	-1.84	3.33	-1.84	3.33
a1	0.58	0.00	0.00	0.00	0.00	0.00
a2	-0.58	0.00	0.00	0.00	0.00	0.00
a5	-0.58	1.00	1.00	1.00	1.00	1.00
X1*	58750000.00	58731574.95	58749969.70	58750016.75	58749969.70	58750016.75
X2*	174812.97	233402.78	174816.96	174812.51	174815.96	174812.51
X3*	-38149813.17	-19919372.08	-71102763.74	-19934809.33	-71103534.19	-19934038.89
Pf	7.08E-04	4.33E-04	9.67E-01	4.33E-04	9.67E-01	4.33E-04

Table I.79: Probability of Failure Calculation H4 Wind Li Spectrum

		Iteration				
H4	Initial values	1	2	3	4	5
σ_Z	10111825	10111340	10111894	10111604	10111894	10111604
μ_Z	29697455	29989368	-17131391	29990678	-17131918	29991204
β	2.94	2.97	-1.69	2.97	-1.69	2.97
a1	0.58	0.00	0.00	0.00	0.00	0.00
a2	-0.58	0.00	0.00	0.00	0.00	0.00
a5	-0.58	1.00	1.00	1.00	1.00	1.00
X1*	58750000.00	58733043.78	58749973.59	58750015.08	58749973.59	58750015.08
X2*	183388.86	246889.00	183393.29	183388.24	183392.15	183388.24
X3*	-40028079.95	-22882078.12	-70019169.39	-22896643.49	-70019695.83	-22896117.06
Pf	1.66E-03	1.51E-03	9.55E-01	1.51E-03	9.55E-01	1.51E-03

Table I.80: Probability of Failure Calculation T200 Wind Li Spectrum

		Iteration				
T200	Initial values	1	2	3	4	5
σ_Z	11792435	11792121	11792503	11792280	11792503	11792280
μ_Z	25348498	23133891	-14624001	23134422	-14624220	23134642
β	2.15	1.96	-1.24	1.96	-1.24	1.96
a1	0.58	0.00	0.00	0.00	0.00	0.00
a2	-0.58	0.00	0.00	0.00	0.00	0.00
a5	-0.58	1.00	1.00	1.00	1.00	1.00
X1*	58750000.00	58737589.53	58749985.02	58750009.47	58749985.02	58750009.47
X2*	203949.77	255822.79	203952.27	203949.21	203951.76	203949.21
X3*	-44376988.33	-29741878.96	-67511721.31	-29752929.32	-67511940.60	-29752710.03
Pf	1.58E-02	2.49E-02	8.93E-01	2.49E-02	8.93E-01	2.49E-02

Table I.81: Probability of Failure Calculation H5 Wind Li Spectrum

		Iteration				
H5	Initial values	1	2	3	4	5
σ_Z	14786191	14786104	14786197	14786145	14786197	14786145
μ_Z	11655747	1543031	-6725206	1543027	-6725198	1543019
β	0.79	0.10	-0.45	0.10	-0.45	0.10
a1	0.58	0.00	0.00	0.00	0.00	0.00
a2	-0.58	0.00	0.00	0.00	0.00	0.00
a5	-0.58	1.00	1.00	1.00	1.00	1.00
X1*	58750000.00	58745448.83	58749999.36	58750002.77	58749999.36	58750002.77
X2*	267529.17	293823.16	267529.31	267528.71	267529.29	267528.71
X3*	-58069591.58	-51340073.49	-59612647.00	-51344320.53	-59612639.00	-51344328.53
Pf	2.15E-01	4.58E-01	6.75E-01	4.58E-01	6.75E-01	4.58E-01

Table I.82: Probability of Failure Calculation T1000 Wind Li Spectrum

		Iteration				
T1000	Initial values	1	2	3	4	5
σ_Z	15812624	15812574	15812589	15812596	15812589	15812596
μ_Z	7374085	-5208908	-4254910	-5208913	-4254912	-5208911
β	0.47	-0.33	-0.27	-0.33	-0.27	-0.33
a1	0.58	0.00	0.00	0.00	0.00	0.00
a2	-0.58	0.00	0.00	0.00	0.00	0.00
a5	-0.58	1.00	1.00	1.00	1.00	1.00
X1*	58750000.00	58747307.58	58750001.88	58750001.53	58750001.88	58750001.53
X2*	288247.76	304119.23	288247.38	288247.46	288247.40	288247.46
X3*	-62351203.99	-58093729.81	-57142226.75	-58096241.22	-57142228.71	-58096239.26
Pf	3.20E-01	6.29E-01	6.06E-01	6.29E-01	6.06E-01	6.29E-01

Table I.83: Probability of Failure Calculation T2000 Wind Li Spectrum

		Iteration				
T2000	Initial values	1	2	3	4	5
σ_Z	16919157	16919145	16919049	16919149	16919049	16919149
μ_Z	1731327	-14107554	-999062	-14107518	-999103	-14107477
β	0.10	-0.83	-0.06	-0.83	-0.06	-0.83
a1	0.58	0.00	0.00	0.00	0.00	0.00
a2	-0.58	0.00	0.00	0.00	0.00	0.00
a5	-0.58	1.00	1.00	1.00	1.00	1.00
X1*	58750000.00	58749409.20	58750004.44	58750000.31	58750004.44	58750000.31
X2*	312805.19	316699.69	312804.18	312805.10	312804.19	312805.10
X3*	-67993908.58	-66994316.12	-53886200.48	-66994829.71	-53886241.18	-66994789.01
Pf	4.59E-01	7.98E-01	5.24E-01	7.98E-01	5.24E-01	7.98E-01

Table I.84: Probability of Failure Calculation T10000 Wind Li Spectrum

		Iteration				
T10000	Initial values	1	2	3	4	5
σ_Z	17393292	17393340	17392924	17393316	17392924	17393316
μ_Z	-10779291	-33837291	6219729	-33837068	6219554	-33836893
β	-0.62	-1.95	0.36	-1.95	0.36	-1.95
a1	0.58	0.00	0.00	0.00	0.00	0.00
a2	-0.58	0.00	0.00	0.00	0.00	0.00
a5	-0.58	1.00	1.00	1.00	1.00	1.00
X1*	58750000.00	58753578.06	58750010.07	58749998.15	58750010.07	58749998.15
X2*	371617.65	342215.62	371614.67	371618.76	371614.41	371618.76
X3*	-80504387.97	-86727879.13	-46666842.45	-86724312.59	-46667018.01	-86724137.03
Pf	7.32E-01	9.74E-01	3.60E-01	9.74E-01	3.60E-01	9.74E-01